Offshore hydrogen production from floating offshore wind - a study of UNITECH Zefyros

An energy and hydrodynamic analysis of an in-turbine electrolyser for offshore hydrogen production and the influence of a variable power source

Master thesis in Ocean Technology
Marine installations

Magnus Vestrheim

Department of Physics and Technology
University of Bergen

i. Preface

This master's thesis is written as a part of my master's degree in Ocean Technology at the Department of Physics and Technology at the University of Bergen, in collaboration with the Western Norway University of Applied Sciences.

The master's thesis is done in collaboration with UNITECH Energy Group. In the summer of 2020, I asked Gunnar Birkeland, CEO of UNITECH Energy Group, if UNITECH were interested in me writing a master thesis about hydrogen production from their floating offshore wind turbine, UNITECH Zefyros. I want to express my gratitude to UNITECH as a company that shared data and information about UNITECH Zefyros. I want to extend a special thank you to Gunnar Birkeland, who facilitated the possibility of this collaboration and spent time answering my questions despite his busy schedule.

The thesis has three supervisors, Velaug Oltedal Myrseth, Torbjørn Egeland-Eriksen and Martin Fernø. I want to express my gratitude for the time spent on meetings and for the valuable input and feedback provided. Also, I want to thank the other master's students writing a thesis about hydrogen for the platform to share information, frustrations, and answers. Of the hydrogen student group, Aurora Baardsen has been a great help to me for the hydrodynamic part of the thesis. I would also like to express my gratitude to Thore Clifford Thuestad for assisting me in the DNV Sesam modelling and for the feedback given despite not being listed as a supervisor for this thesis.

Magnus Vestrheim

31.05.2022

ii. Abstract

The aim of this thesis is to review design considerations and study the effect of a variable power supply of offshore hydrogen production by an electrolyser inside the turbine tower of a floating offshore wind turbine. To achieve this, UNITECH Zefyros, previously known as Hywind Demo, the world's first floating offshore wind turbine, has been studied for the possibility of hydrogen production. Historical 2020 wind and power data collected by Zefyros are used for calculations in the thesis.

The thesis is divided into two cases, shown below.

- **Case 1** An in-turbine electrolyser to show the feasibility of hydrogen production at UNITECH Zefyros.
- **Case 2** A large-scale hydrogen production system to study the effect of an intermittent power supply from wind power on an electrolyser.

The chosen electrolyser must comply with the space constraints in the turbine tower, resulting in a low-rated electrolyser, less than 1 % of the turbine's rated power. Hence, the electrolyser will operate at its rated load if the turbine generates power and cannot be used to study how variable power influences the electrolyser. A second hydrogen production system is thus proposed, where the constraints regarding space inside the turbine tower are not considered. This facilitates for an electrolyser that can use all available energy from Zefyros for hydrogen production, making the load profile dynamic.

For case 1, an in-turbine hydrogen production system is proposed, where the components are reviewed for compatibility in an offshore environment. Safety considerations introduced by in-turbine hydrogen production are identified. Zefyros' responses to 1- and 10-year seas are estimated to identify what displacement and accelerations an in-turbine electrolyser would experience. The annual hydrogen yield in 2020 from the in-turbine electrolyser is estimated.

For case 2, a model is developed in which the electrolyser's energy efficiency is estimated through the cell voltage. The energy efficiencies throughout 2020 and the annual hydrogen yield are estimated to show the effect a variable power source has on an electrolyser.

iii. Samandrag

Målet med denne oppgåva er å vise til vurderingar tilknytt design og å studere effekten av ei variabel kraftkjelde for offshore hydrogen produksjonssystem ved ein elektrolysør integrert i tårnet til ein flytande offshore vindturbin. For å oppnå dette er det tatt utgangspunkt i den offshore flytande vindturbinen UNITECH Zefyros, tidlegare kjent som Hywind Demo, verdas første flytande vindturbin. Historiske 2020 vind- og kraftdata samla av Zefyros er brukt for berekningar i oppgåva.

Oppgåva er delt inn i to casar, som vist under.
Case 1 Ein integrert elektrolysør for å kunne bevise moglegheita for gjennomføring av hydrogenproduksjon på UNITECH Zefyros.
Case 2 Eit storskala hydrogenproduksjonssystem for å kunne studere effekten ei variabel kraftkjelde har på ein elektrolysør.

Elektrolysøren integrert i turbintårnet må være innan avgrensingar tilknytt lokasjon i turbintårnet. Dette vil føre til ein elektrolysør med svært liten merkeeffekt; mindre enn 1 % av Zefyros sin merkeeffekt. Den låge merkeeffekten vil føre til at så lenge turbinen genererer kraft så vil elektrolysøren operere ved sin merkelast, og kan derfor ikkje brukast til å undersøke korleis ei variabel kraftkjelde påverkar ein elektrolysør. Eit anna hydrogenproduksjonsanlegg er derfor også studert i oppgåva kor avgrensingar av plass ikkje er betrakta. Dette mogleggjer hydrogenproduksjon frå all konvertert energi frå Zefyros som fører til ein dynamisk lastprofil.

For case 1 er det tatt utgangspunkt i eit hydrogenproduksjonsanlegg inne i turbintårnet til Zefyros. Komponentar i systemet er vurdert for kompatibilitet med eit offshore miljø. Betraktningar av sikkerheitsutfordringar som introduserast av eit slik anlegg er identifisert. Responsen av Zefyros i 1-års og 10-års sjø er estimert for å identifisera bevegelsar og akselerasjonar ein elektrolysør inne i turbintårnet vil kunne oppleva. Årleg hydrogenproduksjon er estimert.

I case 2 er det konstruert ein modell kor storskala elektrolysøren sin verkningsgrad er estimert gjennom cellespenninga til elektrolysøren. Verkningsgradar gjennom 2020 saman med den årlege hydrogenproduksjonen frå storskala-anlegget er estimert for å vise effekten av ei variabel kraftkjelde på ein elektrolysør.

iv. Table of contents

List of figures

List of tables

v. Nomenclature

Abbreviations

FOWT	Floating Offshore Wind Turbine
FC	Fuel Cell
SCADA	Supervisory Control And Data Acquisition
PEM	Proton Exchange Membrane
AE	Alkaline Electrolysis
AEM	Anion Exchange Membrane
SOEC	Solid Oxide Electrolyser Cell
OER	Oxygen Evolution Reaction
HER	Hydrogen Evolution Reaction
OCV	Open Circuit Voltage
RO	Reverse Osmosis
MEA	Membrane Electrode Assembly
LHV	Lower heating value
STP	Standard Temperature and pressure
UV	Ultraviolet
IR	Infrared
HAZID	Hazard identification study
CTV	Crew Transport Vessel
DoD	Depth of Discharge
SoC	State of Charge
MPM	Most Probable Maximum
MGO	Marine Gasoil
CTV	Crew Transport Vessel

Symbols

P_{wind}	Theoretical power in wind	[W]
P_{WT}	Power from a wind turbine	[W]
A	Area	[m^2]
ρ	Density	[kg/m^3]
u	Wind speed	[m/s]
C_p	Power coefficient	[-]
η_{mech}	Mechanical efficiency	[-]
a	Axial induction factor	[-]
P_{WT}	Power wind turbine	[W]
h	Water depth	[m]
λ	Wavelength	[m]
k	Wave number	[rad/m]
ω	Wave frequency	[rad/s]
T	Temperature	[K]
ξ	Wave surface elevation	[-]
ξ_a	Wave amplitude	[m]
ε_n	Phase angle component	[-]

H_s	Significant wave height	[m]
σ	Standard deviation	[-]
N	Number of samples/waves	[-]
ξ_{a_n}	Wave amplitude irregular wave	[m]
S_ξ	Wave spectrum	[-]
ω_p	Spectral peak	[rad/s]
T_p	Period of spectral peak	[s]
m_{0R}	Area below the response spectrum	[-]
R_a	Response amplitude	[-]
i	Current density	[A/cm^2]
I	Current	[A]
ΔG	Gibbs Free Energy	[J/K*mol]
ΔH	Change in enthalpy	[J/K]
ΔS	Change in entropy	[J/K]
n	Number of electrons	[-]
F	Faraday's constant	[C/mol]
U_{rev}	Reversible voltage	[V]
U_{th}	Thermo-neutral voltage	[V]
U_{cell}	Cell voltage	[V]
U_{OCV}	Open Circuit Voltage	[V]
U_{act}	Activation overpotential	[V]
U_{ohm}	Ohmic overpotential	[V]
U_{con}	Concentration overpotential	[V]
R	Universal gas constant	[J/K*mol]
p_{H_2}	Hydrogen pressure in electrolyser	[bar]
p_{O_2}	Oxygen pressure in electrolyser	[bar]
$p_{cathode}$	Cathode pressure	[bar]
p_{anode}	Anode pressure	[bar]
γ_{H_2}	Partial increase factor hydrogen	[mol/s cm bar]
$p_{H_2O,sat}$	Water saturation pressure	[bar]
γ_{O_2}	Partial increase factor oxygen	[mol/s cm bar]
ε^{Fick}	Diffusivity Nafion membrane	[mol/s cm bar]
$U_{act,anode}$	Anode activation overpotential	[V]
$U_{act,cathode}$	Cathode activation overpotential	[V]
$i_{o,ref\,a}$	Reference exchange current density, anode	[A/cm^2]
$i_{o,ref\,c}$	Reference exchange current density, cathode	[A/cm^2]
T_{cell}	Cell temperature	[K]
T_{ref}	Reference temperature	[K]
$i_{0,a}$	Exchange current density anode	[A/cm^2]
$i_{0,c}$	Exchange current density cathode	[A/cm^2]
$E_{act,a}$	Activation energy OER	[J/mol]
$E_{act,c}$	Activation energy HER	[J/mol]
$\alpha_{cathode}$	Charge transfer coefficient, cathode	[-]
α_{anode}	Charge transfer coefficient, anode	[-]
δ_{mem}	Membrane thickness	[cm]

σ_{mem}	Membrane conductivity	[1/Ω cm]
$C_{an_{O_2}}$	Oxygen concentration in the anode	[-]
$C_{cat_{H_2}}$	Hydrogen concentration in the cathode	[-]
η_T	Electrolyser efficiency	[-]
η_U	Voltage efficiency	[-]
η_F	Faradic efficiency	[-]
j_x	Total gas crossover current density	[A/cm^2]
$j_x^{H_2}$	Hydrogen gas crossover current density	[A/cm^2]
$j_x^{O_2}$	Oxygen gas crossover current density	[A/cm^2]
$P_{H_2}^T$	Diffusive permeability constant hydrogen	[mol/cm s Pa]
d_m	Membrane swelling factor	[-]
a_x	Fitting parameter	[μm]
$E_{Zefyros}$	Energy converted Zefyros	[kWh]
$P_{Zefyros}$	Power converted Zefyros	[kW]
$E_{compression}$	Energy consumption compression	[kWh]
$E_{desalination}$	Energy consumption desalination	[kWh]
$m_{H_2,case\,2}$	Accumulated mass of hydrogen, case 2	[kg H_2]
$E_{compression,case\,2}$	Energy consumption compression, case 2	[kWh]
$E_{desalination,case\,2}$	Energy consumption desalination, case 2	[kWh]
m_{H_2O}	Water consumption electrolyser	[kg]
$m_{H_2O,case\,2}$	Water consumption electrolyser, case 2	[kg]
S_{PEM}	Operational state electrolyser	[-]
E_{PEM}	Energy consumption PEM electrolyser	[kWh]
N_{cell}	Number of cells	[-]
$P_{electrolyser}$	Rated power large-scale electrolyser	[W]
U_{rated}	Cell voltage at rated current density	[V]
i_{rated}	Rated current density	[A/cm^2]
$\dot{m}_{H_2}$	Hydrogen production rate	[kg H_2/10 min]
$E_{electrolyser}$	Specific energy consumption electrolyser	[kWh/kg H_2]
LHV	Lower heating value hydrogen	[J/kg]
A_{cell}	Cell membrane area	[cm^2]
λ_{mem}	Number of molecules per sulphonic group	[-]
T_{wave}	Wave period	[s]
σ_{step}	Step function	[-]

1. Introduction

Norway has a responsibility to reduce greenhouse gas emissions through set climate goals. Some of these goals are listed below. [1]

i. Norway is, by the Paris Agreement, obligated to reduce greenhouse gas emissions by at least 50 % compared to a 1990-level by 2030.
ii. Norway shall be climate neutral within 2030.
iii. Norway has a statutory goal to be a low-carbon society within 2030.

These goals are a call for action for the Government, industry, and academia.

The Norwegian Government presented its offshore wind initiative in February 2022 [2]. It was announced that 1 500 MW of bottom fixed offshore wind turbines are planned for in the field Sørlige Nordsjø II. The Federation of Norwegian Industries requested clarifications of the framework and the licensing process for offshore wind and urged the Government to speed up the process to facilitate for the offshore wind expansion [3]. On the 11th of May 2022, the Norwegian Government presented new ambitions for offshore wind in Norway [4]. The ambition included that within 2040, areas equalling 30 000 MW of offshore wind shall be awarded. The Norwegian Government aims to perform the next round of license awarding within 2025. Regarding hydrogen, more specific examples show the Norwegian Government's initiative. Three hydrogen-related projects from Tizir, Horisont Energi, and Yara are given funds of in total of one billion NOK [5].

In a time of conflict, energy security and cost have been raised as critical issues in the European Union. The Commission President Ursula von der Leyen has stated: "We must become independent from Russian oil, coal, and gas. We simply cannot rely on a supplier who explicitly threatens us. We need to act now to mitigate the impact of rising energy prices, diversify our gas supply for next winter and accelerate the clean energy transition. The quicker we switch to renewables and hydrogen, combined with more energy efficiency, the quicker we will be truly independent and master our energy system…" [6]. The means of storing energy in a future renewable energy mix is vital to the future grid stability [7], in which hydrogen can play its part.

UNITECH Zefyros is the world's first *floating offshore wind turbine*, FOWT. It was installed west of Karmøy, at the METCENTRE, in 2009 as Hywind Demo by Equinor [8] In 2019, UNITECH Offshore A/S purchased the turbine. It is still in production and is also used as a test infrastructure for research projects, technology development, and training [9]. Zefyros is made available as a test infrastructure for third parties through Sustainable Energy Catapult, a part of the Norwegian Catapult Centre [10]. Zefyros is also used as a hub at the METCENTRE [11], where the TetraSpar turbine is connected by an inter-array cable to Zefyros [12]. In the EU Flagship project [13], a 12 MW floating offshore wind turbine shall be installed at the METCENTRE in 2023. Flagship shall be connected to Zefyros, and the onshore grid, by a 66 kV inter-array cable [14]. Zefyros is equipped with a 2.3 MW turbine model SWT-2.3-82 from Siemens Wind Power. The wind turbine is a standard offshore wind turbine with a reinforced tower and a floater motion control system. Zefyros is a semi-submersible FOWT [15], which will be reviewed later in this thesis. UNITECH Zefyros is shown in Figure 1 [16].

Figure 1: UNITECH Zefyros [16]

Directly coupling offshore wind power with an electrolyser for offshore hydrogen production is not a commercially established method. Several pilot projects are planned to prove this concept [17-22], of which some are planning or considering utilizing an in-turbine electrolyser [19, 20]. By in-turbine electrolysis, it is meant that the electrolyser is installed inside the turbine tower. Integrating electrolysis inside the turbine tower would avoid electrical conversion and transport losses between the wind turbine and the electrolyser. This would increase the energy

efficiency of hydrogen production [19]. An in-turbine electrolyser would also eliminate the need for any potential additional constructions for placing the electrolyser, such as a floating structure close to the turbine.

An in-turbine electrolyser is assumed to be used in case 1 of the thesis. UNITECH has stated constraints regarding the space available inside the turbine tower for the electrolyser and for its location. The space constraints will be shown to lead to an electrolyser with low rated power compared to the rated power of Zefyros. The low rated power of the electrolyser will result in that, in case of any power production from Zefyros, the electrolyser would operate at its rated load. This would not explore the effect of wind power intermittency on a directly coupled electrolyser regarding hydrogen production. For this reason, a second hydrogen production system is proposed where space constraints do not apply.

The second electrolyser will be a part of the large-scale hydrogen production system, which is case 2 of this thesis. It is assumed to have a rated power of 2.3 MW, the same as UNITECH Zefyros. The rated power of the electrolyser in case 2 means that the electrolyser can use all energy converted by Zefyros for hydrogen production. This results in the load profile of the electrolyser being dynamic as it follows the energy converted by Zefyros. In this way, the effect of intermittency and variability from wind power on an electrolyser can be studied.

This thesis aims to review design considerations of offshore hydrogen production by an electrolyser inside the turbine tower of UNITECH Zefyros and the effect a variable power supply would have on an electrolyser. The thesis will review considerations regarding placing an electrolyser in an offshore environment. Below, the research questions this thesis aims to answer are shown.

Q1: Installing an in-turbine electrolyser at UNITECH Zefyros to achieve hydrogen production by water electrolysis. Given the restrictions regarding available space and location in the turbine tower, what is the hydrogen yield, and what special considerations must be made considering its offshore location?

Q2: The effect an intermittent power source has on an electrolyser. How do the intermittent power source, and the wind conditions in this area, influence the energy efficiency of an electrolyser?

2. Background

This chapter aims to introduce the theory used in the thesis to answer the research questions raised in the introduction chapter above. Two hydrogen production systems are proposed to answer the research questions. These are the in-turbine and the large-scale hydrogen production system, listed below as cases 1 and 2, respectively.

i. **Case 1** An in-turbine electrolyser to show the feasibility of hydrogen production at UNITECH Zefyros.
ii. **Case 2** A large-scale hydrogen production system to study how the intermittent power supply from wind power affects an electrolyser.

The components necessary for such hydrogen production systems are presented with relevant theory in the following chapters. This chapter also aims to provide the reader with the information required to understand why hydrogen can be used as a medium for energy storage and why offshore wind may be a suitable candidate for hydrogen production.

2.1. Hydrogen energy storage from offshore wind turbines

Hydrogen is the smallest, lightest, and simplest element made up of one electron and the nucleus consisting of one proton. Hydrogen is the most abundant element in the universe, accounting for 75 % of the known mass of the universe [23]. Hydrogen atoms are reactive and can be combined with many elements to form many different compounds, including most biological and organic compounds such as hydrocarbons, polymers, proteins, and DNA. When two hydrogen atoms combine, they form a stable molecule, H_2 [23]. Among the many interesting properties of hydrogen is its use as an energy carrier. Hydrogen does not exist naturally on its own in large quantities on the Earth. Hydrogen has to be separated from compounds such as water or hydrocarbons, which is why hydrogen is an energy carrier, not an energy source [24].

Hydrogen can be separated from water by electrolysis, where the water molecule is split into hydrogen and oxygen. Electrolysis uses electrical energy for the water-splitting process, making hydrogen suitable as energy storage for renewable energy sources. For example, electrical energy from wind turbines or solar power can be converted into chemical energy in the form of hydrogen. To convert the chemical energy in hydrogen, one may combust the hydrogen directly or mix the hydrogen with other compounds like natural gas. It is also possible to convert the chemical energy in hydrogen to electrical energy by using a *fuel cell*, FC. [23]

Wind is air set in motion by pressure differences across the Earth's surface due to uneven heating by solar radiation. Hot air rises in the atmosphere while cold air sinks. Variations in heat transfer to the Earth's atmosphere create differences in pressure in the atmosphere, which causes air to flow from high to low pressure. The higher the pressure gradient, the higher the wind speed. Different surfaces can influence the wind due to differences in pressure fields, surface roughness, solar radiation, and adsorption [25]. Wind turbines are utilized to convert kinetic energy in the wind to electrical energy. The theoretical power in wind speed, P_{wind}, is given by formula 1.

$$P_{wind} = \frac{1}{2}\,\rho\,A\,u^3 \quad [V] \tag{1}$$

In Figure 2, theoretical power in wind speed through an area A is shown as a function of wind speed, u. It is assumed a density, ρ, of 1.225 kg/m^3 and a rotor with a diameter of 85 m in which the wind blows through.

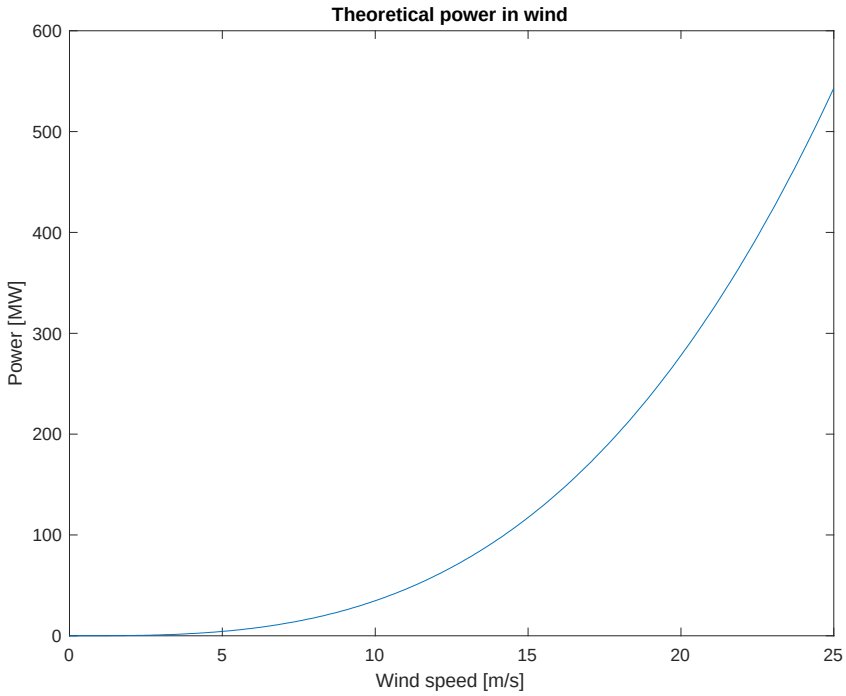

Figure 2: Theoretical power in wind [MW] as a function of wind speed [m/s]

As shown in Figure 2, the power in the wind increases exponentially with the wind speed. This shows the importance of wind speed for energy conversion by wind turbines. Wind speed is one of the reasons why offshore wind farms are emerging around the world [26]; offshore wind resources are generally larger than onshore ones. The main reason is due to the sea's lower surface roughness. However, the surface roughness is not constant. It depends on the wavefield present, which depends on parameters such as the wind speed, fetch, and water depth [27].

Wind speed, in its nature, is intermittent in both time and space [28]. This causes the electrical energy converted by wind turbines to be also highly intermittent. Intermittency is one of the main reasons behind wind power curtailment [28]. Curtailment of wind energy is the reduction in electrical energy conversion from the wind to below what the wind turbines are rated for and represents a loss in revenue and a reduction in energy efficiency [29]. A wind turbine will generate energy if the wind speed is within its operational range. Curtailment may then happen due to transmission congestion or lack of transmission access [30]. The grid must at all times be in balance, meaning the production of energy and the energy usage should be in equilibrium [31]. In areas with high penetration of wind energy in the electricity mix, such as in rural areas in China, curtailment has proven to be a problem [29]. In these areas, the wind curtailment rate, which is the ratio of curtailed electricity to total wind energy generation, typically exceeds 20 % [29]. In 2016 the wind electricity curtailment in China amounted to 49.7 TWh [29]. To put the number into some context, the total Norwegian energy consumption in 2020 was 212 TWh [32].

An offshore wind park whose only purpose is hydrogen production would eliminate the need for an export cable, removing the risk of curtailment [33]. One of the most significant costs associated with a wind farm is the components used to bring the generated electrical energy to shore, namely power cables, transformers, and power electronics [34]. These costs would be eliminated without the use of an export power cable. Subsea hydrogen pipelines, which could be used to transport the hydrogen onshore, have a higher cost per length unit than power cables but also higher energy transmission capacity. Thus, the normalized hydrogen pipeline capital costs are lower. Power cables also have higher transmission losses than hydrogen pipelines [35]. Another solution to the curtailment and intermittency problem is energy storage. In this way, the energy destined to be curtailed now can be stored and later fed into the grid or converted into a new energy carrier. It is possible to convert the hydrogen back to electrical energy using FCs and feed it back to the grid. The hydrogen can be used directly, such as in heating, fuel for hydrogen FC vehicles, or the production of artificial fertilizer [36]. It is also possible to have bunkering stations for potential future maritime vessels utilizing hydrogen as fuel at offshore locations.

It is important to mention the energy loss associated with hydrogen energy storage. To illustrate the energy loss, an electrolyser - fuel cell system is proposed. In such a system, electrical energy is converted to hydrogen using an electrolyser, and converted back into electrical energy using a FC. Values for energy efficiencies for these components vary significantly in the literature depending on the electrolyser and FC technology and if higher or *lower heating value*, LHV, are used. Efficiencies of 50 – 80 % [37-39] and 30 – 70 % [39-41] for electrolysers and FCs, respectively, are to be expected. Using the mean value of the efficiencies, storing 1 MWh of electrical energy as hydrogen, and converting it back to electrical energy would yield 0.325 MWh electrical energy downstream. This energy efficiency value chain of hydrogen storage and conversion is shown in Figure 3, where η represents the components' respective efficiency.

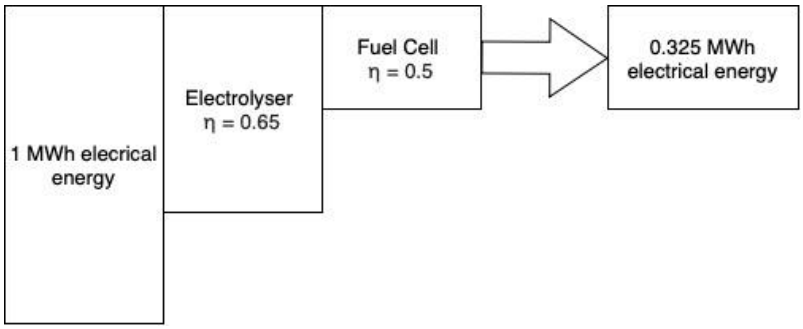

Figure 3: Energy efficiency electrolyser - fuel cell system, η is energy efficiency

Figure 3 shows a graphical representation of the energy losses associated with hydrogen production and the conversion of hydrogen back to electrical energy. The figure only accounts for the electrolysis and fuel cell processes. Cooling, power conversion, post-processing, and other processes would represent further energy losses for the process.

2.1.1. Offshore hydrogen production projects and literature review

This subchapter reviews projects concerning offshore hydrogen production from offshore wind, relevant literature concerning hydrogen production from intermittent power sources, and electrolysis modelling. As mentioned in the introduction, directly coupling offshore wind power with an electrolyser for offshore hydrogen production is not a commercially established method. In the below paragraphs, the projects referred to in the introduction will be reviewed.

The PosHYdon project [21] aims to integrate three energy systems offshore in the North Sea; offshore gas, wind, and hydrogen production. The hydrogen production is from seawater electrolysis and is planned to be located on Neptune Energy's oil and gas platform. [19, 21]

Deep Purple [17] is TechnipFMC's offshore hydrogen production initiative. The Deep Purple system is currently undergoing testing at a land-based location, where the electrolyser load is simulated to equal a wind turbine's power generation. For the offshore hydrogen production, electrolysis of desalinated water is planned. The hydrogen is transported to the seabed, where it is stored under pressure in pressure vessels. During periods of no or low energy generation from the wind turbines, fuel cells will convert the hydrogen back to electrical energy to satisfy the energy demand on the grid. [22]

Lhyfe and Central Nantes plan to install a platform for hydrogen production by electrolysis at the SEM-REV offshore test site [18, 42]. The hydrogen shall be transported onshore, and the oxygen is planned to be reinjected into aquatic ecosystems.

Siemens Gamesa is adapting the FOWT SG14-222 DD to integrate an electrolysis system into its operation [20]. They state on their website, "A modular approach ensures a scalable offshore wind-to-hydrogen solution. Siemens Energy is developing a new electrolysis product that meets the needs of the harsh maritime offshore environment and is in perfect sync with the wind turbine" [20], referring to an in-turbine electrolyser.

In the below paragraphs, research articles that are found to be relevant and have methods and theory applicable to this thesis are presented.

The journal article "Hydrogen production with sea water electrolysis using Norwegian offshore wind energy potentials", K. Meier [33] studies the possibility of hydrogen production at an offshore platform in Norway. In the study, *Solid Oxide Electrolysis Cell*, SOEC, and *Proton Exchange Membrane*, PEM, electrolysis are compared. The economics of the concept is also studied. Results show that 35 % of the total available energy is consumed by the SOEC's auxiliary systems, while the PEM electrolyser's auxiliary system consumes 3 %. The energy efficiency and the amount of hydrogen produced from the SOEC and PEM electrolysers were found to be similar. The concept was found not to be profitable for both SOEC and PEM electrolysis; however, large-scale hydrogen production on an offshore platform was found to be technologically feasible. [33]

The article “Hydrogen Production from Offshore Wind Parks: Current Situation and Future Perspectives”, G. Calado and R. Castro [34] aims to discuss and outline the main features of the integration of hydrogen in offshore wind power and to review the literature on the current state of hydrogen production from offshore wind. The journal article concludes that two hydrogen production systems from offshore wind are currently proposed. This is by offshore or onshore electrolysis. Offshore electrolysis’ advantages include reduced cost of energy transport and reduced transmission losses. Onshore electrolysis’ main advantage is the increased flexibility in the form of facilitating for both hydrogen and electricity sale. The article also concluded that literature shows that costs for green hydrogen production are decreasing. [34]

“Dynamic hydrogen production from PV & wind direct electricity supply – Modeling and techno-economic assessment”, C. Schnuelle, T. Wassermann, D. Fuhrlaender, and E. Zondervan [43] present mathematical models for an *Alkaline Electrolyser*, AE, and a PEM electrolyser coupled with wind and solar power. Hydrogen production, efficiency, and costs are subjects studied in this article. Results show that the AE is preferable from an economic point of view regarding hydrogen production with a directly coupled renewable power source. The PEM electrolyser was found to be more responsive to load changes and offers advantages in terms of load response. [43]

Several research articles on the dynamic modelling of electrolysers have been found [44-47]. These articles all include the estimation of energy efficiency by estimating the cell voltage through a series of formulas. The referred articles [44-47] have inspired the model of this thesis.

2.2. Wind turbine

As previously mentioned, the purpose of a wind turbine is to convert the kinetic energy in the wind to electrical energy. In this chapter, the main components of a wind turbine are to be reviewed. These components are shown in Figure 4.

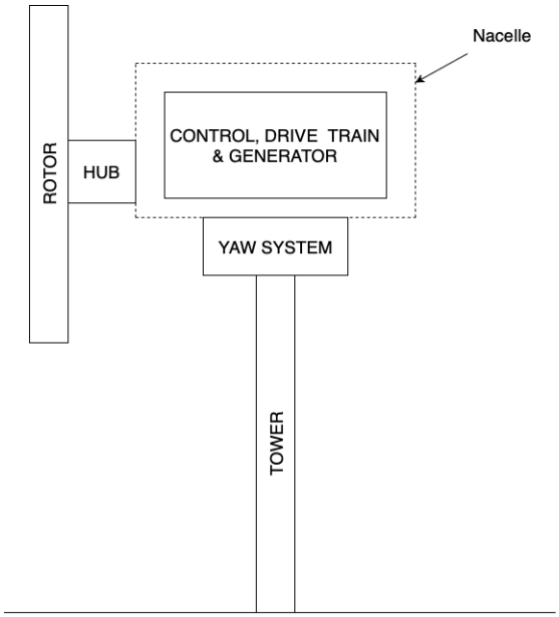

Figure 4: Components of a wind turbine

The rotor converts kinetic energy from the wind into mechanical energy, turning a shaft. The rotor consists of blades, which are connected to a hub. Most turbines today have three blades, based on the Danish design [25]. The nacelle houses the drive train, the generator, and control systems. The drive train may consist of a single shaft or a low-speed shaft, a gearbox, and a high-speed shaft. The generator's purpose is to convert the mechanical energy from the shaft to electrical energy [25]. A yaw system is required to keep the rotor aligned with the wind direction. An active yaw drive contains motors, allowing the nacelle to face the main wind direction. The yaw system is normally controlled by a controller with input from wind measurements from a sensor mounted on the nacelle [25]. The wind turbine tower is the structure to which the nacelle is connected to the ground level.

For the fundament of offshore and onshore wind turbines differ. Offshore wind turbines include bottom fixed wind turbines and *floating offshore wind turbines*, FOWTs. Existing installed offshore wind turbines are mainly wind turbines with bottom fixed foundations such as gravity base, monopile, tripod, and jacket foundations [25, 48]. Bottom fixed wind turbines are utilized

at relatively shallow water depths of less than 50 m [48]. For water depths exceeding 50 m, it is no longer economically viable to utilize bottom fixed wind turbines. Floating installations with a mooring system anchored to the seabed allow offshore wind installations to exceed 50 m water depths. The floating structure must provide sufficient buoyancy to support the weight of the installation and restrain roll, pitch and heave motions from environmental effects [48]. FOWTs foundations include, among others, semi-submersible platforms, spar buoys, and tension leg platforms [48]. However, as FOWTs are receiving increased attention, new concepts for FOWTs foundations are being proposed [49, 50].

2.2.1. Power from wind turbines

The theoretical power convertible from wind is shown in formula 1. For a wind turbine, energy losses and aerodynamic loads must be included in the formula, shown in formula 2 as P_{WT}.

$$P_{WT} = \frac{1}{2}\,\rho\,A\,u^3\,C_p\,\eta_{mech} \quad [W] \tag{2}$$

Where ρ is the air's density, A is the rotor area, u is the wind speed, C_p is the power coefficient, and η_{mech} is the overall efficiency of the wind turbine. The mechanical efficiency η_{mech} represents energy losses from mechanical components in the wind turbine, such as energy losses from the driveshaft and generator as heat [25]. The power coefficient C_p can be derived from 1-D momentum theory, explained in [25]. Here C_p is given by formula 3.

$$C_p = 4a(1 - a^2) \tag{3}$$

Where a is the axial induction factor, given in formula 4.

$$a = \frac{u_1 - u_2}{u_1} \tag{4}$$

Where u_1 is the wind speed far enough away from the rotor such that it is unaffected by the wind turbine. u_2 is the wind speed at the rotor plane. The maximum C_p can be calculated by taking the derivative of formula 4 and setting it equal to zero. The result is shown in formula 5.

$$C_{p_{max}} = \frac{16}{27} \tag{5}$$

This is known as Betz' limit, which states that at maximum $\frac{16}{27}$ of the power in the wind is extractable by a wind turbine. [25]

Every wind turbine has a power curve associated with its generator, in which the power output is presented as a function of wind speed. In Figure 5, measurements from Zefyros are used to show Zefyros' power curve.

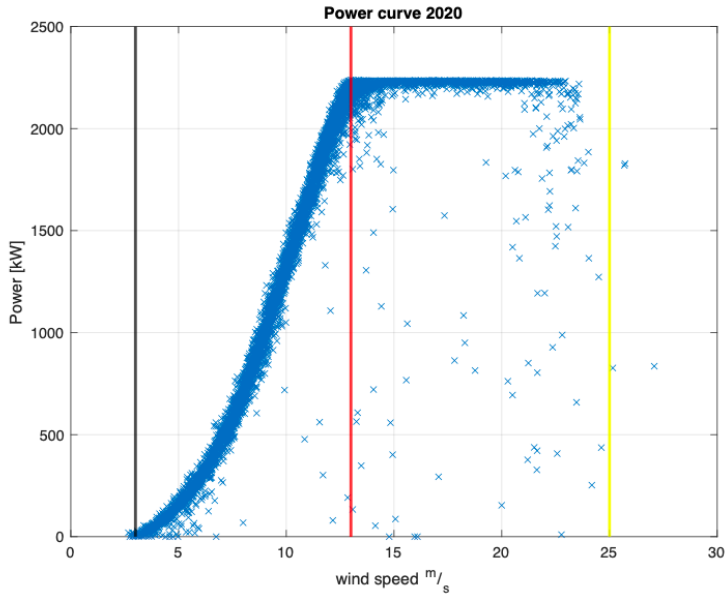

Figure 5: UNITECH Zefyros' power curve [MW], black line represents cut-in wind speed, red rated wind speed, and yellow cut-off wind speed [m/s]

As shown in Figure 5, the power output from the wind turbine increases exponentially with wind speed between the cut-in wind speed and the rated wind speed. When wind speed reaches rated wind speed and above, the power output is constant until cut-off wind speed. This is done to reduce aerodynamic loads that may inflict damage to the wind turbine and is done by rotating or feathering the rotor blades to decrease their surface area [51]. The cut-off wind speed eventually stops the rotor when the wind speeds are too high for feathering to help reduce loads. The cut-off wind speed shown in Figure 5 is stated by the specifications of a standard Siemens SWT-2.3-82 wind turbine generator to be 25 m/s [52]. Figure 5 shows that the turbine shuts down prior to its cut-off wind speed. This may be because the cut-off wind speed is altered for the offshore environment existing at Zefyros. The power curve in Figure 5 is unfiltered, such that some samples deviate from the dense part of the curve. These samples are few in the dataset of 46157 samples [53], such that the power curve is assumed to be the part of the figure with the densest population of measurement samples.

2.3. Hydrodynamics

This chapter, a review of the hydrodynamic response of UNITECH Zefyros is performed, and formulas used for estimating the response are presented. Any floating structure in the sea will experience motion due to relevant sea conditions such as waves, current, and wind, where the motion is defined in the degrees of freedom, shown in Table 1 [54].

Table 1: Definition of the degrees of freedom [54]

Degree of freedom	Description
Surge	Translation along the longitudinal axis, the main wind direction, x-axis
Sway	Translation along the lateral axis, normal to the main wind direction y-axis
Heave	Translation along the vertical axis, z-axis
Roll	Rotation about the x-axis
Pitch	Rotation about the y-axis
Yaw	Rotation about the z-axis

The coordinate system used for the definition in Table 1 is shown in Figure 6.

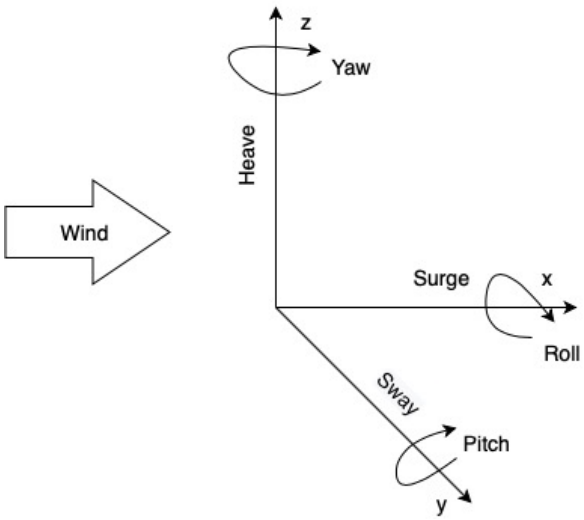

Figure 6: Degrees of freedom

Zefyros has a spar buoy foundation. The spar buoy is a gravity stabilized structure with a very large draft; the draft of Zefyros is 100 m. The large draft results in the spar buoy foundation usually having good stability and experiencing small heave motions. The deep draft also makes the construction less affected by wind, waves, and current [54].

Waves can be generated in many ways. A single mathematical solution for all problems related to the different types of waves does not exist; approximations are required. Limitations and simplifications are important to be aware of, especially for nonlinear effects. Wind-generated waves can be classified into two categories, surface waves and swell. Surface waves are a chain

of waves driven by the local wind field. They are short-crested and highly irregular; tall waves are followed by unpredictably low waves and vice versa [55]. Swell is waves that have propagated out from an area and the local wind in which they were generated [55]. They are no longer dependent on the wind to propagate. Individual waves are more regular, the crest is more rounded compared to surface waves, and the length of the crests is also longer. The wave height is more predictable [55]. Although both types of waves mentioned above are irregular to different degrees, they can be seen as a superposition of many simple regular and harmonic wave components, each with its amplitude, length, frequency or period, and direction of propagation. The harmonic components, such as the relation between wave period and wavelength, the phase difference, are necessary to analyse wave systems' properties. [55]

A wave can be described through potential theory. In the potential theory, the basic assumption is that the fluid is incompressible, inviscid, and irrotational [54]. A regular wave is represented by a sine or cosine wave, shown in Figure 7, extracted from [55].

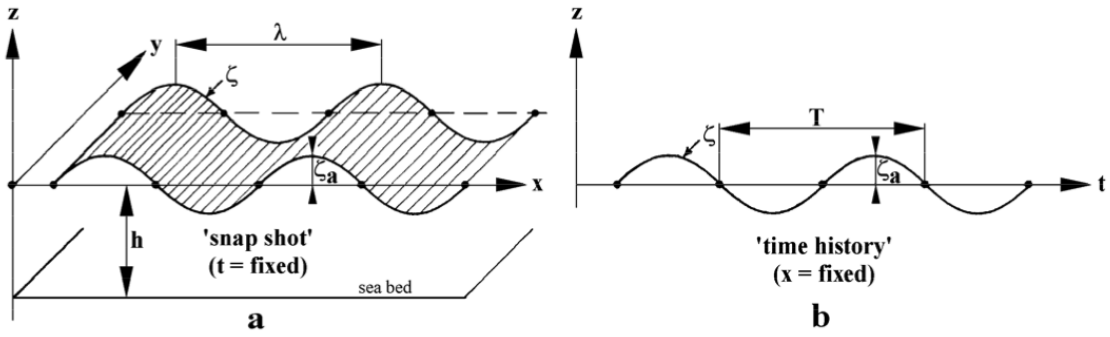

Figure 7: A periodic wave as shown from different perspectives. a: time is fixed, b: position is fixed [55]

Waves change in both time and space, which is why the two perspectives in Figure 7 are mentioned. In the figure, the z-coordinate is directed upwards, the water depth h is measured from still water level to the seabed, ξ_a is the wave amplitude, T_{wave} is the wave period, λ is the wavelength, and ξ is the wave surface elevation. Sine and cosine waves are expressed in terms of angular arguments; hence, the wavelength and period are converted into angles using formulas 6 and 7. [55]

$$k = \frac{2\pi}{\lambda} \quad \left[\frac{rad}{m}\right] \tag{6}$$

$$\omega = \frac{2\pi}{T_{wave}} \quad \left[\frac{rad}{s}\right] \tag{7}$$

Where k is the wavenumber and ω is the wave frequency. If the wave moves in the positive x-direction, the wave surface elevation of a regular wave can be expressed as a function of space and time, x and t, shown in formula 8.

$$\xi = \xi_a \cos(kx - \omega t) \tag{8}$$

Irregular waves can be expressed using a linear superposition of wave components. In Figure 8, extracted from [55], this is shown by the sum of two waves.

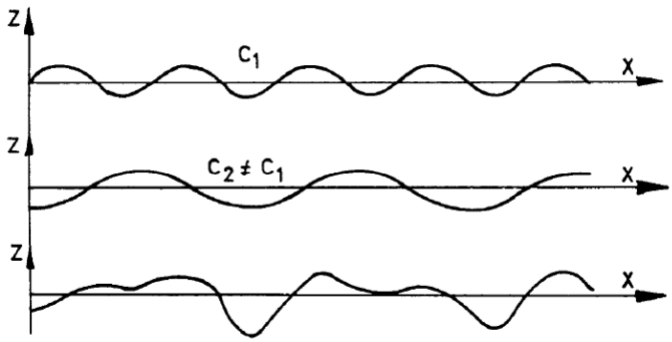

Figure 8: Superposition of two periodic waves propagating in the same direction [55]

Irregular waves can be described as a sum of several periodic wave components in a Fourier series, shown in formula 9. [55, 56]

$$\xi(t) = \sum_{n=1}^{N} \xi_{a_n} \cos(k_n x - \omega_n t + \varepsilon_n) \tag{9}$$

Where ε_n is a random phase angle component and n is the number of the wave in the set of waves N. A common representation to describe the sea over time is to use significant wave height H_s. H_s is given by the average wave height of the highest third of individual waves over a given period, seen in formula 10. [55, 56]

$$H_s = \frac{1}{\frac{N}{3}} \sum_{j=1}^{N/3} H_j \quad [m] \tag{10}$$

Where j is the ranking of the largest wave heights, where 1 is the largest, 2 is the next largest, and so on. A series of wave profiles can be analysed statistically by a Gaussian or normal distribution [55]. This normal distribution, if the water level has a mean value equal to zero, still water level, is given by formula 11.

$$f(x) = \frac{1}{\sigma\sqrt{2\pi}} \exp\left[-\left(\frac{x}{\sigma\sqrt{2}}\right)^2\right] \tag{11}$$

Where x is the variable being studied and σ its standard deviation. With this distribution, the probability that the wave surface elevation ξ exceeds a threshold b is given by formula 12.

$$P\{\xi > b\} = \int_b^\infty f(x)\,dx = \frac{1}{\sigma\sqrt{2\pi}} \int_b^\infty \exp\left[-\left(\frac{x}{\sigma\sqrt{2}}\right)^2\right] dx \tag{12}$$

If the range of frequencies of the series of wave profiles is not too long, it becomes a narrow banded frequency spectrum [55]. This is the case for most waves, both surface waves and swell [55]. If this is the case, and the wave surface elevation is assumed to be normally distributed, then the wave amplitude statistics will obey a Rayleigh distribution. A wave spectrum is used to describe the sea's stochastic behaviour. The wave spectrum shows the wave's energy that occurs at different frequencies. The wave amplitude of the irregular wave, ξ_{a_n}, can be expressed in a wave spectrum $S_\xi(\omega_n)$, as shown in formula 13. [55, 57]

$$\sum_{n=1}^{N} S_\xi(\omega_n) \cdot \Delta\omega = \sum_{n=1}^{N} \frac{1}{2}\xi_{a_n}^2(\omega) \tag{13}$$

Where $\Delta\omega$ is the difference between two successive frequencies, multiplying this formula with $\rho\ g$, the density of the seawater and the gravitational constant, yields the energy per unit area of the waves in the frequency interval $\Delta\omega$, shown in Figure 9 extracted from [55].

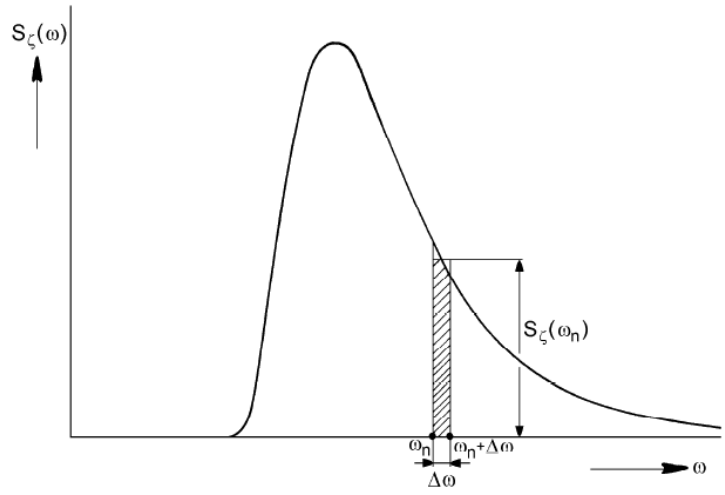

Figure 9: Wave energy density spectrum [55]

It has been attempted to describe irregular seas in a standard form, such as the Bretschneider and JONSWAP wave spectrums [55]. In this thesis, the JONSWAP wave spectrum is utilized. JONSWAP, Joint North Sea Wave Project, was an extensive wave measurement program carried out at the North Sea [55]. The JONSWAP wave spectrum is given in formula 14.

$$S_{\xi}(\omega_n) = \frac{320 \cdot H_s^2}{T_p^4} \cdot \omega^{-5} \cdot \exp\left(\frac{-1950}{T_p^4} \cdot \omega^{-4}\right) \cdot 3{,}3^{A} \tag{14}$$

Where T_p is the peak period of the spectral peak. A is given by formula 15, and ω_p the frequency at spectral peak is given by formula 16. σ_{step} is a step function of ω. σ_{step} changes if the wave frequency is larger than the frequency at spectral peak, 0.09, or not, 0.07. [55]

$$A = \exp\left[-\left(\frac{\frac{\omega}{\omega_p} - 1}{\sigma_{step}\sqrt{2}}\right)^2\right] \tag{15}$$

$$\omega_p = \frac{2\pi}{T_p} \left[\frac{rad}{s}\right] \tag{16}$$

Short-term statistics are used to calculate the response of Zefyros. The basis of calculating such a response is the transfer function of that response [55]. The transfer function of the response can be derived from the energy density of the response. Short-term statistics are a sea state registration over a relatively short time interval, three to six hours [56]. Inside this time interval, the sea state is assumed to be stationary. Assuming a normal distributed incoming wavefield and a Rayleigh distributed wave amplitude, the structure's response amplitudes can be approximated to be Rayleigh distributed [55]. The short-term Rayleigh distributed probability density function of the structure's response is given by formula 17. [55]

$$f_{ST}(R_a) = \frac{R_a}{m_{0R}} \cdot \exp\left(-\frac{R_a^2}{2m_{0R}}\right) \tag{17}$$

Where m_{0R} is defined as the area below the response spectrum and R_a is the response amplitude being studied.

2.4. Hydrogen production

In this chapter, methods of producing hydrogen will be reviewed. Different electrolyser technologies will be reviewed, and the choice of electrolyser will be made for the hydrogen production systems for cases 1 and 2. The chosen desalination technology to provide the electrolyser with water with sufficient purity is presented.

The most common method for hydrogen production today is steam reforming. It is estimated that 68 % of the world's hydrogen production comes from this process [58]. Hydrocarbons in natural gas react with steam in the presence of a nickel catalyst at a high temperature, 500 – 1100 ℃, and a pressure of 0.3 – 2.5 MPa [59]. Hydrogen, carbon monoxide, and carbon dioxide are released. This is shown in formula 18.

$$CH_4 + H_2O \rightarrow CO + 3H_2 \tag{18}$$

The steam reforming process includes emissions of around 7 kg CO_2/kg H_2 and has an energy efficiency of about 80 % [60]. Hydrogen can also be produced by water electrolysis. Here, water in its liquid or vapor form can be dissociated into its elemental components, molecular oxygen and hydrogen. This is shown in formula 19 [61]. The electrolysis process is powered by electrical energy, so the emissions from this process depend on the emissions included in the electrical energy used.

$$H_2O \rightarrow H_2(g) + \frac{1}{2}O_2(g) \tag{19}$$

An electrolytic cell consists of two electrodes placed face to face, separated by a thin membrane layer. In an electrolytic cell, electrical energy is provided from an external power source to split water molecules into gaseous hydrogen and oxygen. Half-cell reactions depend on the electrolyser technology utilized [61]. An electrolyser consists of multiple cells put together in stacks. By combining cells and stacks, the hydrogen output can be modified [39].

Electrolyser technologies are differentiated by their operating temperature, low- or high-temperature, and by their electrolyte. Low-temperature electrolysers include, among others, *Proton Exchange Membrane*, PEM, electrolysis, *Alkaline Electrolysis*, AE, and *Anion Exchange Membrane*, AEM, electrolysis. The electrolysis technologies mentioned above are differentiated by their electrolyte, proton exchange membrane, potassium hydroxide, and polymer membrane, respectively [39]. These electrolyser technologies have an operating temperature of 60 – 80 ℃. High-temperature electrolysers include, among others, *Solid Oxide*

Electrolyser Cell, SOEC, with an oxide ceramic electrolyte and an operating temperature of 700 – 900 ℃ [39]. The mentioned electrolysis technologies, the AE, PEM electrolyser, the AEM electrolyser, and the SOEC will be reviewed in the following subchapters.

2.4.1. Proton Exchange Membrane

The Proton Exchange Membrane, PEM, electrolytic cell consists of two electrodes, a solid electrolyte, circulating deionized water, a power supply, and a membrane of proton-conducting polymer electrolyte, often manufactured by Nafion® [62]. The membrane carries ionic charges and separates electrolysis products, preventing recombination into water. The electrolysis process also requires electrical energy through a potential difference between the electrodes [61]. During electrolysis, the following half-cell reactions occur for the anode and the cathode in formulas 20 and 21, respectively. [62]

$$H_2O(l) \rightarrow \frac{1}{2}O_2(g) + 2H^+ + 2e^- \tag{20}$$

$$2H^+ + 2e^- \rightarrow H_2(g) \tag{21}$$

PEM electrolysers can operate at a high current density due to a smaller area of the electrolyte [62]. In electrochemistry, current density, i, is defined as electrical current through an element, I, divided by the cell area, A_{cell} [63]. This is given in formula 22.

$$i = \frac{I}{A_{cell}} \quad \left[\frac{A}{cm^2}\right] \tag{22}$$

The high current density reduces operational costs and potentially the overall cost of electrolysis [62]. The low gas crossover rate of the proton exchange membrane yields hydrogen with high purity and allows the PEM electrolyser to operate under a wide range of power inputs. This is because the proton transport across the membrane responds rapidly to the power input and is not delayed by inertia, such as in liquid electrolytes. PEM electrolysis covers most of the nominal power density range, 10 – 100 % [62]. The start-up time of PEM electrolysis is approximately 15 minutes [64]. A solid electrolyte allows for a compact design with good structural properties and high operational pressures, yielding high-pressure hydrogen downstream. For context, the electrolyser manufacturer NEL states a delivery pressure of hydrogen up to 30 bar from their PEM electrolyser line-up [65]. The higher pressure delivered hydrogen leads to less required energy consumption in case of further compression.

Problems related to the high operational pressure also exist. Cross-permeation, the risk of permeation of hydrogen to oxygen side and vice versa, increases with pressure. Hydrogen and oxygen produced at both sides of the electrode permeate through the PEM and mix. This mixing increases the risk of gas explosion and decreases the overall efficiency of the electrolysis cell [66]. The corrosive, acidic environment caused by the PEM requires the use of distinct materials. These materials must resist harsh corrosive conditions and sustain high applied voltage. This is true for components such as the catalyst and the separator plates. Only a few materials are applicable: platinum group metals, such as platinum, iridium, ruthenium, and titanium-based separator plates. These materials are costly and will result in high CAPEX for the PEM electrolyser [62]. In subchapter 2.5.1, a more comprehensive review of the PEM electrolyser design is presented.

2.4.2. Alkaline Electrolyser

The Alkaline Electrolyser, AE, consists of two electrodes, a liquid electrolyte, a membrane, and a power supply. In an AE, the electrodes are immersed in liquid potassium hydroxide, the electrolyte. A porous solid material, the membrane placed between the electrodes, allows transport of hydroxyl ions (OH^-) between the electrodes and, due to the low permeability of oxygen and hydrogen, restricts transport of the mentioned gases. The AE electrolysis process requires electrical energy through a potential difference between the two electrodes [61]. When a sufficient difference of potential between the electrodes is reached, reduction and oxidation reactions occur simultaneously at the anode and cathode shown in formulas 23 and 24, respectively. [61]

$$4OH^- \rightarrow O_2 + 2H_2O + 4e^- \quad (23)$$

$$4H_2O + 4e^- \rightarrow 2H_2 + 4OH^- \quad (24)$$

The main advantage of AE is that it can be made of abundant and inexpensive materials; simple iron or nickel steel electrodes are used to produce hydrogen and nickel for oxygen production [62]. Disadvantages associated with AE include low operating pressure, load range, and limited current density. The start-up time of an AE is about one hour [64]. Due to the liquid electrolyte of AE when operating at a low load, less than 40 % of rated power [62], the rate of hydrogen and oxygen production reduces while the hydrogen permeability through the diaphragm remains constant. This yields a higher concentration of hydrogen at the anode, or oxygen side, creating a hazardous environment. The AE has low achievable current densities due to high

ohmic losses across the electrolyte and membrane. The liquid electrolyte results in an inability to operate at high pressure. [62]

2.4.3. Anion Exchange Membrane

Anion Exchange Membrane, AEM, electrolysis is the electrochemical splitting of water into oxygen and hydrogen utilizing an AEM. Electrical energy is required for the electrolysis process. The overall reaction consists of two half-reactions, the *Oxygen Evolution Reaction*, OER, and *Hydrogen Evolution Reaction*, HER. Water is circulated from the anode side to the cathode side through the membrane, where it is reduced to form hydrogen and hydroxyl ions, OH^-. The hydroxyl ions diffuse through the membrane to the anode side, recombining as water and oxygen. The OER and HER reactions are presented in formulas 25 and 26, respectively. [67]

$$4OH^- \rightarrow O_2 + 2H_2O + 4e^- \quad (25)$$

$$4H_2O + 4e^- \rightarrow 2H_2 + 4OH^- \quad (26)$$

The main difference between PEM and AEM electrolysis is the replacement of the proton exchange membrane with an anion exchange membrane. A transition metal catalyst can be utilized in an AEM electrolyser, making the materials used in the membrane for an AEM cheaper than in a PEM [67]. In an AEM electrolyser, distilled water or a low concentration of an alkaline solution can be used as an electrolyte. [67]

2.4.4. Solid Oxide Electrolysis Cell

High-temperature electrolysis of steam with an operating temperature of 700 – 900 °C may be performed using a Solid Oxide Electrolysis Cell, SOEC. The SOEC consists of an anode and a cathode separated by a dense ionic conducting electrolyte. Steam is fed to the cathode side of the SOEC, where it is reduced to H_2. Oxide ions, O^{2-}, pass through the electrolyte to the anode, where they recombine into oxygen, releasing two electrons. This is shown for the anode and cathode in formulas 27 and 28, respectively. [68, 69]

$$H_2O + 2e^- \rightarrow H_2 + O^{2-} \quad (27)$$

$$O^{2-} \rightarrow \frac{1}{2}O_2 + 2e^- \quad (28)$$

The electrical energy demand for high-temperature electrolysis is lower than low-temperature electrolysis due to the high operating temperature. This is shown in Figure 10, extracted from [70].

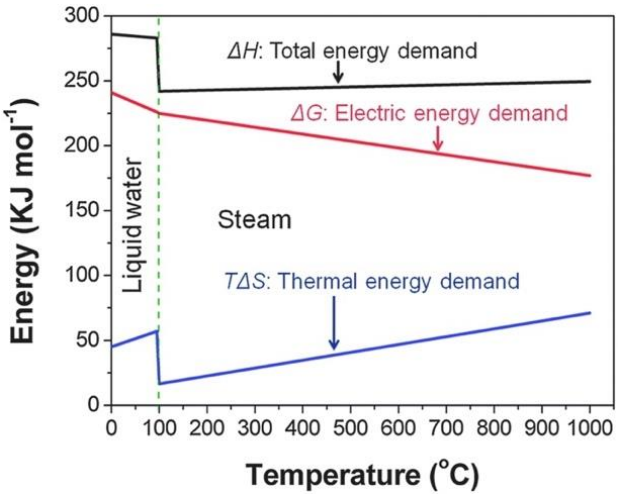

Figure 10: Total ΔH, Electrical ΔG. and Thermal $T\Delta S$ energy demand [kJ/mol] as a function of operating temperature [°C]. *Collected from [70]*

Figure 10 shows that the electrical energy required for electrolysis decreases with increasing temperature while the thermal energy demand increases. If utilizing waste heat from nearby exothermal processes, the energy efficiency of the SOEC can reach 95 % using hydrogen's higher heating value [68].

The SOEC is in a research and development stage, but research and attention have increased rapidly over the last years, reaching advanced stages [39]. Bosch is planning for Solid Oxide Fuel Cell commercialization in 2024 [71]. The durability of the ceramic catalyst at high temperatures and long-term operation remains a problem to be solved. [62]

2.4.5. Electrolyser choice for offshore hydrogen production

This subchapter will assess the reviewed electrolyser technologies to find the optimal technology for use in offshore hydrogen production coupled with wind power. In Table 2, what is deemed as the advantages and disadvantages of the reviewed electrolyser technologies are presented and compared.

Table 2: Comparison of electrolyser technologies [62, 67, 69]

AE	PEM Electrolysis	AEM Electrolysis	SOEC
Advantages			
Well established technology	High current densities and voltage efficiency	Non-noble metal catalyst	Non-noble catalyst
Relatively low cost and cost effective	Rapid system response and good partial load range	Non-corrosive electrolyte	High efficiency
Non-noble catalysts	Dynamic operation	Low cost	Syngas (CO) production
MW range stacks	High gas purity	High operating pressure	Waste heat utilization
Long-term stability	Compact system design	Compact system design	
Disadvantages			
Low current densities, partial load range and dynamics	High cost of components	Laboratory stage	Laboratory stage
Low operational pressure	Stacks below MW range	Low current density	Durability

The SOEC and AEM are not seen as feasible due to the market state of the technologies. Furthermore for the SOEC, there is no supply of waste heat at Zefyros, and a steam production process at the turbine would further complicate and enlarge the system [67]. The AE cannot operate below a specific load, typically 20 – 40 % of the nominal load, for safety reasons. This constraint does not apply to the PEM electrolyser [62, 72]. Also, the AE has a liquid electrolyte, potassium hydroxide KOH [62]. Since Zefyros is in constant motion in the six degrees of freedom, it is uncertain how this would affect the AE and its liquid electrolyte. Also, the AE electrolysis requires a larger area than PEM electrolysis [73]. The intermittency of wind power would result in frequent load changes of the electrolyser. Considering the longer start-up time of AE electrolysis compared to PEM electrolysis [64], PEM electrolysis is seen as the most promising option for electrolysis technology for the proposed hydrogen production system, and is assumed to be used in the hydrogen production system of cases 1 and 2.

2.4.6. Desalination

PEM electrolysers require fresh water for the electrochemical splitting of the water molecule. At an offshore location, seawater is readily available. Hence, desalination and seawater purification result in an inexhaustible supply of feedwater to the electrolyser. Two primary technologies of desalination exist, thermal and pressure operated. In this thesis, the pressure-driven technology *reverse osmosis*, RO, is chosen because it is the most available and developed technology [73]. RO desalination utilizes the osmotic principle, where two solutions have different concentrations of salt particles and are separated by a membrane that only allows for the salt-free solvent to pass through. The clean solvent will flow from the side with the lowest concentration of salt particles to the membrane and into the side with the highest salt particle concentration. The salt concentration will eventually reach equilibrium for the sides. By applying external pressure, this process is reversed. This way, freshwater is produced on one side and concentrated seawater brine on the other side. Before the seawater is fed through the membrane, it must be pre-processed by filtration and by adding chemicals [73]. RO desalination can be done in multiple steps to increase water purity. 1-step RO desalination yields water with purity 200 – 500 ppm with an energy consumption of 2.5 – 3 kWh/ ton water [73]. 2-step RO desalination yields water with purity < 10 ppm and with an energy consumption of 3.3 – 4 kWh/ton water, which is assumed to be the desalination method used in cases 1 and 2 of this thesis. [73]

2.5. PEM electrolysis design and thermodynamics.

In this chapter, the design of a PEM electrolyser is reviewed, and the electrolyser thermodynamic formulas used in the model of the large-scale electrolyser in case 2 will be presented.

2.5.1. PEM electrolysis design

A PEM electrolyser consists of multiple cells, which form a stack. The main components of a PEM electrolysis cell are the proton exchange membrane, the catalyst layers, the gas diffusion layers, and the bipolar plates [74]. A schematic of a PEM electrolytic cell is shown in Figure 11, where the cell's main components are included. [75, 76]

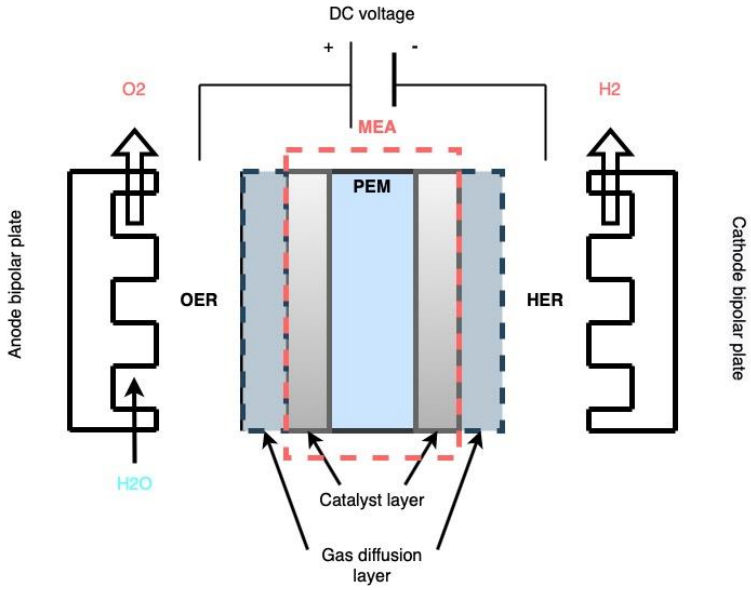

Figure 11: Schematic of a PEM electrolytic cell

The *Membrane Electrode Assembly*, MEA consists of the PEM, an ionomer solution, and the cathode and anode catalysts. Nafion® membranes are the most commonly used membranes due to their ability to operate at higher current densities, 2 A/cm^2, high durability, and high proton conductivity [74]. PEMs are fabricated by different methods; however, the most common is that the catalyst is coated on the membrane. The catalyst decreases the activation energy for the electrolytic process. The ionomer solution improves the proton transport from the electrode layers to the membrane, decreasing the ohmic losses in the cell. It also provides structure to the catalyst layer [74]. The MEA is sandwiched between the gas diffusion layers, which are thin layers of titanium in the shape of foams, felts meshes, or sintered plates [45]. The gas diffusion layers need to be highly conductive. They must operate in the harsh operating conditions of a PEM electrolyser and manage product distribution and transportation [45]. The bipolar plates

are embedded with flow fields that transport the reactants, oxygen and hydrogen, to the membrane electrode and electrolysis products away from the cell [45].

Degradation of a PEM electrolyser is expected, where multiple operating parameters and factors may cause the degradation [45]. Traditionally electrolysis is powered by a constant supply of power. By introducing a variable power supply, for example, by directly coupling the electrolyser with a wind turbine, the electrolytic cell will experience voltage fluctuations, leading to corrosion and durability issues [45]. This is a well-documented phenomenon for the PEM fuel cell technology [77]. Insufficient feed water purity is one of the major contributors to stack degradation in a PEM water electrolyser. Low water purity may lead to an accumulation of impurities, resulting in increased ohmic resistance and degradation, hence increasing the risk of failure [77].

2.5.2. Electrolyser thermodynamics

Electrolysis requires electrical energy to split the water molecule. The minimum theoretical energy for water electrolysis is shown in formula 29. [45, 74]

$$\Delta G = \Delta H - T\Delta S = n\,F\,U_{rev} \quad \left[\frac{J}{mol\ K}\right] \tag{29}$$

Where ΔG is the Gibbs free energy, T is the temperature, ΔS is the change in entropy, ΔH is the change in enthalpy, n is the number of electrons, F is Faraday's constant, and U_{rev} is the reversible voltage. The minimum theoretical energy, ΔG, at *standard temperature and pressure*, STP is 237.2 kJ/mol [45], yielding U_{rev} as shown in formula 30. [74]

$$U_{rev} = \frac{\Delta G}{n\,F} = 1.23 \quad [V] \tag{30}$$

Once the current passes through the cell, the actual voltage for electrolysis increases from the reversible cell potential due to irreversible losses. These irreversible losses are described in the following sections.

Cell voltage

The required formulas for estimating the cell voltage are presented in the following sections. Later, a model will be developed based on these formulas. The proposed model is based on existing models in the literature [44-47, 78-80], and will be presented in chapter 3.1.4.

To estimate the electrolyser efficiency, the cell voltage of the PEM electrolyser cell must be estimated. The cell voltage is represented by the sum of the open circuit voltage and three overpotentials; activation, ohmic, and concentration overpotential. This is shown in formula 31. [47]

$$U_{cell} = U_{OCV} + U_{act} + U_{ohm} + U_{con}\ [V] \tag{31}$$

Open Circuit Voltage U_{OCV}

The *Open Circuit Voltage*, OCV, is the potential between the electrodes in the cell when no current is passing through the circuit. The OCV is given by the sum of the reversible cell voltage and a part that relates to the reactants involved in the electrolysis process. The OCV is given in formula 32. [45]

$$U_{OCV} = U_{rev} + \frac{R\,T_{cell}}{2\,F}\ln\left(\frac{p_{H_2}}{p_{cathode}\sqrt{\frac{p_{O_2}}{p_{anode}}}}\right)\ \ [V] \tag{32}$$

U_{rev} is the reversible cell voltage, R is the universal gas constant, T_{cell} is the cell temperature in Kelvin, p_{H_2} is the hydrogen pressure, $p_{cathode}$ is the pressure at the cathode side, p_{O_2} is the oxygen pressure, and p_{anode} is the pressure at the anode side. The reversible cell voltage can be estimated through a temperature-dependent formula, shown in formula 33. [46]

$$U_{rev} = 1.23 - 0.9 \cdot 10^{-3}(T_{cell} - 298)\ \ [V] \tag{33}$$

The hydrogen pressure is given by the sum of the pressure at the cathode side and the partial increase factor for hydrogen and subtracting the water saturation pressure. This is shown in formula 34. [45, 79]

$$p_{H_2} = p_{cathode} + \gamma_{H_2}\, i - p_{H_2O,sat}\ \ [bar] \tag{34}$$

Where γ_{H_2} is the partial increase factor for hydrogen, i is the current density, and p_{H_2O} is the water saturation pressure. The water saturation pressure can be calculated from formula 35 [47].

$$p_{H_2O,sat} = 10^{A-\frac{B}{C+T_{cell}}}\ \ [bar] \tag{35}$$

Where A, B and C are given parameters. Values for A, B and C with temperature in ℃ and $p_{H_2O,sat}$ in $mm\ Hg$ is given in Table 3 [47].

Table 3: Parameters in formula 35 with temperature in ℃, yielding water saturation pressure in mm Hg [47]

A	**B**	**C**
8.07131	1730.63	233.426

The partial pressure increase factor for hydrogen, γ_{H_2}, is dependent on the type of catalyst. For a Pt/C catalyst, platinum on carbon, γ_{H_2} is 2.4 $\frac{bar\ cm^2}{A}$ [45]. The oxygen pressure, p_{O_2}, is given by formula 36. [45, 79]

$$p_{O_2} = p_{anode} + \gamma_{O_2}\, i - p_{H_2O,sat} \quad [bar] \tag{36}$$

Where γ_{O_2} is the partial pressure increase factor for oxygen which again is determined by the type of catalyst. Assuming the cathodic and anode catalyst layers have similar thickness and structure, γ_{O_2} at the anode is expressed as shown in formula 37. [79]

$$\gamma_{O_2} = \frac{\varepsilon_{H_2}^{Fick}}{\varepsilon_{O_2}^{Fick}} \frac{\gamma_{H_2}}{2} \quad \left[\frac{bar\ cm^2}{A}\right] \tag{37}$$

Here, ε^{Fick} is the diffusity for Nafion® membranes. [45]

Activation overpotential U_{act}

The activation overpotential, U_{act}, represents the kinetic electrochemical behaviour and describes an energetic barrier that must be surpassed to start the electrochemical reactions at the electrodes. Some of the applied voltage is lost in transferring electrons to or from the electrodes. The activation overpotential for the electrolysis cell is given by the sum of the anode and cathode overpotential, shown in formula 38. [44, 45]

$$U_{act} = U_{act,anode} + U_{act,cathode} \quad [V] \tag{38}$$

The anode and cathode overpotentials are given in formulas 39 and 40, respectively.

$$U_{act,anode} = \frac{R\,T}{\alpha_{anode}\,F} \operatorname{arcsinh}\left(\frac{i}{2\,i_{o,ref\ a}}\right) \quad [V] \tag{39}$$

$$U_{act,cathode} = \frac{R\,T}{F} \operatorname{arcsinh}\left(\frac{i}{2\,i_{o,ref\ c}}\right) \quad [V] \tag{40}$$

Where $i_{0,ref}$ is the reference exchange current density of either the anode or cathode and α is the charge transfer coefficient. The anode and cathode exchange current densities are calculated using formula 41. [45]

$$i_{0,a/c} = i_{0,ref\ a/c} \exp\left(\frac{E_{act,a/c}}{R}\left(\frac{1}{T_{ref}} - \frac{1}{T_{cell}}\right)\right) \quad \left[\frac{A}{cm^2}\right] \tag{41}$$

Where T_{ref} is the reference temperature of the electrolysis cell and $E_{act,a/c}$ is the activation energy for the OER or the HER, anode or cathode, respectively. [45]

In Table 4, values that are found in the relevant literature, [44, 81-84], for charge transfer coefficients for anode and cathode and reference exchange current density of the anode and cathode are presented. These values are extracted from [46]. The conceptual basis of the reference charge transfer coefficient α requires a value of less than one for both the anode and cathode [44].

Table 4: Values used for reference exchange densities and charge transfer coefficients in literature [46]

$i_{0,ref\ a}$	$i_{0,ref\ c}$	α_a	α_c	Reference
$1 * 10^{-7}$	$1 * 10^{-1}$	0.8	0.25	[44]
$0.5 * 10^{-3}$	$0.4 * 10^{-6}$	0.5	0.25	[81]
$1 * 10^{-9}$	$1 * 10^{-3}$	0.5	0.5	[82]
$1 * 10^{-7}$	$1 * 10^{-3}$	0.5	0.5	[83]
$2 * 10^{-7}$	$2 * 10^{-3}$	2	0.5	[84]

As can be seen from Table 4, values for the different parameters vary greatly, especially for the reference exchange current densities. Later, in Table 8, chosen parameters for reference exchange densities and charge transfer coefficients will be presented.

Ohmic overpotential U_{ohm}

Ohmic overpotential, U_{ohm}, is related to the material's internal ohmic resistance. The magnitude of U_{ohm} depends on the material's properties [46]. The ohmic overpotential is simplified in this thesis to reduce the number of specific electrolyser design choices. This thesis only accounts for ohmic losses from the membrane. This is a justified assumption because the membrane is the dominant source of resistance in the cell [47]. The simplified formula for ohmic overpotential is shown in formula 42.

$$U_{ohm} = \frac{\delta_{mem}}{\sigma_{mem}}\, i \quad [V] \tag{42}$$

Where δ_{mem} is the membrane thickness, and σ_{mem} is the membrane conductivity. The membrane conductivity can be expressed in an empirical formula for Nafion® membranes, shown in formula 43.

$$\sigma_{mem} = (0.005139\lambda_{mem} - 0.00326)\exp\left(1268\left(\frac{1}{303} - \frac{1}{T_{cell}}\right)\right) \quad \left[\frac{1}{\Omega\ \mathrm{cm}}\right] \tag{43}$$

Where λ_{mem} is the number of molecules per sulphonic group, representing the water content in the membrane. Standard membrane preparation, heating to operating temperature, leads to the membrane having a λ_{mem} of approximately 0.5, 12 – 14 when exposed to water-saturated gas and 22 when exposed to liquid water [44]. In [45], it assumed a water content of the membrane of 21, a well-hydrated membrane. This is also the case for the developed model to be presented in chapter 3.1.4. Seen in formula 43, the ohmic resistance increases if the membrane is dry.

Concentration overpotential U_{con}

U_{con} occurs due to the change in concentration of the reactants at the electrode surface during electrolysis. U_{con} develops when the current density is high enough to restrict the electrolysis process by overpopulating the membrane surface with oxygen gas bubbles, slowing down the reaction speed. U_{con} is given by formulas 44 and 45, the sum of concentration overpotential at the anode and cathode. [44, 47]

$$U_{con} = U_{con}^{anode} + U_{con}^{cathode} \quad [V] \tag{44}$$

$$U_{con} = \frac{R\,T}{4\,F}\ln\left(\frac{C_{an_{O_2},1}}{C_{an_{O_2},0}}\right) + \frac{R\,T}{2\,F}\ln\left(\frac{C_{cat_{H_2},1}}{C_{cat_{H_2},0}}\right) \quad [V] \tag{45}$$

Where index 1 is for the operating condition, index 0 is for a reference operating condition, $C_{an_{O_2}}$ is the oxygen concentration at the anode, and $C_{cat_{H_2}}$ is the hydrogen concentration at the cathode. In formula 45, assuming that the concentration of oxygen at the anode is the partial pressure of oxygen at the current operating conditions, and the standard condition is given by the partial water saturation pressure subtracted from the anode pressure, the anode concentration overpotential can be estimated [80]. The same methodology is applied for the cathode overpotential. This is shown in formulas 46 and 47. [44, 80]

$$U_{con}^{anode} = \frac{R\,T}{4\,F}\ln\left(\frac{p_{O_2}}{P_{anode} - p_{H_2O,sat}}\right) \quad [V] \tag{46}$$

$$U_{con}^{cathode} = \frac{R\,T}{2\,F}\ln\left(\frac{p_{H_2}}{P_{cathode} - p_{H_2O,sat}}\right) \quad [V] \tag{47}$$

Electrolysis energy efficiency

The energy efficiency of the electrolyser, η_T, can be calculated by the product of the voltage efficiency, η_U, and the faradaic efficiency, η_F. This is shown in formula 48. [45, 78]

$$\eta_T = \eta_F \, \eta_U \tag{48}$$

η_U is given by formula 49 [44, 45].

$$\eta_U = \frac{Thermo - neutral\ voltage}{Cell\ voltage} = \frac{U_{th}}{U_{cell}} = \frac{\frac{\Delta G \; T\Delta S}{nF}}{U_{cell}} = \frac{1.482}{U_{cell}} \tag{49}$$

Electrolysis generates entropy as heat. Considering that no external heat is available, the energy required for the electrolysis process must be delivered in terms of electrical energy. That means that the thermal energy required, $T\Delta S$, must be added, see Figure 10 in subchapter 2.4.4. Hence, the thermo-neutral voltage, U_{th}, is considered the minimum required voltage for electrolysis for calculating η_U, shown in formula 48. U_{th} is given by formula 50 [45, 46, 74].

$$U_{th} = \frac{\Delta G + T\Delta S}{n \; F} = 1.482 \;\; [V] \tag{50}$$

The faradaic efficiency, η_F, expresses the charge transfer efficiency of electrons in the electrolyser. For a PEM electrolyser, this translates to the efficiency at which oxygen and hydrogen generation occurs. η_F is calculated in terms of current density, shown in formula 51. [45, 78]

$$\eta_F = 1 - \frac{j_x}{i} \;\; \left[\frac{A}{cm^2}\right] \tag{51}$$

Where j_x is the total gas crossover current density, shown in formula 52. [45, 78]

$$j_x = j_x^{H_2} + j_x^{O_2} \;\; \left[\frac{A}{cm^2}\right] \tag{52}$$

Where the gas crossover for hydrogen is given in formula 53. [45, 78]

$$j_x^{H_2} = 2 \; F \; P_{H_2}^T \frac{p_{H_2}}{d_m \delta_m} + \frac{a_x}{d_m \delta_m} \; i \;\; \left[\frac{A}{cm^2}\right] \tag{53}$$

Where $P_{H_2}^T$ is the effective diffusive permeability coefficient for hydrogen, which is temperature-dependent, and d_m is the membrane swelling. $P_{H_2}^T$ is given in formula 54. [45, 78]

$$P_{H_2}^T = 3 \cdot 10^{-20} \exp(0.026 \; T_{cell}) \;\; \left[\frac{mol}{cm \; s \; Pa}\right] \tag{54}$$

a_x is a fitting parameter, given in formula 55. [45, 78]

$$a_x = \frac{1}{425}\ \delta_m\ \ [\mu m] \tag{55}$$

The oxygen permeability coefficient, $P_{O_2}^T$, is twice that of the corresponding $P_{H_2}^T$ for a Nafion® membrane [44, 45, 79]. It is assumed that the current density effect on the permeation is the same for both electrodes [44, 45]. This yields j_x shown in formula 56. [45, 78]

$$j_x = 2\left(F\ P_{H_2}^T \frac{p_{H_2} + p_{O_2}}{\delta_m} + \frac{a_x}{\delta_m}\ i \right)\ \left[\frac{A}{cm^2}\right] \tag{56}$$

2.6. Hydrogen storage

Hydrogen's gravimetric energy density is 33.33 kWh/kg [85], which is very high compared to traditional fossil fuels such as petrol 12.2 kWh/kg and diesel 12 kWh/kg [86]. Gravimetric energy density indicates how much energy exists per mass unit, for example in kWh/kg while volumetric energy density indicates energy unit per volume unit, for example in kWh/m^3 [87]. Hydrogen produced by electrolysis typically results in gaseous hydrogen under relatively low pressure, resulting in a low density of the hydrogen gas. The volumetric energy density of hydrogen can be calculated from the density of the gas, resulting in a low volumetric energy density compared to fossil fuels. Hydrogen gas at STP has a density of approximately 0.09 kg/m^3 [88], yielding a volumetric energy density of 3 kWh/m^3. Diesel has a volumetric energy density of approximately 9611 kWh/m^3 [89]. This means that to store 9611 kWh, one would require 1 m^3 diesel or 3204 m^3 hydrogen. Therefore, some form of processing of the hydrogen gas must be done to increase the hydrogen's volumetric energy density to store hydrogen in a realistic storage volume. Figure 12 shows some of the methods for storing hydrogen. [90]

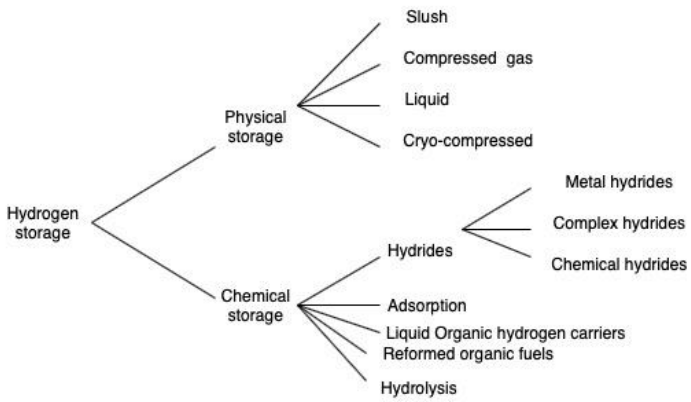

Figure 12: Hydrogen storage methods

Hydrogen's physical storage includes compressed gaseous, liquid, cryo-compressed, and slush hydrogen. Chemical hydrogen storage includes hydrides, adsorption of hydrogen, liquid organic hydrogen carriers, reformed organic fuels, and hydrolysis [90]. Some of these storage methods will be reviewed in this chapter.

The most common method for storing and transporting hydrogen is to compress the gaseous hydrogen into a higher storage pressure, increasing the density of the gas [91]. In a piston compressor, a piston reduces the available volume for hydrogen gas in the piston cylinder, much like in an internal combustion engine. Piston compressors can reach high end pressure by multistage hydrogen compression. The first step increases the hydrogen pressure to a couple of atmospheres before reaching the targeted hydrogen pressure through the next steps. The estimated energy consumption for compressing hydrogen gas from atmospheric pressure to 250 bar by multistage compression is 2-4 kWh/kg [92, 93]. Compressed hydrogen is stored in pressure vessels. Pressure vessels are separated by their structure material into types, as shown in Table 5. [94]

Table 5: Hydrogen pressure vessel types, materials, rated pressure and gravimetric hydrogen density [94, 95]

Pressure vessel	Material	Rated pressure [MPa]	Gravimetric hydrogen density [wt %]
Type I	Metallic	20 - 30	1.7
Type II	Metallic with Polymer liner wrap on cylindric part	20	2.1
Type III	Composite material with metal liner	70	N/A
Type IV	Composite material with polymer liner	70	5.7

In Table 5, gravimetric hydrogen density describes the ratio of the weight of stored hydrogen to the weight of the pressure vessel.

It is also possible to liquefy hydrogen. At atmospheric pressure, hydrogen has a boiling point of 20 K [91]. By reducing the temperature below this temperature, hydrogen becomes a liquid. Liquid hydrogen is stored in cryogenic storage tanks. These tanks are isolated to minimize heat exchange with the environment and are often spherical due to the surface area to volume ratio [94]. Heat exchange with the environment will occur, leading to some stored liquid hydrogen changing phase into hydrogen gas. This phase change will increase the pressure in the storage tank. The hydrogen gas is released through a pressure relief valve to avoid rupture of the

cryogenic tank. This venting of the hydrogen is called hydrogen boil-off and represents a loss in stored hydrogen. [95]

Storing hydrogen in organic fuels such as methane and methanol is also possible. Among reformed fuels, ammonia, NH_3, is considered promising for hydrogen storage due to its hydrogen density, 17.8 wt% [90], established production facilities, applications, and ease of transport [90]. Ammonia is a standardized product with a well-established distribution network, handling method, and regulations covering its storage and transportation [96]. Ammonia can be combusted directly, mixed with hydrogen or methane fuels, or be used as fuel in fuel cells. One of the disadvantages of ammonia is the release of NO_x when combusted. [97]

Hydrogen can also be stored in a solid state using nanostructured materials by the adsorption of molecular hydrogen in metal hydrides and nanostructured materials, such as carbon nanotubes and metal organic framework systems, by either physisorption or chemisorption processes [98]. These storage methods are not considered in the thesis due to the low volumetric energy density of these methods and their market states. [98, 99]

In the thesis, it is assumed that hydrogen is stored as a compressed gas at 250 bar. Storing hydrogen as a compressed gas is the most established storage method of hydrogen [100]. The small annual hydrogen yield, space restrictions, and degree of complexity make compressed gaseous hydrogen storage the most suitable storage technology for the proposed in-turbine electrolysis system. The choice of storing at 250 bar was made due to the availability of pressure vessels rated for this pressure [101].

2.7. Hydrogen transportation and bunkering

Methods for hydrogen transportation must be selected with a background in several parameters. These parameters include hydrogen amount, the state of the stored hydrogen, the distance from production to customer, and land or sea transport. [58]

Hydrogen transport

For small amounts of hydrogen, it may be beneficial to store hydrogen in storage tanks and transport it using trucks. For transportation by truck, the storage density of the transported hydrogen should preferably be high to allow for as much hydrogen to be transported in one turn. The total weight of the transport is also important to minimize and is done for compressed gaseous hydrogen by utilizing composite storage tanks [58]. Factors such as storage time, the

distance of the transport route, cost, and fuel usage also have to be considered in the logistics of hydrogen transport by truck [58].

Transporting hydrogen in large quantities over long distances, 1000 – 4000 km [58], transport of compressed gaseous hydrogen in pipes is the most viable option. This could be done by mixing the hydrogen into, for example, natural gas or the transportation of pure hydrogen [58]. A subject that has received increased attention in the last years is the possibility of hydrogen transport in existing pipe networks [102-105]. This would eliminate the need for all new pipelines to be built and significantly reduce costs for hydrogen transport by pipes. In the SINTEF HyLine project [102], utilizing already established pipeline networks at the North Sea for oil and gas transport for hydrogen transport is reviewed. The main topics to be addressed are at what rate hydrogen can get into the pipe material and how much hydrogen it takes for the material to lose its structural properties. [106]

It is also possible to use marine tankers for transportation. The world's first liquid hydrogen tanker, Susio Frontier, was launched in December 2019 in Kobe, Japan [107]. Susio Frontier will transport liquid hydrogen produced in Australia to Japan. The project aims to prove the feasibility of bulk liquid hydrogen shipping by sea. [107]

Hydrogen bunkering

In this section, bunkering methods for hydrogen are reviewed. Since the hydrogen storage method is assumed to be compressed hydrogen, only bunkering methods for compressed hydrogen are considered.

Bunkering of hydrogen is the hydrogen transfer from its storage to a consumer, supplying fuel for maritime vessels. The bunkering method depends on the hydrogen storage method. There are two leading technologies of gaseous hydrogen bunkering; compressing the gas onto the vessel, or by pressure balancing [108]. For compressing, a high throughput compressor is used to move the hydrogen from low-pressure storage at the bunkering facility to the vessel. This bunkering method allows for control of the hydrogen flow but requires costly equipment; the compressors [108]. In pressure-balancing, hydrogen is stored at a higher pressure at the bunkering location than the storage pressure of the vessel. The hydrogen would flow from high to low pressure, from storage to vessel, by opening a valve. This method does not require compressors to transfer the hydrogen but requires considerable storage capacity at the

bunkering facility since a lot of the stored hydrogen is inaccessible. When the storage pressure drops below the pressure of the vessel storage, hydrogen transfer by pressure balancing would not be possible. [108]

It is also possible to utilize swappable portable tank containers. This is containerized storage, replacing the transfer and handling of the hydrogen. Hydrogen is transferred by replacing the full containerized hydrogen storage with a new empty containerized storage. This solution simplifies distribution but would increase the cost of storage due to more pressure vessels required. [109]

In the thesis, it is assumed that the stored compressed hydrogen on Zefyros is compressed on board a vessel to transport the hydrogen onshore.

2.8. Hydrogen consumption

Today, more than half of the world's hydrogen production is being used to produce ammonia, where 90 % of the ammonia is further used to produce artificial fertilizer [58]. About 25 % of the world's hydrogen is used for petroleum refining and 10 % for methanol production. Hydrogen is also used in the production of steel, metal alloys, glass, electronics, and synthetic resins [58]. Below, potential consumers of hydrogen will be reviewed.

In the transport sector, hydrogen light-duty vehicles, trucks, trains, maritime vessels, and planes are potential hydrogen consumers [58]. Hydrogen-powered vehicles, FC vehicles, have existed since 2015; however, FC vehicles have not experienced the same growth as electric cars [110]. This is shown in Figure 13, which shows the Norwegian carpool in 2020 by fuel. Data is collected from [111].

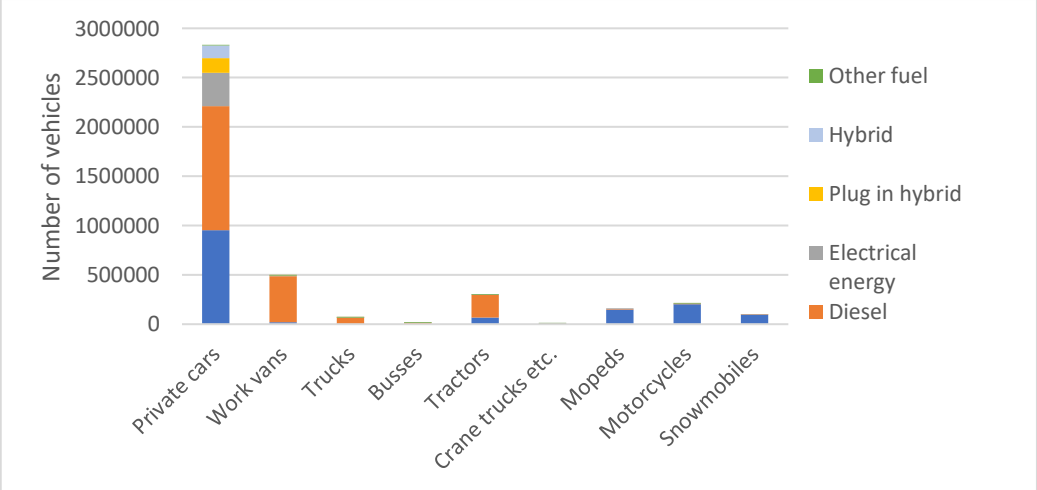

Figure 13: The Norwegian car pool in 2020 by fuel, other fuels include e.g. natural gas and hydrogen [111]

Figure 13 shows that the share of vehicles powered by non-traditional fuels is low. The low share of hydrogen vehicles may be due to Norway's number of hydrogen filling stations. Currently, two hydrogen filling stations in Norway are open to consumers; Høvik and Hvam [112, 113]. Three hydrogen filling stations are currently under construction, and one filling station is privately owned by Asko [114]. The world's first hydrogen ferry, Norled's MF Hydra, will travel the route Hjelmeland – Nesvik – Skipavik in Rogaland, Norway. The ferry is currently powered by diesel generators [115], and fuel cells are planned to be installed in autumn 2022 [116]. Eidesvik's Viking Energy will become the world's first supply vessel powered by ammonia-driven fuel cells by Wärtsilä. The launching date of the vessel is planned to be in 2024 [117]. Airbus has stated that they aim to develop the world's first zero-emission commercial aircraft by 2035, the ZEROe concepts [118]. Here, liquid hydrogen would be combusted with air in modified gas turbines. Hydrogen fuel cells will also be used to complement the gas turbine and power electrical equipment on the aircraft. [118]

The use of hydrogen as means of heating in residential buildings is an option to reduce greenhouse gas emissions from countries with an existing gas network for heating. These countries include, among others, Australia, Canada, Netherland, the USA, and the UK, where natural gas is used for heating and cooking. Winlaton in northeast England uses a gas mixture of natural gas and hydrogen for heating and cooking, where hydrogen makes up 20 % of the gas mixture. The gas mixture is transported through public supply pipelines, supplying 668 homes, a school, and some small businesses [119].

Industry accounts for approximately a third of the world's energy consumption and carbon emissions [58]. Around 40 % of these carbon emissions are from heating by fossil energy sources. By using hydrogen as fuel, these carbon emissions can be decreased [58]. In Odda, Norway, Tizir Titanium & Iron is planning to replace coal with hydrogen in their process of producing titanium oxide, potentially decreasing the carbon emissions by 90 % and increasing the energy efficiency by 40 % [120].

As mentioned in chapter 2.1, hydrogen can be used to store surplus energy. Due to the intermittent nature of renewable energy sources, such as wind and solar power, and the grid capacities, it may be possible to either have a surplus or shortage of power available on the grid. This imbalance of power production and demand is mainly an issue in areas with high penetration of intermittent energy sources in the energy mix and low grid capacities. Here,

hydrogen can act as energy storage in periods of surplus energy production. Hydrogen can later be converted back to electricity using fuel cells and fed into the grid during periods of a shortage in energy production.

A review of how and where the produced hydrogen from the proposed in-turbine hydrogen production system can be used is shown in the results chapter of the thesis.

2.9. Hydrogen safety

Hydrogen is a standardized product, such that standards and regulations for handling and managing hydrogen are available worldwide. In Norway, The Norwegian Directorate for Civil Protection is the expert authority for flammable substances, including hydrogen. The following references are examples of regulations for handling and transport of hydrogen [121-125]. Storulykkeforskriften, The Major Accident Prevention Policy, [123], must be followed if the amount of stored hydrogen exceeds 5 tons. Hydrogen safety is the key to increasing social acceptance of hydrogen in society. [90]

Hydrogen has low ignition energy and has a very wide flammability range, 0.017 mJ, and 4.1 – 74.8 vol%, respectively [90]. This means that hydrogen requires a low amount of energy to ignite and is flammable in a very wide range of concentrations in air. In addition, hydrogen also has a low electro-conductivity rate, which means that hydrogen flow has the potential to trigger an electrostatic spark that may ignite the hydrogen, whether in the liquid or gaseous phase. Hence, isolating hydrogen from the surrounding environment, external heat sources, and system grounding is important [90]. When burning, hydrogen has a nearly invisible pale blue flame. The combustion produces water such that inhaling the smoke from hydrogen combustion is safe, with no risk of smoke asphyxiation. [90]

A gas detector is necessary to detect hydrogen leaks. Gas detectors suitable for detecting a hydrogen leak include mainly catalytic bead detectors [126]. The catalytic bead gas detector consists of a pair of platinum wire wound resistors with ceramic beads, where one of them is coated with a catalyst. When a combustible gas meets the catalytic surface, it gets oxidized. Heat is released, causing the resistance in the platinum wire coated with the catalyst to change while the other catalyst's resistance remains unchanged. The sensors detect the change in current due to this change of resistance [126]. Since hydrogen is lighter than air, it rises rapidly

and disperses quickly. It is important to place the gas detectors nearby and directly above where leaks are more likely to happen, such as in a valve stem or in a connection. [126]

Hydrogen presents several challenges related to the detection of a potential flame. The nearly invisible hydrogen flame requires technology to detect flames in the non-visible spectrum of electromagnetic radiation; *ultraviolet*, UV and *infrared*, IR radiation. It is also possible to utilize thermal sensors to detect an increase in temperature due to the flame [126]. A thermal sensor must be placed near the hydrogen flame to detect the flame. The energy from the flame is radiated primarily in the UV spectrum. UV detectors excel at detecting hydrogen flames; however, they are sensitive to sparks, arcs, welding, and other UV-rich sources. When UV-rich sources are present, false alarms could happen [126]. Multispectral IR flame detectors use a combination of IR sensor filters and analysis software to detect flames and reduce false alarms. Multispectral IR detectors can be designed to specifically detect the low amount of IR radiation caused by a hydrogen flame. These have a good detection range with a low response time and do not cause false alarms of the same nature as the UV detectors [126].

In the report, "Report on offshore structural integrity and safety performance of H2 production, processing, storage and transport", R. Koelewijn, M. v. Dam, and C. Hulsbosch-Dam [126], a *hazard identification study,* HAZID, of offshore hydrogen production at an offshore platform. A HAZID is a qualitative study for the early identification of risk. In the report [126], risk is defined as the frequency of the occurrence of harm and the severity of that harm. Several potential risks and recommendations resulted from this HAZID [126]. In the event of a hydrogen leak, a cloud could form and create an explosive environment. Planned release of oxygen can result in an oxygen-rich environment causing an increased risk of flammability or explosion, and higher corrosion rates [126].In the event of a hydrogen jet flame caused by a leak, the HAZID recommends that the flame is not extinguished. The leak could continue to form clouds and potentially create a more dangerous explosive environment by extinguishing the flame [126]. The report [126] concludes that catalytic bead gas detectors and multiple IR flame detectors are best suited for hydrogen application. It also concluded that further studies for hydrogen safety are necessary, such as the venting of hydrogen and oxygen and the effect of hydrogen flame temperature on structural steel [126].

Hydrogen production inside the turbine tower of Zefyros would create a potentially explosive environment. The use of electrical equipment and the safety systems onboard Zefyros would

have to comply with the regulation “Forskrift om utstyr og sikkerhetssystem til bruk i eksplosjonsfarlig område” [125]. In this regulation, it is specified that all components used in an explosive environment must be EX-certified and marked. [127]

Lhyfe and Central Nantes plan to install a platform for hydrogen production by electrolysis at the SEM-REV offshore test site [18, 42]. DNV will lead a safety study for this project to identify the main environmental, safety, and operational risks for offshore hydrogen production facilities [128]. At the time of writing this thesis, this study is not available.

In the results chapter, safety hazards for an in-turbine electrolyser are identified, and gas and flame detectors and their locations are specified.

2.10. Material selection

For the successful use of materials for the storage of compressed hydrogen, some unique properties of the compressed hydrogen gas must be considered. These properties include hydrogen embrittlement, hydrogen attack, and hydrogen permeation, and will be reviewed in this chapter. [91]

Hydrogen embrittlement occurs when hydrogen is in contact with metal. The contact may happen during manufacturing, for example, by arc welding, which could be a source of hydrogen atoms [91]. Hydrogen permeation due to the hydrogen solubility of the metal leads to a certain concentration of hydrogen inside the metal. This hydrogen causes a reaction within the metal structure, leading to hydrogen embrittlement [91]. Hydrogen embrittlement results in a hardening of the metal and a reduction in ductility, which in turn causes the metal to crack below the expected yield stress [91]. The risk of hydrogen embrittlement increases with the pressure of the hydrogen [91]. Materials that can be utilized without any specific precautions regarding hydrogen embrittlement include brass and most copper alloys, aluminium, and aluminium alloys, and beryllium copper alloys [91].

In carbon steels, hydrogen in the steel may react with the carbon and form methane at the grain boundaries and voids. The methane does not diffuse through the steel; it accumulates in the voids at high pressure, which causes cracks to form. This is called hydrogen attack, where the risk increases with increased temperature and pressure of the hydrogen. Increasing the fraction of certain materials such as chromium, molybdenum, titanium, and wolfram in the storage

material reduces the risk of hydrogen attack [91]. Other materials such as aluminium, manganese, and nickel increase the risk of hydrogen attack. [91]

For permeation through metals, diatomic hydrogen, H_2, is absorbed through the metal surface to produce atomic hydrogen, H. The hydrogen atoms will diffuse through the metal and recombine into H_2, which will exit the metal wall [91]. Hydrogen permeation increases with temperature. Structural materials for use in hydrogen storage must have low hydrogen permeability to enclose the stored hydrogen [91]. A layer of a low permeable material inside a storage tank is also an option to reduce permeability [91]. For pressure vessels, mainly low-alloy steel, austenitic stainless steels, and ferritic steel are used as structural materials. [91]

In the results chapter, a review of suitable materials utilized in the proposed in-turbine hydrogen production system is performed.

3. Method

In this master's thesis, an energy- and hydrodynamic analysis of an in-turbine electrolyser at UNITECH Zefyros FOWT is performed. Results have shown that an in-turbine electrolyser at Zefyros would not describe the electrolyser's efficiency when powered by a variable power source. Hence, the thesis is divided into two cases. Case 1 considers the in-turbine system, and case 2 considers the large-scale hydrogen production system. To design these two cases and to answer the research questions raised in the introduction chapter, the hierarchical approach shown in Figure 14 is followed.

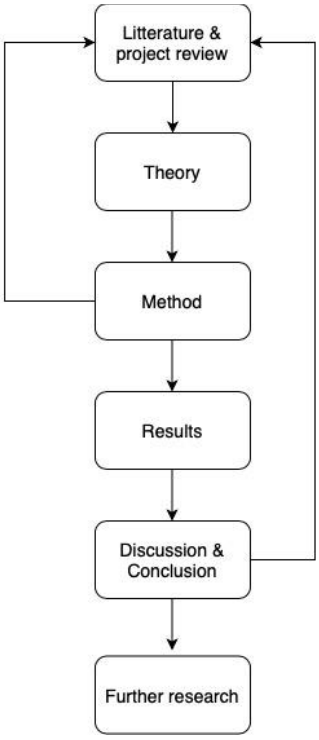

Figure 14: Methodology of the master's thesis

First, a review of relevant literature is performed to identify what research has been done for offshore hydrogen production by electrolysis and what projects exist in the industry. The review shows that most of the concepts include electrolysers coupled with wind power placed at a maritime structure of its own for offshore hydrogen production [17, 18, 21, 22]. The literature review is done with a background in all concepts for hydrogen production from intermittent power sources [33, 34, 43], and for PEM electrolysis modelling [44-47]. Applicable methodologies, results, theory, and concepts found in the literature study have inspired this thesis's work [45].

The thesis's theory chapter, or background, is done to achieve the knowledge required to perform the calculations, modelling, and simulations in the results chapter of the thesis. The theory chapter's purpose is also to provide the reader with relevant theory to understand the research questions listed in the introduction chapter and any simplifications and assumptions made to answer them.

The method chapter aims to describe how the problem is approached. This is an iterative process; when describing the approach, new relevant questions to the problems were found that needed to be addressed. The same is the case for the results chapter, where the results of the calculations, modelling, and simulations are shown.

In the discussion chapter, the results of the thesis are discussed along with the results' limitations, assumptions, and simplifications. A discussion of the results' applicability in a real-life scenario is made along with the value of the results to UNITECH as a company. The choices of components in the two hydrogen production systems are defended. In the concluding chapter, the research questions are answered.

Considering the concept that is offshore hydrogen production, a repeating challenge is to maintain the scope of the thesis at an achievable level. Areas for further study are suggested in the future research chapter.

3.1. Approach

In the background chapter, the hydrogen value chain, general hydrodynamic formulas, and a short introduction to offshore wind turbines have been introduced. In the approach chapter, the two proposed cases shall be explained along with the method of approaching the research questions and how they are answered.

3.1.1. Case descriptions

As mentioned, the thesis is divided into two cases. This is done to answer the research questions presented in the introduction chapter. Case 1 includes the in-turbine hydrogen production system. Case 2 includes the large-scale hydrogen production system. This subchapter aims to describe the two cases.

Conversations with UNITECH revealed that in the case of hydrogen production at Zefyros, an in-turbine concept was considered the feasible concept. UNITECH stated the space available

for an electrolyser inside the turbine tower to be 1 m x 1.5 m x 2 m at a level 17 m above still water level [129]. Results have shown that the space constraints largely limit the choice of electrolyser. The rated power of the assumed in-turbine electrolyser is but a small fraction of the rated power of UNITECH Zefyros. To answer research question **Q2**, a new hydrogen production system is proposed. This hydrogen production system is referred to as case 2, the large-scale hydrogen production system. Here, no space constraints apply, and only the energy aspect of the system is reviewed. This is done to estimate the variable power source's influence on the electrolyser efficiency and the hydrogen production from Zefyros.

To answer research question **Q1**, a hydrodynamic analysis of Zefyros is performed. This is done to identify the displacement and acceleration the in-turbine hydrogen production system from case 1 would experience at Zefyros. An assessment of material selection for case 1 is done with a background in the offshore environment at Zefyros.

The in-turbine electrolyser, case 1, refers to the hydrogen production system where space constraints apply. The large-scale hydrogen production system, case 2, refers to the hydrogen production system where space constraints do not apply. System overviews of the small- and large-scale hydrogen production systems are shown in Figures 15 and 16, respectively.

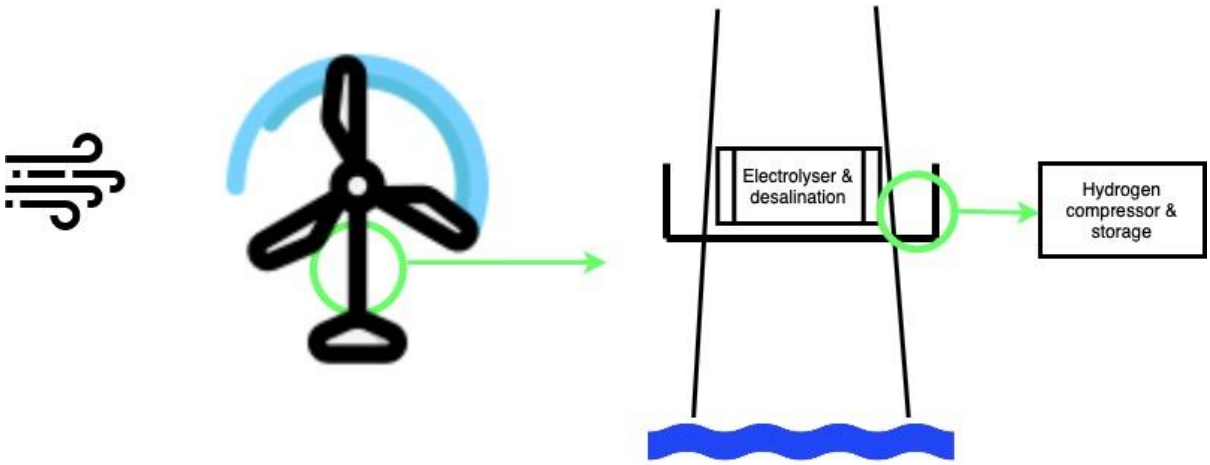

Figure 15: Case 1: System overview, in-turbine electrolysis

In Figure 15, the system overview for the proposed in-turbine electrolysis system, case 1, is shown. The wind rotates the rotor blades, generating electrical energy. The electrical energy powers a desalination unit to supply the electrolyser with feedwater with sufficient purity. The electrolyser and the desalination unit are placed inside the turbine tower to perform hydrogen production. The hydrogen gas is compressed to 250 bar and stored in pressure vessels. The

compressor and hydrogen storage must be placed on the outside platform due to no additional space inside the turbine tower.

Figure 16: Case 2: System overview; large-scale hydrogen production system

The system overview for the proposed large-scale hydrogen production system, case 2, is shown in Figure 16. In the figure, the hydrogen production system, consisting of an electrolyser, a desalination unit, and a compressor, is shown not to have a specified location. This is because the location of the large-scale hydrogen production system is not considered in the thesis. The storage of the produced hydrogen is not included in the scope of case 2.

3.1.2. Wind conditions and power production

The data used in this thesis for energy analysis for both the in-turbine and large-scale hydrogen production systems are historical *SCADA*, Supervisory Control And Data Acquisition, data from Zefyros in 2020 provided by UNITECH [53]. This dataset has a sampling interval of 10 minutes. This means that what happens outside these samples is unknown. This thesis assumes that the state of the measured parameter is constant until the following sample is available. For example, at 14:00, the measured wind speed is 10 m/s. Even though the wind speed will change during the next 10 minutes, it is treated as constant. A new measurement is executed at 14:10, where the assumption repeats itself. The dataset starts on the 22nd of January 2020 and ends on the 20th of January 2021; however, only 2020 values are used to simplify the modelling process. The data used from the dataset are shown in Table 6.

Table 6: SCADA data used in thesis

Parameter	Unit
Wind speed	m/s
Active Power	kW
Current	A
Voltage	V

Figure 17 presents the wind conditions at Zefyros for the year 2020. In the provided dataset, there are some gaps in the measurements, which may have been caused by turbine shutdown, planned installations, or other shutdown reasons. These gaps are treated as having no value.

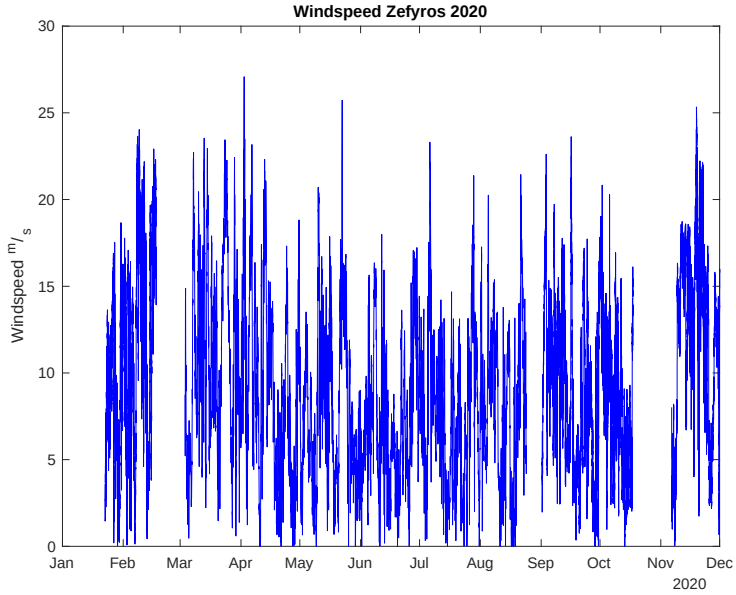

Figure 17: Onsite wind conditions Zefyros 2020, [m/s]

Illustrated in Figure 17 is the intermittent nature of wind speed. The wind conditions from May 2020 are shown in Figure 18 to illustrate the intermittency more clearly. May is chosen due to having power production during the whole month.

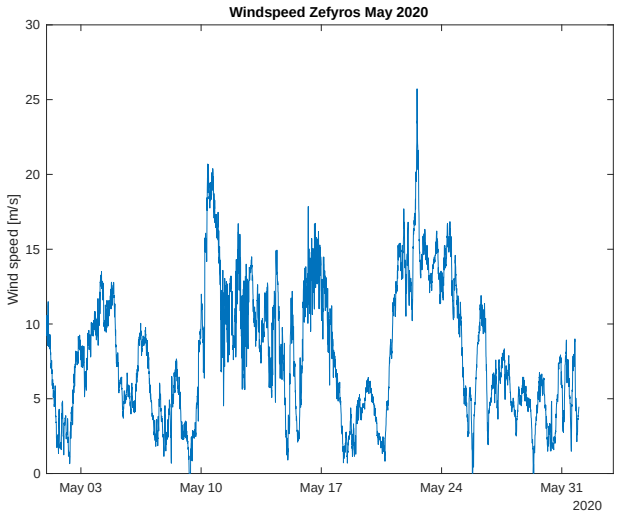

Figure 18: Wind speed Zefyros May 2020, [m/s]

The intermittency of wind speed in Figure 18 results in variable power production. The power production from Zefyros in 2020 is shown in Figure 19.

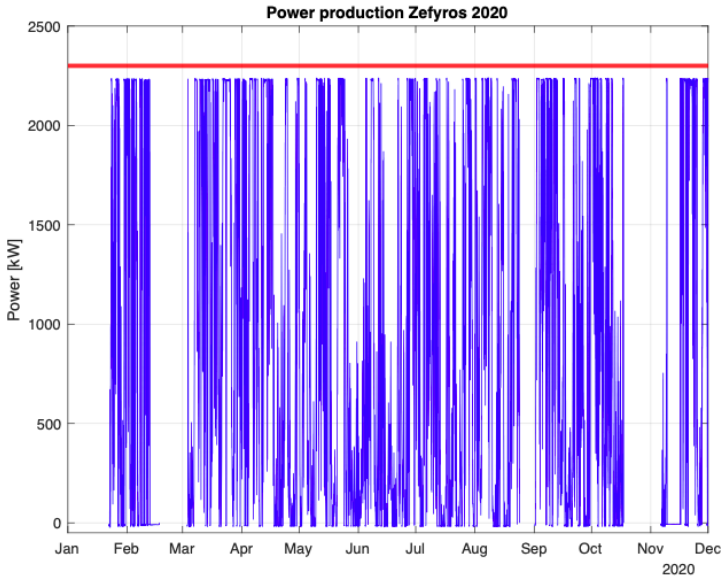

Figure 19: Power production UNITECH Zefyros 2020 [kW]. Red line shows the rated power of the turbine 2300 kW.

Figure 19 shows that power production directly correlates with wind speed. The power production from Zefyros is less than its rated power due to certain energy losses, such as from η_{mech}. The reason why the power conversion is limited is related to the power curve of the turbine, shown in Figure 5 in subchapter 2.2.1. When the wind speed exceeds a certain value, in this case 13 m/s, the power conversion is limited to reduce loads on the turbine. When this is no longer sufficient to keep loads on an operational level, the turbine shuts down. At Zefyros, this occurs at a wind speed of 25 m/s [52].

To illustrate the changes in wind speed throughout 2020, the monthly variation of wind speed is shown in Figure 20.

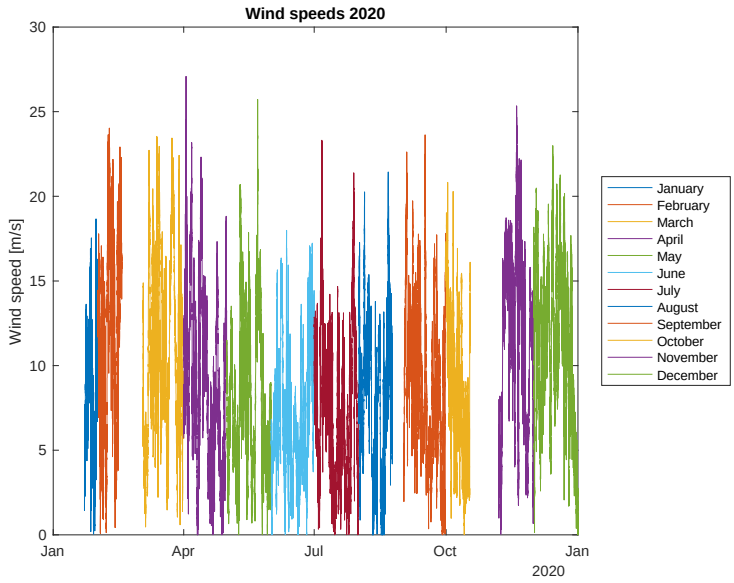

Figure 20: Monthly variation in wind speed [m/s]

In Figure 20, it is difficult to conclude the average wind speed for the respective months. In Figure 21, a bar diagram of the monthly average wind speed is shown to illustrate this.

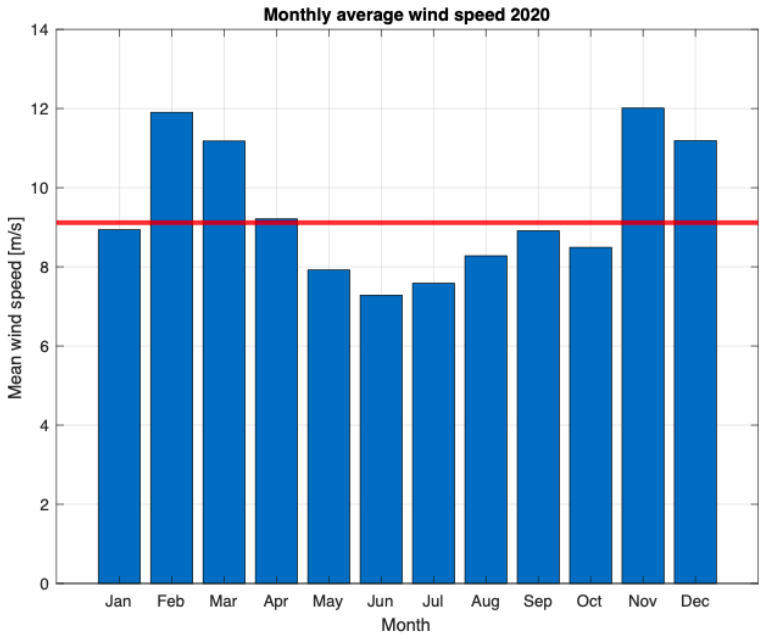

Figure 21: Monthly average wind speeds [m/s].Red line shows the average wind speed in 2020, 9.12 m/s

Shown in Figure 21 is that the winter, early spring, and late autumn months have the highest average wind speed. As mentioned, the dataset starts on the 22nd of January 2020, making the average wind speed in this month unrepresentative.

3.1.3. Case 1: In-turbine hydrogen production

In this subchapter, the components of case 1, the in-turbine hydrogen production system, and their energy demands will be reviewed.

The power measurements from the generator are utilized to estimate the hydrogen production from the proposed in-turbine hydrogen production system. The power generation from the generator is in the dataset stated in kW. The power generation from the generator is divided by 6 to calculate the amount of energy generated in the 10 minutes in which the sample lasts. This is shown in formula 57.

$$E_{Zefyros} = P_{Zefyros} \cdot \frac{1}{6} \quad [kWh] \tag{57}$$

The energy consumption of the proposed in-turbine NEL S series PEM electrolyser, E_{PEM}, is 67.85 kWh/kg H_2, and the hydrogen production rate is 0.0944 kg H_2/h or 0.0157 kg H_2/10 min [130]. Since the in-turbine electrolyser will operate at a constant load, the energy consumption is also assumed to be constant.

The specific energy consumption of compression and desalination is assumed to be constant per mass unit product; 3.5 kWh/kg H_2 and 3.6 kWh/ton H_2O for the compression and desalination, respectively [73, 92, 93]. The energy demand of the compressor and desalination unit during the 10 minutes is estimated using formulas 58 and 59, respectively.

$$E_{compression} = 3.5 \cdot 0.0157 \quad [kWh] \tag{58}$$

$$E_{desalination} = 3.6 \cdot \ m_{H_2O} \quad [kWh] \tag{59}$$

Where m_{H_2O} is the water consumption of the electrolyser. The electrolyser manufacturer states the electrolyser's specific water consumption to be 0.9 l/Nm^3 or 10.01 kg H_2O/kg H_2 [130]. The electrolyser's water consumption during the 10 minutes is calculated by formula 60.

$$m_{H_2O} = 0.0157 * 10.01 \quad \left[\frac{kg\ H_2O}{10\ min}\right] \tag{60}$$

Where 0.0157 kg H_2/10 min is the hydrogen production rate in the 10-minute sampling interval.

The energy consumption of the components in the in-turbine hydrogen production system is subtracted from the energy generation from Zefyros. If this result is positive, the hydrogen production system is on; if negative, off and the electrolyser is in standby mode. This is shown in formula 61.

$$S_{PEM} = E_{Zefyros} - E_{PEM} - E_{compressor} - E_{desalination} \begin{cases} 0, & S_{PEM} < 0 \\ 1, & S_{PEM} \geq 0 \end{cases} \tag{61}$$

Where S_{PEM} is the operational state of the electrolyser, on or off, represented by 1 and 0, respectively.

A battery is implemented in the system to provide the electrolyser with energy for entering a standby mode when the operational state is "off". At standby, the power demand is assumed to be 2 % of rated power [131]. The standby mode keeps the electrolyser at operating temperature and pressure [131]. When in standby, the load response of the electrolyser is less than 10 seconds [132]. In the thesis, the load response is assumed to be instant due to the sampling interval of the dataset. The battery is assumed to have a C-rate of 1 and a *Depth of Discharge*, DoD, at 80 %. Through an iterative process to find a battery capacity that suited the dynamics of the operating mode, a 5 kWh battery was found to be suitable. This would cover the standby

load for most of the year, apart from the long periods of downtime in 2020, shown in Figure 17 in subchapter 3.1.2. If there is any remaining energy from Zefyros after hydrogen production and battery charging, it will be exported to the grid through the export cable.

Figure 22 shows a schematic of the design of the in-turbine hydrogen production. The purpose of this figure is to graphically show the description of the case 1 in-turbine hydrogen system proposed in this subchapter.

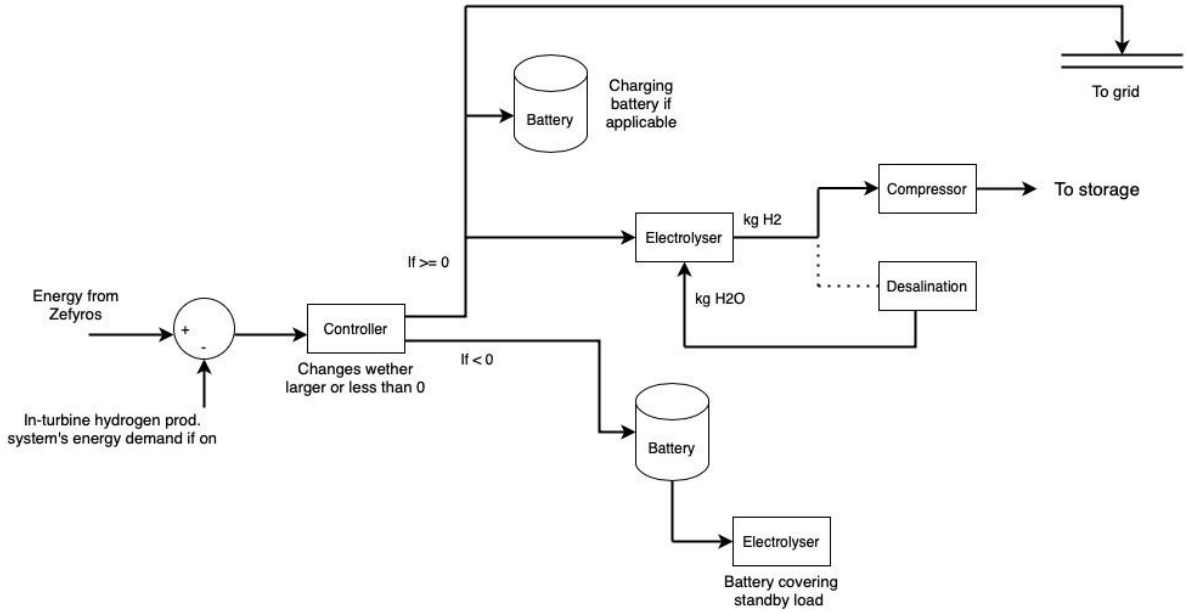

Figure 22: Design of the proposed in-turbine hydrogen production, case 1

In formula 59 it is shown that the energy demand of the desalination unit is estimated by the water consumption of the electrolyser, which depends on the hydrogen production. Hydrogen production data must then be transmitted to the desalination unit to estimate its energy consumption. The dotted line in Figure 22 illustrates this.

DNV Sesam

This section describes the methodology used for estimating the hydrodynamic response of the turbine. The response of the turbine is relevant for case 1, the in-turbine electrolyser. A potential electrolyser manufacturer can review what displacement and accelerations their components would experience onboard the turbine. DNV Sesam is used for this purpose. DNV Sesam is a collection of software applications for maritime structures' design and strength assessment [133]. The DNV Sesam application GeniE is used to build the 3D models of Zefyros. The model is imported into HydroD for analysis. The response of the turbine is collected in Postresp. Further details about the applications GeniE, HydroD, and Postresp can be found in [134],

[135], and [136], respectively. Two finite element models are built in GeniE, the panel model and the mass model, shown in Figure 23.

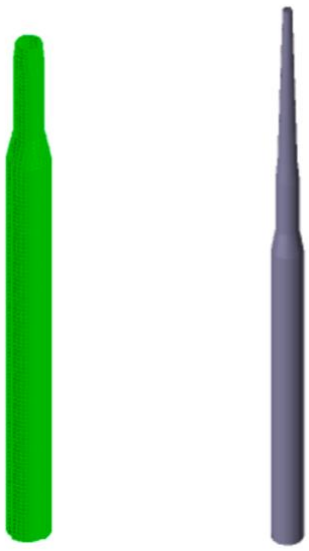

Figure 23: GeniE models, panel model and mass model, respectively

No mooring systems are considered in the model to reduce the scope of the thesis. This means that the turbine's surge, sway, and yaw response cannot be calculated. Hence, only heave, roll, and pitch have been considered. Due to the symmetry of the turbine, heave and pitch responses are identical. This will be shown in chapter 4.1.2.

UNITECH provided a spreadsheet of the mass properties of Zefyros [137]. The properties utilized in the model are listed in Table 7. These values are added in the HydroD analysis model. The weight of the proposed in-turbine hydrogen production system is not included. This is justified by the weight of the turbine being much greater than the proposed in-turbine hydrogen production system.

Table 7: Structural properties UNITECH Zefyros

Part of structure	Weight [ton]	KG [m]
Nacelle	136	165
Tower	172	131.8
Substructure	1305.22	59.2

In Table 7, KG is the vertical distance between the very bottom of the turbine and the centre of gravity along the centreline of the turbine.

According to the DNVGL-OS-C102 standard [138], the minimum design sea state for operational conditions shall reflect a 1-year response level. This standard is for offshore ship-shaped units. It is assumed that the electrolyser must be designed with the same guidelines for

design conditions. The standard states that the survival conditions must be accounted for. Survival condition is defined as: "..the condition for the most severe environmental loads the unit is exposed to" [138]. This is related to the 100-year response level. Since the expected lifetime of the electrolyser is less than 100-years [139], this is not included in the thesis. The standard states that topside areas should use 10-year return period seas for short-term response analysis [138]. DNVGL-OS-C102 [138] states that the *Most Probable Maximum*, MPM, should be applied when performing a short-term response analysis. The probability of that measurement n out of the number of measurements N in the records exceeding its most probable maximum amplitude is shown in formula 62. [55]

$$P(R_a) = \frac{n}{N} \tag{62}$$

Combining formula 17 in chapter 2.3 and formula 62 yields formulas 63 and 64.

$$-\frac{R_a^2}{m_{0R}} = \ln(n) - \ln(N) \tag{63}$$

$$P(R_a) = 1 - e^{\ln(n) - \ln(N)} \tag{64}$$

When n is one and N goes toward infinity, the MPM response is shown in formula 65.

$$P(R_a) = 1 - e^{-1} = 0.63 \tag{65}$$

Resulting in the probability of exceedance of the MPM amplitude being 63 %. The probability of exceedance is high; however, a large exceedance of the most probable maximum response is not probable due to the shape of the probability density function [57].

In the HydroD model, important input parameters are the wave spectrum's H_s and T_p, significant wave height and spectral peak, respectively. UNITECH has provided the site assessment of Zefyros, where wave measurements are from 1970 to 1986 [140]. In the site assessment, H_s and T_p for the 1 – year return period is 9.3 m and 13.9 s, respectively. Similarly, for the 10 – year return period, H_s and T_p is 11.4 m and 15.1 s, respectively. These values are calculated in terms of short-term statistics, where the duration of the sea state is three hours [140]. In Postresp, a specific point is made to identify the displacement and acceleration of the point where the electrolyser is planned to be located. This point is 17 m above still water level.

By using the parameters described above, the response amplitudes of displacement and acceleration in heave and pitch are estimated. This will be shown in subchapter 4.1.2.

3.1.4. Case 2: Large scale hydrogen production

This subchapter describes how the thesis estimates the energy efficiency of the electrolyser in the large-scale hydrogen production system, from case 2, when powered by a variable power source. A model that estimates the cell voltage and the energy efficiency depending on the load of the electrolyser is developed and described in the section below.

Case 2, electrolyser model

The model is built in SIMULINK. SIMULINK is an extension of MATLAB and is a programming and numeric computing platform. In the thesis, SIMULINK is used as a graphical modelling tool. Both tools, SIMULINK and MATLAB are developed and owned by MathWorks [141].

The formulas expressed in subchapter 2.5.2 are implemented in Simulink. The model's input is the power measurements from the SCADA data provided by UNITECH [53]. In periods of downtime of the turbine, the power from Zefyros is negative due to various power demands at Zefyros despite no production from the turbine. The negative values are set to zero in the model due to occurring problems if the input value is negative. Also, the load response of the electrolyser is assumed to be instant, meaning the electrolyser is assumed to be in standby when not producing hydrogen. The rated current density of the electrolyser is assumed to be 2 A/cm^2. The current is assumed to be uniformly distributed on the PEM. The electrolytic cell membrane area is assumed to be 160 cm^2. The rated power of the electrolyser is assumed to be 2.3 MW, equal to Zefyros. Given these assumptions, the number of cells necessary to reach the assumed rated power of 2.3 MW can be estimated. This is shown in formula 66.

$$N_{cell} = \frac{P_{electrolyser}}{U_{rated} \cdot i_{rated} \cdot A_{cell}} \tag{66}$$

$P_{electrolyser}$ is the rated power of the electolyser in case 2, U_{rated} is the cell voltage at the rated current density i_{rated}, and A is the cell membrane area. The input current density i is calculated using the active power from Zefyros as the input. This is shown in formula 67.

$$i = \frac{P_{Zefyros}}{U_{rated} \cdot N_{cell} \cdot A_{cell}} \quad \left[\frac{A}{cm^2}\right] \tag{67}$$

It is assumed that the electrolyser operates at a constant temperature. This is done to restrict the thesis's scope and to reduce specific electrolyser design choices. The temperature is assumed to be 60 ℃. The rated cell voltage is then the cell voltage at 60 ℃. The electrolyser's energy efficiency, η_T, is estimated as described in subchapter 2.5.2 in formula 48. The hydrogen production rate can be estimated by dividing the power input to the electrolyser by the *lower heating value*, LHV, of hydrogen. This is shown in formula 68.

$$\dot{m}_{H_2} = \frac{P_{electrolyser}\,\eta_T}{LHV} \cdot 600 \quad \left[\frac{kg\ H_2}{10\ min}\right] \tag{68}$$

Where 600 represents how many seconds there are in the 10 minutes, that is the sampling interval of the provided dataset. The hydrogen production is then used as input to estimate the energy required for the compression and desalination. The energy consumption for the compression and desalination for the model, applying for case 2, is assumed to be as shown in formulas 69 and 70, respectively. The specific energy consumptions of compression and desalination are assumed to be the same for case 2 as for case 1 to restrict the scope of the thesis.

$$E_{compression,case\ 2} = 3.5 \cdot m_{H_2,case\ 2} \quad [kWh] \tag{69}$$

$$E_{desalination,case\ 2} = 3.6 \cdot m_{H_2O,case\ 2} \quad [kWh] \tag{70}$$

$m_{H_2,case\ 2}$ is the mass of hydrogen produced during the 10-minute sampling interval, and $m_{H_2O,case\ 2}$ is the electrolyser's water consumption during the same 10 minutes, estimated by formula 71.

$$m_{H_2O,case\ 2} = m_{H_2,case\ 2} \cdot 10.1 \quad \left[\frac{kg\ H_2O}{10\ min}\right] \tag{71}$$

Here, 10.01 kg H_2O/kg H_2 is the assumed specific water consumption of the electrolyser [130]. Formulas 69, 70, and 71 for case 2 are different from formulas 58, 59, and 60 for case 1 in that for case 2, the large-scale hydrogen production system, the hydrogen production rate is not constant like in case 1. This means that the energy demand for the electrolyser, compressor, and desalination unit in case 2 changes depending on the available input power from Zefyros.

The energy consumption of compression and desalination is converted to power and subtracted from the input from Zefyros to the model. The new power input, now with the energy

consumption from compression and desalination subtracted, is used to estimate the hydrogen production. In this way, the compression and desalination energy consumptions are higher than they would be in practice due to the input power being reduced and thereby also the hydrogen production. To reduce the scope of the thesis, it is assumed that the energy consumptions of the compression and desalination processes are very low compared to the energy consumption of the electrolyser, which is reasonable to assume. The difference in the resulting hydrogen production due to the mismatch of the energy consumption of compression and desalination, and the initial hydrogen production rate with those energy consumption not subtracted, is then assumed negligible.

In Figure 24, the design of the proposed large-scale hydrogen production system is illustrated. This figure aims to graphically show the description of the system proposed in this chapter.

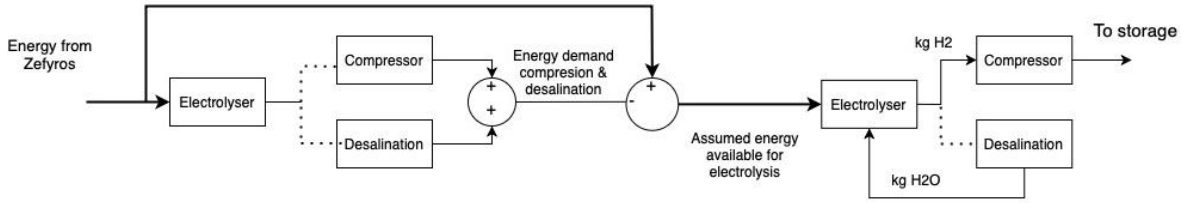

Figure 24: Design of the proposed large-scale hydrogen production system, case 2

An illustration of how the model works in Simulink is shown in Figure 25.

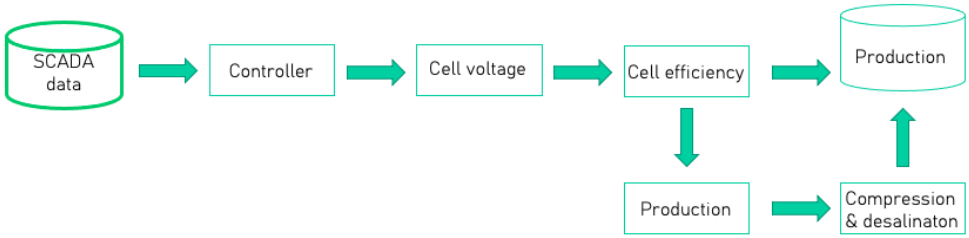

Figure 25: Methodology for the large-scale hydrogen production model

The power measurements from the provided dataset are converted to current density. The current density estimates the cell voltages at the respective input current density. From the cell voltage, the energy efficiency of the electrolyser is estimated. The energy efficiency is used to estimate the first hydrogen production which is used to estimate the energy demand for the compression and desalination processes. These energy demands are subtracted from the energy available from Zefyros. This yields the final estimated hydrogen production.

In Table 8, the parameters utilized in the model are presented. The parameters are extracted from PEM electrolysis modelling journal articles [45, 46, 79, 142], and some are assumed. Through an iterative process where several different parameters are tested, the selected

parameters are chosen to present a conservative estimation of PEM electrolyser energy efficiency [62, 143, 144].

Table 8: Parameters utilized in SIMULINK model

Symbol	Description	Value	Unit	Source
$\boldsymbol{P_{anode}}$	Pressure anode side	1	bar	Assumed to be equal to [65]
$\boldsymbol{\gamma_{O_2}}$	Partial pressure increase factor oxygen	Formula 37	$\frac{bar\ cm^2}{A}$	[45] [79]
$\boldsymbol{\gamma_{H_2}}$	Partial pressure increase factor hydrogen	2.4	$\frac{bar\ cm^2}{A}$	[45] [79]
$\boldsymbol{\varepsilon_{O_2}^{Fick}}$	Diffusivity Nafion membrane oxygen side	$2 \cdot 10^{-11}$	$\frac{mol}{s\ cm\ bar}$	[45] [79]
$\boldsymbol{\varepsilon_{H_2}^{Fick}}$	Diffusivity Nafion membrane hydrogen side	$4.7 \cdot 10^{-11}$	$\frac{mol}{s\ cm\ bar}$	[45] [79]
$\boldsymbol{P_{cathode}}$	Pressure hydrogen side	30	bar	Assumed to be equal to [65]
$\boldsymbol{R}$	Universal gas constant	8.3144	$\frac{J}{K\ mol}$	
$\boldsymbol{F}$	Faraday's constant	96485	$\frac{C}{mol}$	
$\boldsymbol{\alpha_{anode}}$	Anode charge transfer coefficient	0.5	-	[45, 46]
$\boldsymbol{\alpha_{cathode}}$	Cathode charge transfer coefficient	0.5	-	[45, 46]
$\boldsymbol{i_{0,ref\ a}}$	Reference exchange current density anode	$1.3 * 10^{-7}$	$\frac{A}{cm^2}$	[45, 46]
$\boldsymbol{i_{0,ref\ c}}$	Reference exchange current density cathode	$1 * 10^{-3}$	$\frac{A}{cm^2}$	[45, 46]
$\boldsymbol{E_{act,anode}}$	Activation energy anode	30000	$\frac{J}{mol}$	[45, 142]
$\boldsymbol{E_{act,cathode}}$	Activation energy cathode	90000	$\frac{J}{mol}$	[45, 142]
$\boldsymbol{\delta_{mem}}$	Membrane thickness	127	μm	[45]
$\boldsymbol{d_{mem}}$	Membrane swelling	1	-	[45]
$\boldsymbol{LHV}$	Lower heating value H_2	120	$\frac{MJ}{kg}$	
$\boldsymbol{A}$	Cell area	160	cm^2	[45]

4. Results

In the method chapter, the two different cases of the thesis are described. The results chapter is divided into two chapters; chapter 4.1, the in-turbine hydrogen production system, and chapter 4.2, the large-scale hydrogen production system.

In chapter 4.1, the design of the in-turbine electrolyser of case 1 will be analysed. Here, the hydrodynamic response of Zefyros will be estimated to identify the Zefyros' response in 1-year and 10-years seas in pitch, roll, and heave. Required components' locations and safety measures are also reviewed. The operation in 2020 of the in-turbine hydrogen production system is shown. The low rated power of the chosen electrolyser compared to the rated power of UNITECH Zefyros yields that the electrolyser will operate at rated power if the turbine is in production. Therefore, the variable load that is induced by intermittent wind power would not occur.

To show the effect intermittency has on the efficiency of an electrolyser, a second hydrogen production system, the large-scale hydrogen production system of case 2 is proposed in chapter 4.2. Here, constraints regarding space do not apply. For case 2, the energy aspects of the system will be reviewed, and the electrolyser energy efficiency is estimated.

For both systems, the in-turbine and large-scale hydrogen production system, it is assumed that PEM electrolysers are utilized for the electrochemical splitting of water. This is because PEM electrolysers enable the possibility of dynamic operation, have high market availability, and utilization of a PEM as an electrolyte eliminates the need for a liquid electrolyte, which would increase maintenance frequency and expenses [43, 62, 67]. Also, the AE requires a larger area compared to PEM electrolysis [73]. For both hydrogen production systems, the in-turbine and large-scale hydrogen production systems, compressed hydrogen is assumed to be the method of storage. In the in-turbine hydrogen production, the choice of storing as compressed hydrogen was made due to the small amount of hydrogen produced. It is also the most common method of hydrogen storage and is a less complicated technology compared to the other means of storage. The same specific energy consumption of the compression and desalination is assumed for both hydrogen production systems, case 1 and 2. This assumption is made to reduce the scope of the thesis.

4.1. Case 1: Design of the in-turbine hydrogen production

A schematic layout of Zefyros is shown in Figure 26, provided by UNITECH [137].

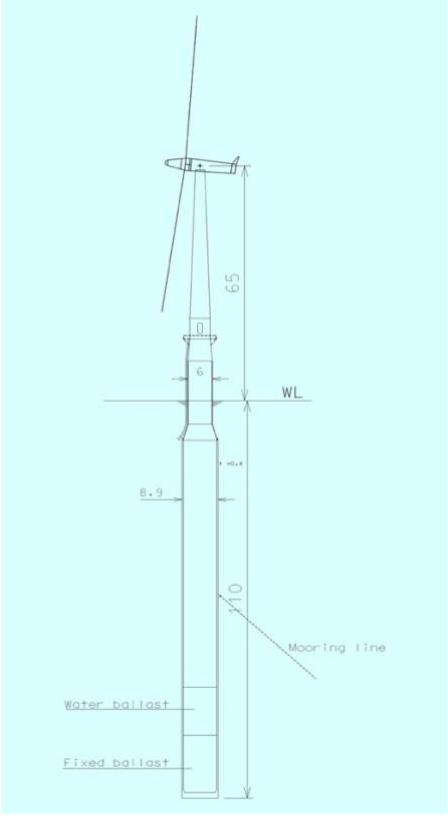

Figure 26: Schematic of UNITECH Zefyros [137]

Through discussions with UNITECH [129], the maximum dimensions of the in-turbine electrolyser were identified to be 1 m x 1.5 m x 2 m (W x D x H) inside the turbine, 17 m above still water level. In Figure 27, a sketch is made to illustrate this location.

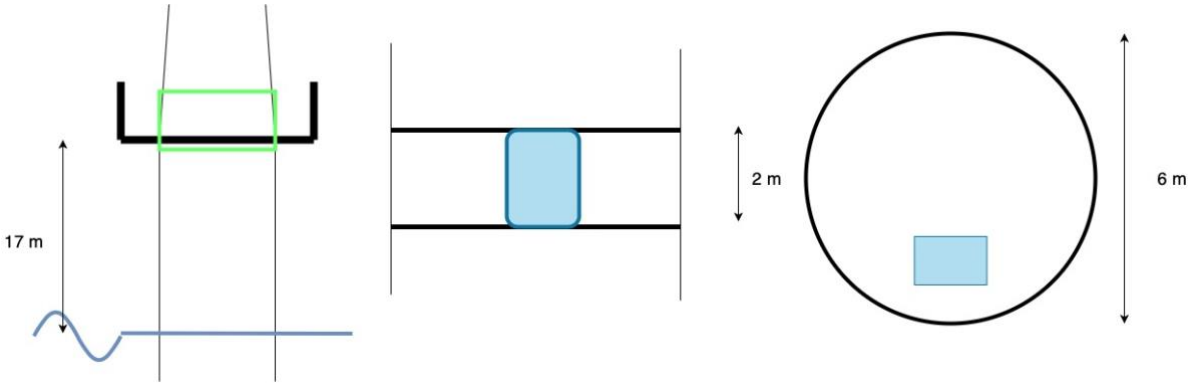

Figure 27: Sketch illustrating the specified location by UNITECH for an in-turbine electrolyser. From the left; the height of the location relative to the waterline, length and height of location restricted by the floor above, width and length restrictions due to other equipment at the location

Based on the space restrictions stated by UNITECH and illustrated in Figure 27, a suitable PEM electrolyser has been identified. This is shown in Table 9.

Table 9: Electrolyser for Zefyros hydrogen production

Name	Dimensions (WxDxH)	Rated power [kW]	Reference
NEL S40	0.8 m x 1 m x 1.1 m	6.41	[130]

The NEL S40 was selected due to the size of the electrolyser, the data available for the electrolyser, and the lack of other catalogue PEM electrolyser options available. Relevant specifications for the S40 electrolyser presented on the Nel website are presented in Table 10.

Table 10: Nel S40 specifications [130]

Nominal Production rate [Nm^3/h, 0 ℃ 1 bar]	1.05
kg per 24 h	2.27
Power consumption by system [kWh/Nm^3]	6.1
Delivery pressure [bar]	13.8

When Zefyros has incoming wind speed at the rated wind speed, the energy generation for one hour is approximately 2300 kWh. When both the electrolyser and the generator are operated at their rated power, the electrolyser consumes 0.27 % of the energy generated by Zefyros. This means that if Zefyros is generating power, the NEL S40 will operate at its rated load, yielding a constant energy consumption.

The water consumption of the NEL S40 is 0.9 l/Nm^3 [145], which translates into 10.1 kg water/ kg H_2. In Greenstat's report "Optimal utnyttelse av energi fra havvind i Sørlige Nordsjø II" [73], an area of 0.02 m^3/ton water produced per day is occupied by a 2-step RO desalination unit. The daily demand water demand is very low, yielding a very low area requirement for the desalination unit. The area specification stated in [73] is assumed to not apply to such a small system. However, it is assumed that there is available space inside the turbine tower for the 2-step RO desalination unit.

No specific hydrogen compressor with available dimensions has been found suitable for this system. L&W compressors have high-pressure compressors in their line-up, which includes compression of hydrogen gas from atmospheric pressure to 200 bar and 300 bar [146]; however, not for 250 bar, and no dimensions are available. Their product range has dimensions for a similar compressor with dimensions of 1.28 m x 0.51 m x 0.826 m [147], which is assumed also applies to a hydrogen compressor. Assuming that a hydrogen compressor has the dimensions stated above, there is no available space inside the turbine tower for the compressor. This means that the compressor must be placed outside the turbine tower along with the hydrogen pressure vessels used for storage.

The hydrogen production rate of 1.05 Nm^3/h translates to a production rate of 0.0944 kg/h. As shown in Table 10, the pressure of the produced gaseous hydrogen is 13.8 bar. The energy consumption of the hydrogen compression from 13.8 bar to 250 bar is assumed to be 3.5 kWh/kg H_2 [92, 93]. The energy consumption of 2-step RO desalination is 3.3 – 4 kWh/ton water [73], as stated in subchapter 2.4.6, and is further assumed to be 3.6 kWh/ton water.

4.1.1. In-turbine electrolyser operation

In this subchapter, the operation of the in-turbine hydrogen production system is explained. The system is assumed to have two operating modes, on or off. The electrolyser will either be in standby mode or operate at the rated load. The control of this system will monitor the power generation from Zefyros; when power generation from Zefyros is below the system's power consumption, the electrolyser is set to its standby mode, and the other components, desalination and compression, are switched off. When the power generation from Zefyros exceeds the system's power consumption, the hydrogen production system is started. This is shown in formula 61 in subchapter 3.1.3.

A battery is implemented in the system to cover the energy consumption of the electrolyser in standby mode to ensure rapid response to load changes. The load response of the electrolyser is further assumed to be instant. If the battery is not at its full capacity, the battery is charged by surplus energy generated by Zefyros after powering the hydrogen production system. The remaining energy after charging the battery is exported to the grid by its export cable. Figure 28 shows the operating modes for the year 2020, where 1 is on and 0 is off.

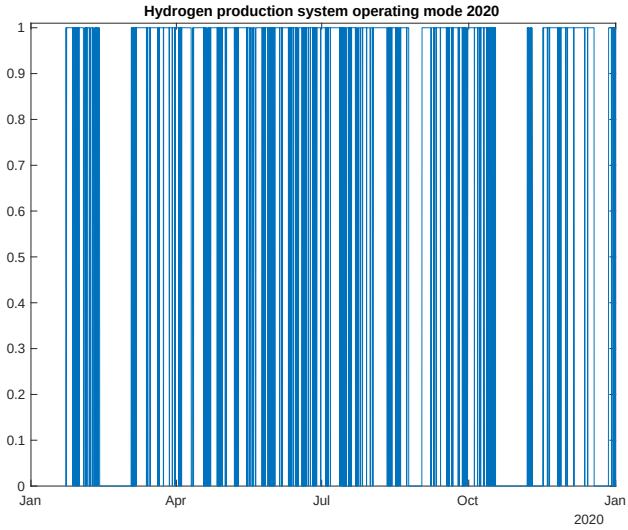

Figure 28: Alternation of operating mode UNITECH Zefyros 2020, 1 is on, 0 is off

As seen in Figure 28, the operating mode of the hydrogen production system alternates very frequently in 2020. To better illustrate the changes in operating mode, the operating modes for June are shown in Figure 29. June is chosen due to its high frequency of alternating the operating mode.

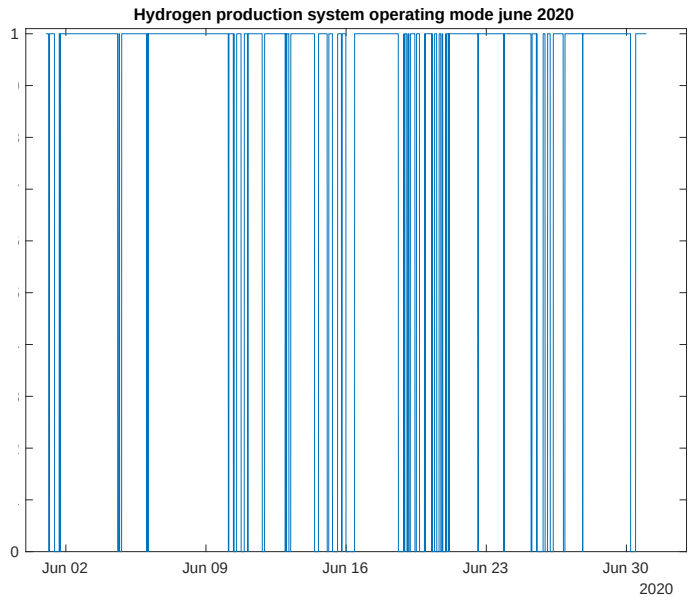

Figure 29: Alternation of operating mode UNITECH Zefyros June 2020, 1 is on, 0 is off

In Figure 29, the operating mode is shown to switch from on to off often in June, especially around the 20th of June. This may present a problem due to the start-up time of the electrolyser. The operating modes during the 20th of June 2020 are shown in Figure 30 to review this.

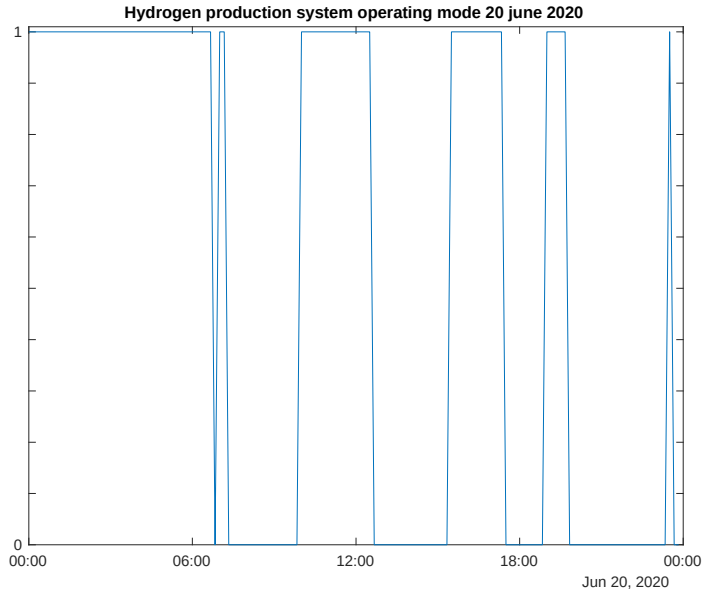

Figure 30: Alternation of operating mode UNITECH Zefyros June 20th of 2020, 1 is on, 0 is off

In Figure 30, between 6 o'clock and 12 o'clock, the hydrogen production system changes operating modes four times, where three of the operating mode changes are within 40 minutes of each other.

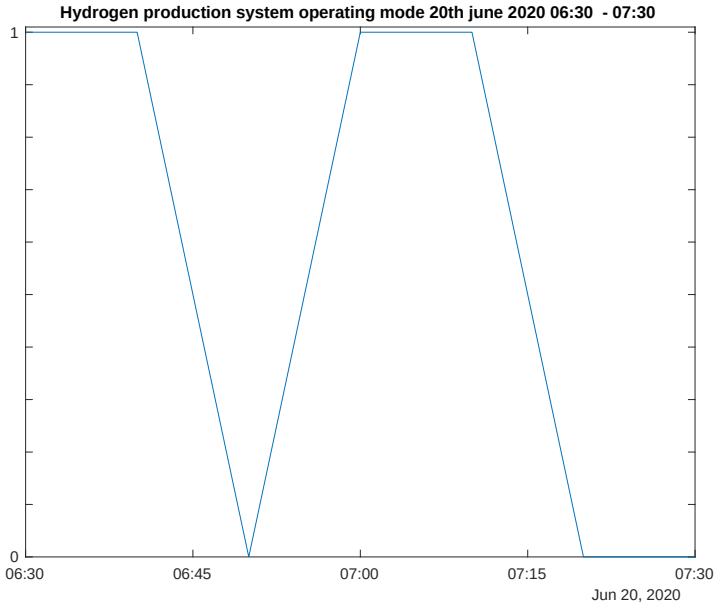

Figure 31: Alternation of operating mode UNITECH Zefyros 20th of June 2020 between 06:30 and 07:30, 1 is on, 0 is off

In Figure 31, the hydrogen production system switches from off at 06:50 to on at 07:00. As mentioned, the start-up time of a PEM electrolyser is approximately 15 minutes [64]. This shows the need for short-term energy storage to supply the standby load of the electrolyser. The start-up time in standby mode is significantly shorter, less than 10 seconds [132]. However, since the sampling interval in the provided dataset is 10 minutes, the start-up time is assumed to be instant when on standby. The short-term energy storage is assumed to be a battery with a capacity of 5 kWh and an assumed *Depth of Discharge*, DoD of 80 %. A 5 kWh battery was found suitable through an iterative process. The battery's *State of Charge*, SoC, during 2020 is shown in Figure 32.

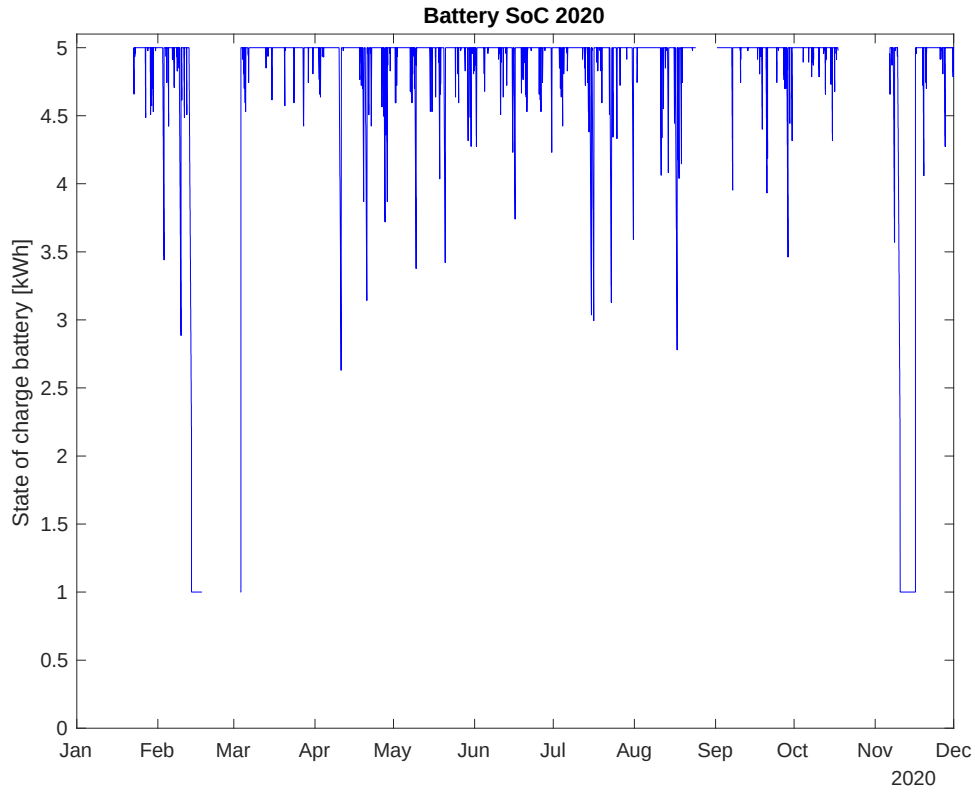

Figure 32: Battery State of Charge, SoC 2020 [kWh]

In Figure 32, the battery's SoC is within approximately 3 kWh most of the year. In the more extended periods of no production, such as in the month change February to March and in November, the SoC reaches the DoD. It is assumed that in the periods of downtime, the SoC of the battery is equal to the last sample before shutdown. The battery would experience self-discharge [148]; however, this is assumed to be negligible due to the low capacity of the battery. Hence, it is not included in the estimation of the battery SoC.

The sum of the hydrogen production for every 10-minute sampling interval yields the hydrogen production in 2020 to be 581 kg hydrogen.

4.1.2. Zefyros' hydrodynamic response

A model is developed in DNV Sesam to identify the displacement and acceleration in heave, roll, and pitch the in-turbine electrolyser would experience at Zefyros. No research has been found on how displacement and acceleration affect the electrolyser and the other components in a hydrogen production system. The methodology is then to identify the displacement and acceleration the in-turbine electrolyser from case 1 would experience for a potential electrolyser supplier to review their component for compatibility.

Given the symmetry of the spar buoy foundation of Zefryos, pitch and roll motion characteristics are identical [54]. This is shown in Figure 33, extracted from the results in Postresp.

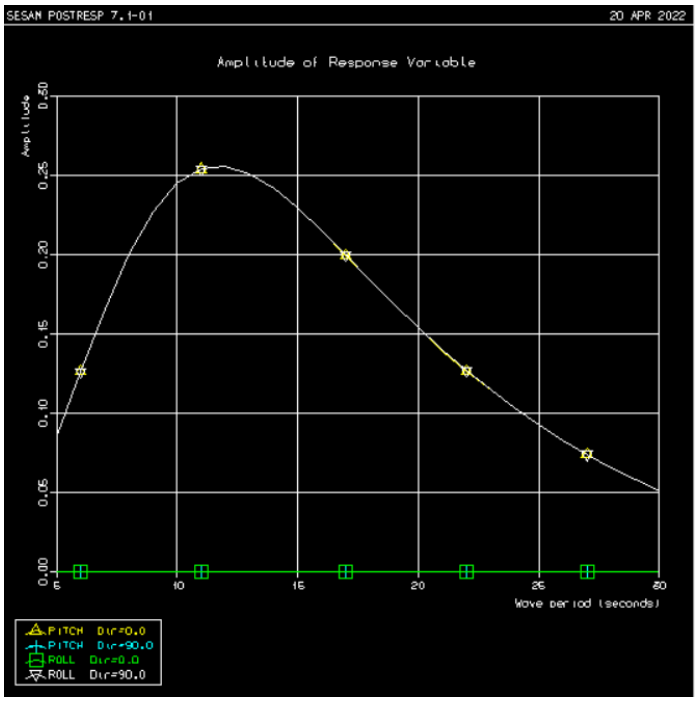

Figure 33: Amplitude of pitch and roll responses as a function of wave period

As seen in Figure 33, the amplitude of the pitch response when the incoming wavefield is at 0° is identical to the amplitude of the roll response when the incoming wavefield is at 90°. Hence, only the pitch response is presented in the thesis' results. In the Sesam model, the direction of the wave field that yields the largest response in pitch and heave is further processed in Postresp. The short-term statistics of the displacement and the acceleration in heave and pitch are calculated in DNV Sesam for two different return period seas, described in subchapter 3.1.3.

The most probable maximum displacement and acceleration in heave and pitch in a sea with 1-year return period are shown in Table 11.

Table 11: Heave and pitch response in a sea with 1 – year return period

Degree of freedom	Displacement		Std.dev displacement	Acceleration		Std.dev acceleration
Heave	1.329	[m]	0.363	0.3109	[m/s^2]	0.0840
Pitch	0.5874	[deg°]	0.1587	0.2024	[deg°/s^2]	0.0536

The most probable maximum displacement and acceleration in heave and pitch in a sea with 10-year return period are shown in Table 12.

Table 12: Heave and pitch response in a sea with 10 – year return period

Degree of freedom	Displacement		Std.dev displacement	Acceleration		Std.dev acceleration
Heave	1.7890	[m]	0.4921	0.3684	[m/s^2]	0.0098
Pitch	0.7011	[deg°]	0.1903	0.2172	[deg°/s^2]	0.0576

4.1.3. Storage

The amount of compressed gaseous hydrogen that can be stored at one time at UNITECH Zefyros is limited by the space available at the turbine for storage. It is assumed that a volume is available at the main platform for storing the hydrogen of 2 x 2 m x 6 m.

As stated in chapter 2.6, the hydrogen gas is assumed to be stored at 250 bar. The density of the hydrogen gas is then approximately 23 kg/m^3 [149]. This means 25.6 m^3 is the necessary storage volume for the annual hydrogen production from the in-turbine electrolyser. This required storage volume is only the volume of hydrogen produced; the volume of the tanks and other components must be added. Hexagon Type 4 pressure vessels, Hexagon Purus [101], are assumed to be utilized for storing the hydrogen at 250 bar. Type I pressure vessels could be used to cut costs. However, due to the lack of specifications available on such pressure vessels at the assumed storage pressure and the fact that economics is not in the scope of this thesis, the Hexagon Purus is assumed to be used. The capacity of a Purus pressure vessel is 27.8 kg. The shape of the pressure vessel is cylindrical, and it has a length of 5689 mm and a diameter of 653 mm [101]. The use of Hexagon Purus pressure vessels results yields a 3 x 3 matrix to store the compressed hydrogen, considering the assumed available space for storage. The capacity of the storage is 250.2 kg hydrogen. This means that the hydrogen tanks must be emptied three times within 2020, given that the estimated hydrogen yield in 2020 is 581 kg hydrogen. It is assumed that the storage tanks and the hydrogen compressor are placed in an area protected from environmental factors, such as waves, sea spray, and rain. The area must be closed off from the atmosphere to achieve this.

4.1.4. Components, materials, and safety

In this subchapter, the auxiliary systems, materials, and safety measures for the in-turbine hydrogen production are reviewed. Materials' and components' compatibilities in an offshore environment are assessed.

The Nel S series electrolyser is in essence a plug-and-play system. This means that the electrolyser can be installed easily in a few hours, although this is meant for land-based

installations [130]. The NEL S series electrolyser has integrated several integrated components including a heat exchanger, hydrogen gas dryer, hydrogen phase separator, oxygen phase separator, de-ionized water polishing bed, water pump, and hydrogen gas detector [130]. In "Evaluation of materials and components degradation of a PEM electrolyzer for marine applications" A. Di Blasi *et al.* [150], an experiment was performed to investigate the degradation of the components in a PEM electrolyser in marine applications. Desalinated and de-ionized seawater was used as the water feedstock for the electrolyser. Corrosion tests were also performed in a corrosive environment to simulate the offshore environment. The results stated that no significant reduction in performance was shown using desalinated water as the feedstock, and no evidence of poisoning, sodium and chlorine, was caused by the marine environment. No notable degradation of materials in the PEM electrolyser due to corrosion was shown. [150]

The desalination unit is assumed to require a water pump and a water tank. A water tank can be used as a storage of purified water for the electrolyser. The water consumption of the electrolyser is 10.1 kg water/ kg H_2. Since the hourly hydrogen production from the electrolyser is approximately 0.1 kg H_2/h, the hourly water consumption is 1.01 kg water/h. Considering this low water consumption, the energy requirement of the pump that shall lift the seawater to the desalination unit is assumed negligible.

Low output hydrogen compressors may be air-cooled [151], which eliminates any potential extra water consumption for cooling. The energy requirement for cooling is assumed to be included in the assumed energy consumption of the compression from 13.8 bar to 250 bar at 3.5 kWh/kg [92].

To account for the successful use of materials for the storage and components in the in-turbine hydrogen production system, hydrogen embrittlement, hydrogen attack, and hydrogen permeation must be considered [91]. The selection of materials for the system is based on the industry standard for hydrogen handling. These materials are further reviewed for compatibility with an offshore environment.

Oxygen-free copper is normally used for hydrogen piping at lower pressures for hydrogen distribution, and copper alloys for equipment for hydrogen storage such as a braze material and for equipment such as valves [91]. The permeability of hydrogen through copper is very low, lower than austenitic stainless steel [152]. Copper shows less resistance to electrochemical

corrosion from seawater than its alloys [153]; however, the inside of the turbine tower is separated from the marine environment, and it is assumed that no notable elevated salt-rich atmosphere occurs. For sealing and lining of components, typically, non-metallic materials are used. These materials could be in direct contact with hydrogen gas and must withstand mechanical and thermal loads. Filling and emptying the storage tanks results in temperature changes in the stored hydrogen: - 40 ℃ during emptying and 90 ℃ during filling [91], and are challenging conditions for the sealing material to withstand [91]. For storage of the hydrogen, Hexagon Purus is assumed to be used. The Purus pressure vessel is a glass-fiber/carbon-fiber composite with a plastic inner lining [154]. In the journal article "Evaluation of mechanical properties and morphology of seawater aged carbon and glass fiber reinforced polymer hybrid composites" D. K. Jesthi and R. K. Nayak [155], an experiment is performed to review the mechanical properties of seawater aged glass fiber/carbon fiber composites. The materials were immersed in seawater at room temperature for 90 days. Seawater immersion may be relevant to consider for the storage onboard Zefyros. The highest registered wave at the site is 19 m, submerging the main platform at Zefyros. The article [155] concluded that glass fiber/carbon fiber composite materials are applicable in an offshore environment.

Regarding safety, an in-turbine electrolyser is not a tested method. In the Lhyfe hydrogen project, DNV will perform a study to identify the main risk of offshore hydrogen production [128]; however, this is for an electrolyser placed on an offshore platform, not inside the turbine tower [156]. The paragraphs below present what are deemed as safety risks introduced by an in-turbine electrolyser.

Hydrogen gas is lighter than air. In case of a potential leak, the hydrogen gas would rise inside the turbine tower to escape through the nacelle or accumulate inside the tower and nacelle structure. Hydrogen has, as mentioned, low ignition energy and a wide flammability range [90]. In the nacelle, electrical equipment or heat released from components may ignite the hydrogen. In addition to the grounding of the system to avoid sparks, it is suggested that the electrolyser is located close to a hydrogen exhaust ventilation fan, which is a product available on the market [157]. This also applies to the area where hydrogen storage and compressor are placed. In case of a leak, it must be possible to vent the room to avoid the accumulation of hydrogen. The in-turbine electrolyser will experience the same displacements and acceleration as the turbine, as described in subchapter 4.1.2. This may cause a problem by the mixing of the product gasses, hydrogen and oxygen. This is relevant both for the phase separator and inside the electrolyser

itself. No research has been found that proves this, but it is deemed as likely that an electrolyser that experiences accelerations would have an increased risk of product gas mixing. The flammability range of hydrogen, 4.1 – 74.8 vol% [90], would mean that the mixing of product gasses increases the risk of explosions. Gas mixing also decreases the energy efficiency of the electrolyser [66].

Hydrogen gas detectors should be placed near areas more likely to experience leaks, such as valve stems and connections or couplers. Gas detectors should also be placed in the nacelle of the turbine since hydrogen gas is lighter than air and would rise inside the turbine. Catalytic bead detectors are recommended as gas detectors for hydrogen [126]. Hydrogen flame detection is necessary to identify and locate a potential hydrogen flame. Flame detectors should be placed close to the electrolyser, hydrogen-containing pipes, and connections. Flame detectors should also be placed in the nacelle due to the risk of hydrogen accumulation in the nacelle. Multiple IR flame detectors are best suited for hydrogen application [126]. All components in the in-turbine hydrogen production system must be Ex-certified and marked according to the regulation "Forskrift om utstyr og sikkerhetssystem til bruk i et eksplosjonsfarlig område" [125].

4.1.5. Utilization of produced hydrogen and transportation

The small amount of hydrogen produced from the in-turbine hydrogen production limits the potential end-users of the produced hydrogen. 250 kg hydrogen, the proposed storage capacity at Zefyros, is 8.33 MWh. *Marine Gasoil*, MGO, is a commonly used fuel in the maritime sector. 8.33 MWh translates to approximately 0.833 m^3 MGO [158]. A general purpose vessel, a tanker transporting refined fossil products, typically carries 12 000 – 30 000 m^3 MGO in its fuel storage [159]. This means that for the in-turbine hydrogen production from Zefyros, it is not feasible for use as a bunkering station or fuel supply for potential future hydrogen-powered vessels in the North Sea. A potential end-user of the hydrogen produced at Zefyros would be research and test centres nearby. At Stord, there is a test facility for hydrogen-powered maritime engines and fuel cells 90 km from Skudeneshavn, where Zefyros is located [10]. UNITECH's R&D centre at Bømlo, 100 km from Zefyros, may also be a potential end-user of the hydrogen [160].

For the bunkering solution, two methods are seen as feasible; compressing the gas from storage at Zefyros onto a vessel or container swapping. Pressure balancing is not deemed feasible due

to the required extra storage volume onboard the turbine. The choice of the bunkering technology must be seen in context with the potential consumers and the amount of hydrogen produced. It would be possible to transport the hydrogen from Zefyros to Bømlo using a ship. A *Crew Transport Vessel*, CTV, is used when UNITECH is performing service or installations at Zefyros. This same CTV could be used to transport the hydrogen to Bømlo.

Performing container swapping, the hydrogen storage at Zefyros would have to be lifted from the main platform, 17 m above the still water level. The height and the fact that both the CTV and Zefyros would move in the six degrees of freedom would make the container swapping process difficult. For compressing the stored hydrogen from Zefyros onboard a ship, a compressor, a hose, and hydrogen storage at the ship are necessary. The expected heave and pitch responses of Zefyros are identified in subchapter 4.1.2. The heave motions of the CTV would follow the wave height. Considering this, the location of the CTV during pressure balancing could be determined along with the length of the hose required for the process.

A product not mentioned prior to this is the oxygen also produced from water electrolysis. Oxygen is a product used in several industries such as the steel industry, chemical processing, and health services [161]. A potential consumer of oxygen that may become relevant in the case of offshore hydrogen production is fish farms. To reduce the scope of the thesis, oxygen production and identifying potential end users are not further considered.

4.2. Case 2: Large-scale hydrogen production

In this chapter of the thesis, the results of the model developed for case 2 are presented. The large-scale hydrogen production system of case 2 is dimensioned to facilitate for all the power generated from Zefyros being used for hydrogen production, thereby not considering the space constraints stated by UNITECH [129].

The large-scale hydrogen production is designed to illustrate the wind energy and electrolysis interaction. In chapter 4.1, the in-turbine hydrogen production system, case 1, has two operating modes, on or off. The rated power of the electrolyser in case 1 is small compared to the Zefyros' rated power. As long as the turbine generates power, the electrolyser will operate at its rated load. In the large-scale hydrogen production system, case 2, an electrolyser with a much larger rated power is proposed. The rated power of the electrolyser is assumed to be 2.3 MW to be able to use all energy converted from Zefyros for hydrogen production. Since UNITECH Zefyros' rated power also is 2.3 MW, the load profile of the electrolyser would be dynamic. By dynamic, it is meant that the load percentage of the electrolyser changes over time depending on the power output from the turbine.

A PEM electrolyser has higher energy efficiency when operated below its rated load [72]. This is illustrated in Figure 34, where data is extracted from "Current status of water electrolysis for energy storage, grid balancing and sector coupling via power-to-gas and power-to-liquids: A review", Buttler and H. Spliethoff [162].

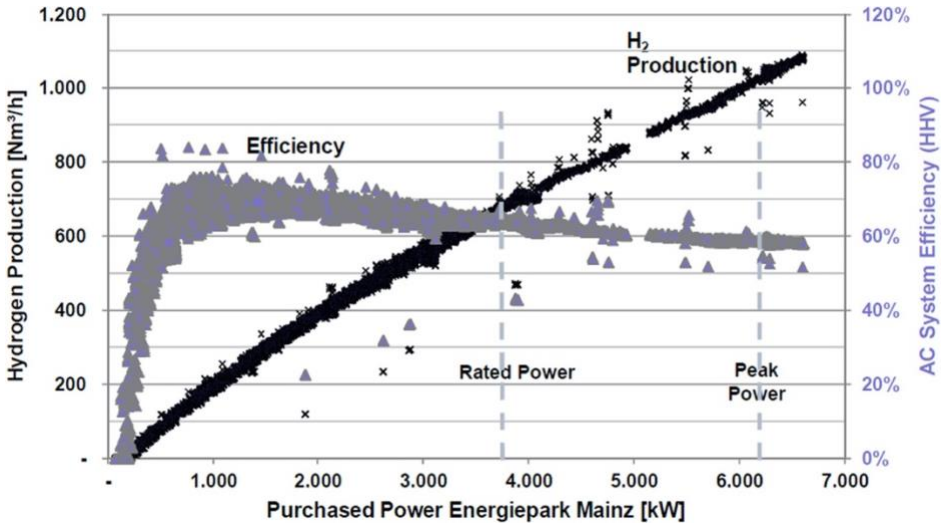

Figure 34: Hydrogen production [Nm^3/h] and system efficiency as a function of power consumption [kW], Siemens PEM electrolysis system Energiepark Mainz [162]

Figure 34 shows that the maximum energy efficiency of the PEM electrolyser occurs at around 15 – 20 % of the rated load. In [162], it is stated that the efficiency curve of the PEM electrolyser includes losses from all energy consumers. That includes compression, cooling, purification, and control of the PEM electrolysis system at Energiepark Mainz [162]. The system's efficiency is calculated based on electrical energy consumption and the higher heating value of hydrogen [162]. Also shown in Figure 34 is that while the PEM electrolyser has higher energy efficiency in part-load, the hydrogen production increases approximately linearly with the load. [162].

4.2.1. Model results and validation

In this subchapter, the results from the developed model for case 2 are presented and compared with results in a relevant research article to validate the developed model.

The polarization curve of the modelled electrolyser in case 2 is shown in Figure 35. The cell voltage is divided into its contributors; activation overpotential, concentration overpotential, open circuit voltage, and ohmic overpotential. The figures in this subchapter start with a current density of 0.015 A/cm^2 due to occurring problems in the model when using values below this threshold and stop at the electrolyser's assumed rated current density of 2 A/cm^2.

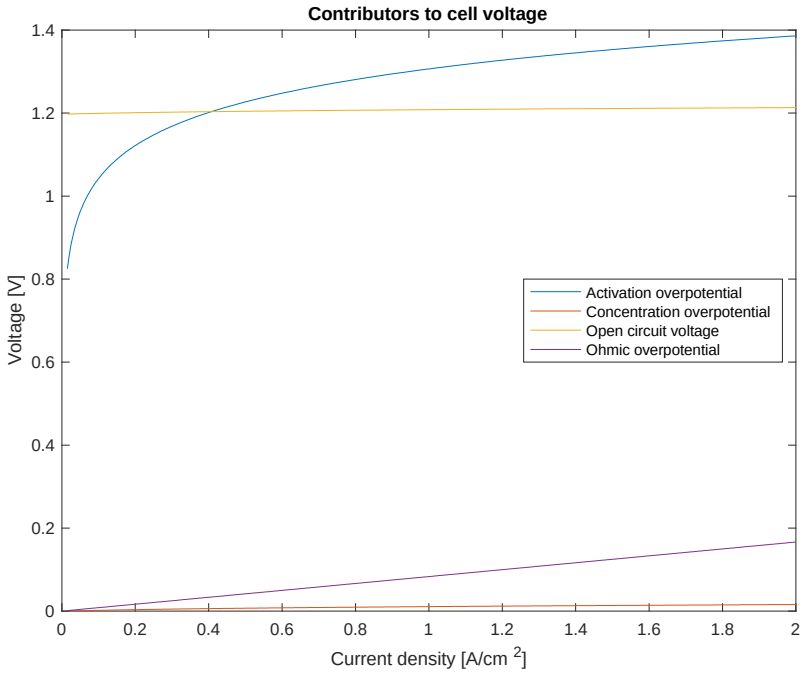

Figure 35: Cell voltage contributors [V] as a function of current density, [A/cm^2]. Temperature assumed constant at 60 °C. Activation overpotential (blue), Concentration overpotential (red), Open Circuit voltage (yellow) and Ohmic overpotential (purple).

In “Modelling and simulation of a proton exchange membrane (PEM) electrolyser cell”, Z. Abdin, C. J. Webb, and E. M. Gray, [44], the cell voltage contributors are presented as a function of current density with a rated current density of 1.2 A/cm^2, an operating temperature of 55 ℃, and a cathode pressure of 10 bar. The thesis’ model assumes an operating temperature of 60 ℃, a rated current density of 2 A/cm^2, and a cathode pressure of 30 bar. The parameters used in [44] are not necessarily the same as used in the model of this thesis. In the paragraphs below, results from [44] are compared to the results from Figure 35. When mentioning the article, it is referred to the journal article “Modelling and simulation of a proton exchange membrane (PEM) electrolyser cell” [44]. The voltages used to compare the article’s and the thesis’ results are the mentioned voltages values at a current density of 1.2 A/cm^2.

The *Open Circuit Voltage*, OCV, in the article is around 1.2 V. In Figure 35, the OCV is also around 1.2 V. The same formula is used for estimating the OCV in the thesis and the article, seen in formula 32. The activation overpotential in the thesis is higher compared to the article, 1.3 V and approximately 0.8 V, respectively. The same formula is used for both the thesis and the article, seen in formulas 39 and 40. However, the parameters used to calculate the activation overpotential in the thesis and the article are different. This is shown in Table 13. [44]

Table 13: Comparing parameters used for estimating activation overpotential of thesis and article [44]

Parameter	Thesis	Article [44]
α_{anode}	0,5	0,8
$\alpha_{cathode}$	0,5	0,25
$i_{0,anode}$	$1{,}3 * 10^{-7}$	$1 * 10^{-7}$
$i_{0,cathode}$	$1 * 10^{-3}$	$1 * 10^{-3}$

The concentration overpotential has a small contribution to the cell voltage, approximately 0.01 V in both the thesis and the article. The same formula is used in both the thesis and the article, seen in formula 45. However, in the thesis, a simplification is made. It is assumed that the concentration of the product gas is equal to the partial pressure of the product gas, divided by the pressure at the respective electrode subtracted by the water saturation pressure at this electrode.

The ohmic overpotential is in the article divided into ohmic overpotential from the electrodes, the flow field plates, and the PEM, where the PEM has the highest contribution to the ohmic overpotential [44]. The contribution of the ohmic overpotential to the cell voltage is small, around 0.15 V in the thesis and around 0.2 V in the article. In the thesis, only the ohmic

overpotential from the PEM is included. Therefore, the ohmic overpotential is higher in the article than in the thesis. The same formula is used to estimate the ohmic overpotential in the thesis and the article, seen in formula 42. The water content in the membrane, λ_{mem}, is the same in the thesis and the article. The membrane thickness is higher in the article than in the thesis; 0.0254 cm and 0.0127 cm respectively, explaining why the ohmic overpotential is higher in the article.

To reduce the scope of the thesis, the operating temperature of the electrolyser in case 2 is assumed to be constant at 60 ℃. It is important to know how the operating temperature influences the cell voltage and, therefore, the energy efficiency of the electrolyser. In Figure 36, the electrolyser polarization curve is shown for two different operating temperatures; 60 ℃ and 80 ℃.

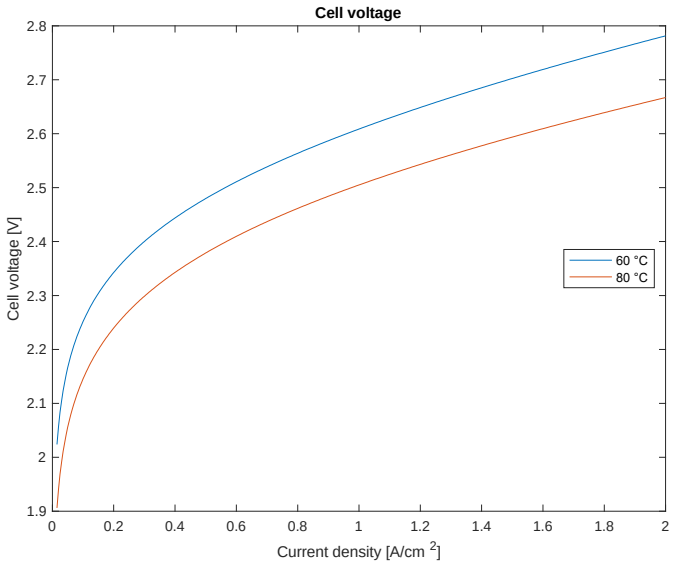

Figure 36: Cell voltage [V] with temperature of 60 ℃ (blue) and 80 ℃ (red) as a function of current density, [A/cm^2]

In Figure 36, it is shown that the cell voltage decreases with increasing temperature. This can be related to Figure 10, where the electrical energy required for electrolysis decreases with temperature.

In Figure 37 below, the energy efficiency of the electrolyser is shown as a function of current density. The energy efficiency is estimated by the cell voltage, shown in formula 48. The hydrogen production rate is also shown as a function of current density to illustrate that the production rate increases with the current density even though the energy efficiency decreases.

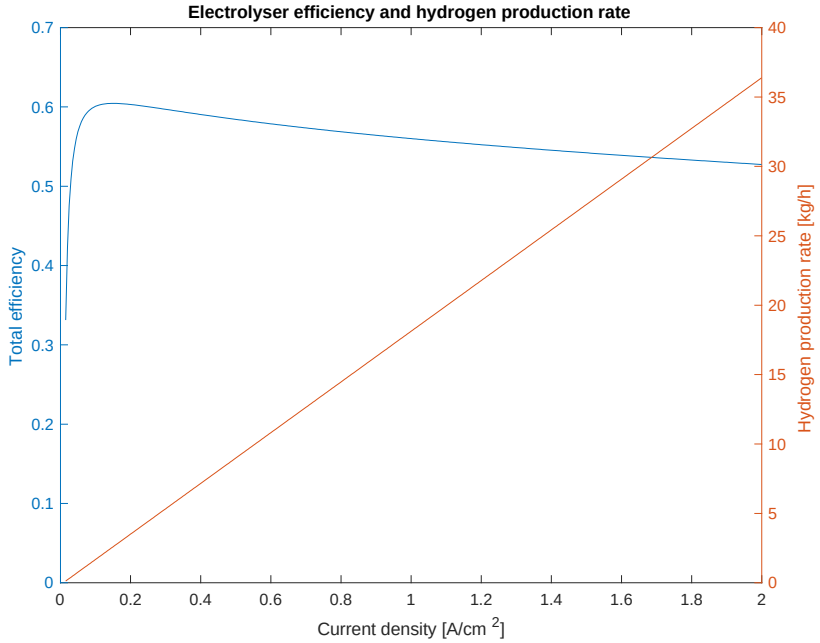

Figure 37: Electrolyser energy efficiency and hydrogen production rate [kg/h] as a function of current density [A/cm^2]

As seen in Figure 37, the electrolyser's energy efficiency increases rapidly up to 0.15 A/cm^2 followed by a steady decrease with increased current density, while the hydrogen production rate increases with increased current density. This result correlates with the PEM electrolyser from Energiepark Mainz shown in Figure 34 [162]. To illustrate how the efficiency affects the hydrogen production rate, the modelled hydrogen production rate with the estimated efficiency from Figure 37 is shown in Figure 38 as a function of current density along with the hydrogen production rate with 100 % efficiency.

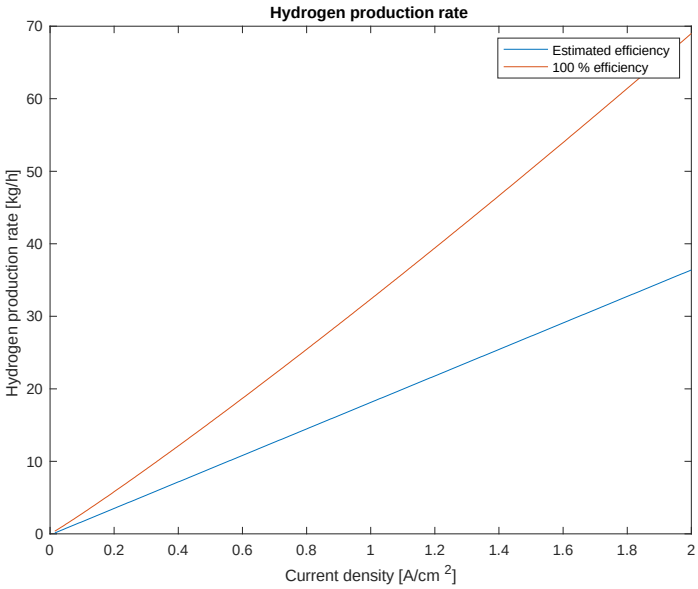

Figure 38: Hydrogen production rate [kg/h] with estimated energy efficiency (blue) and 100 % efficiency (red) as a function of current density, [A/cm^2]

4.2.2. Electrolyser efficiency and hydrogen production

In this subchapter, the dataset provided by UNITECH [53] is used to estimate the hydrogen production from the assumed 2.3 MW PEM electrolyser in case 2, using the developed model presented in subchapter 3.1.4.

The input of the model is the power delivered by Zefyros, $P_{Zefyros}$. $P_{Zefyros}$ is used to estimate the input current density, shown in formula 67 in subchapter 3.1.4. In the SCADA dataset from Zefyros [53], the power is negative during periods of no production. This is because of various components' power demand while the turbine is not in production. Negative values are not applicable in the model hence, negative values are set to zero. The input current density in 2020 is shown in Figure 39.

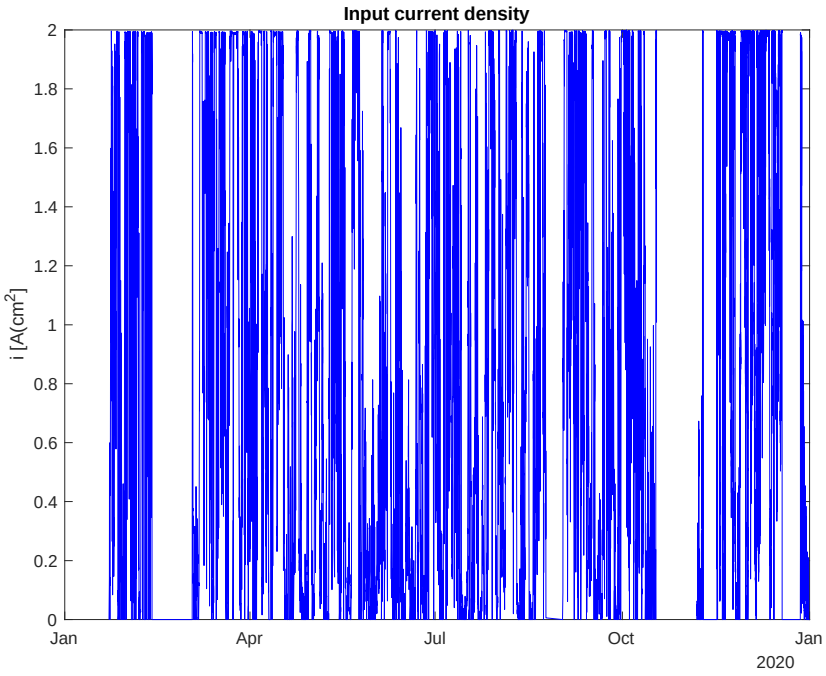

Figure 39: Input current density in 2020, [A/cm^2]

The gaps in measurements in Figure 39, such as between February and March, are due to no available data in the provided dataset. This also applies to the remaining figures in this subchapter. From the current density, the cell voltage is estimated by the sum of the open-circuit voltage and the three overpotentials, shown in formula 31. Using the cell voltage, the energy efficiency of the electrolyser throughout 2020 can be estimated. This is shown in Figure 40.

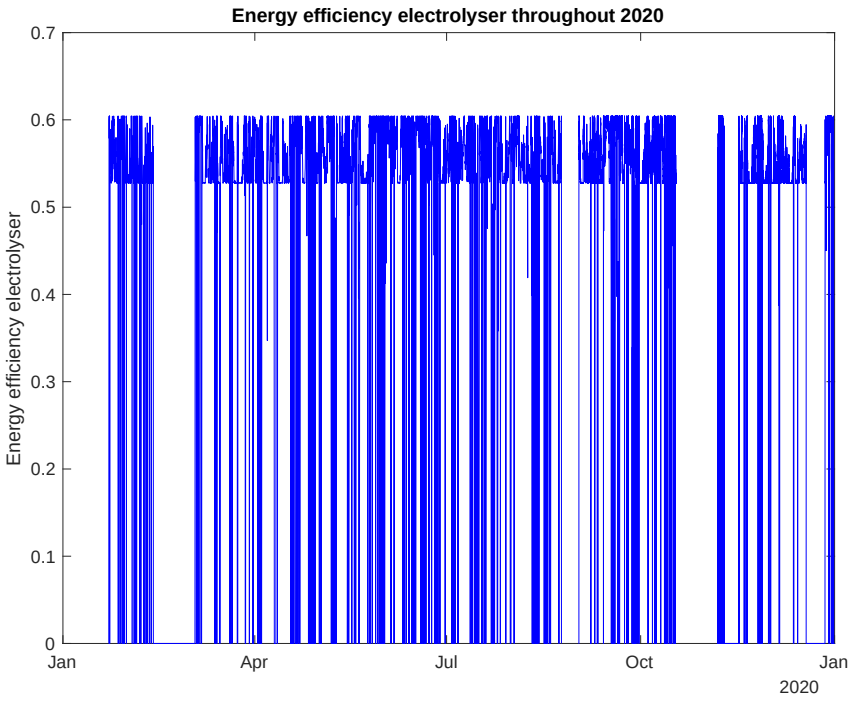

Figure 40: Electrolyser energy efficiency throughout 2020

The electrolyser's energy efficiency in June is shown in Figure 41 to illustrate the variability of the energy efficiency more clearly. The figure also shows the input current density in June 2020 to display how the current density, or the load, affects the electrolyser energy efficiency.

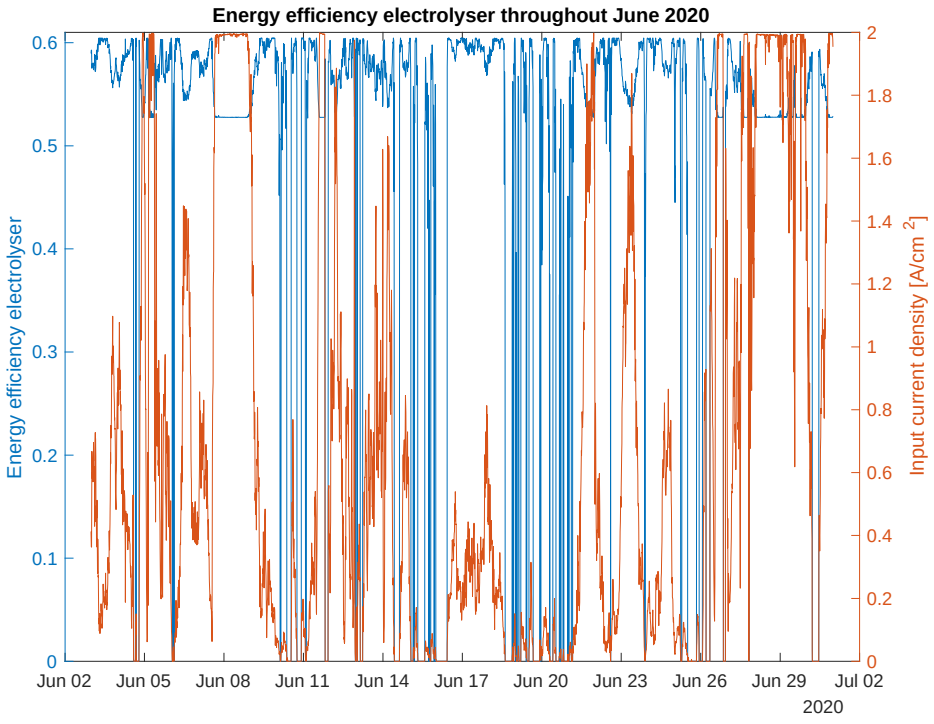

Figure 41: Electrolyser energy efficiency (blue) and input current density (red) [A/cm^2] in June 2020

When the current density is at its rated value, the energy efficiency of the electrolyser is at its lowest. This is more clearly shown in the period between the 7th to the 9th of June, in Figure 42 below.

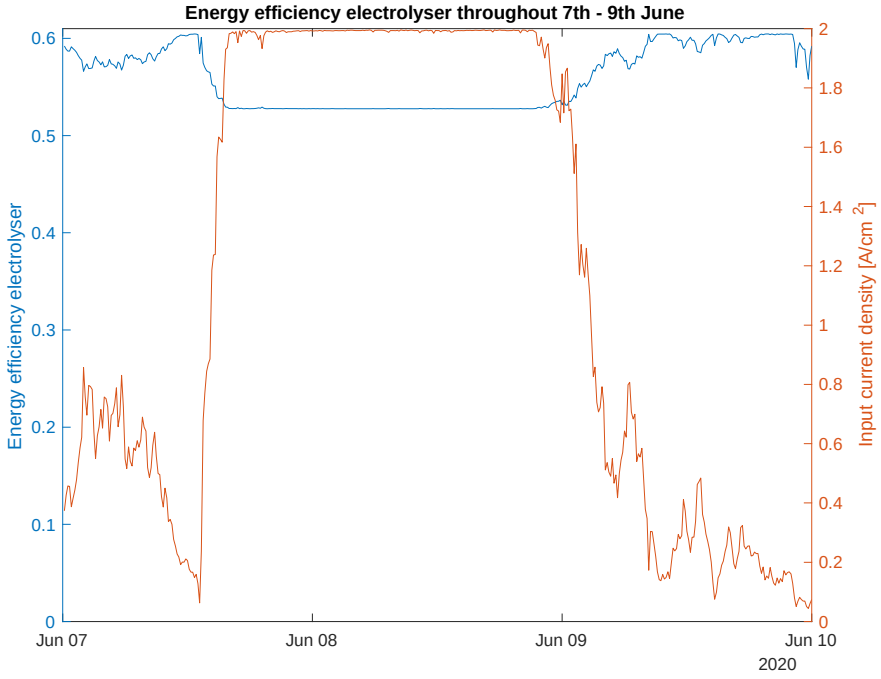

Figure 42: Electrolyser energy efficiency (blue) and input current density (red) [A/cm^2] 7th to 9th of June 2020

Using the electrolyser energy efficiency, the hydrogen production rate can be estimated by formula 68. This is shown in Figure 43.

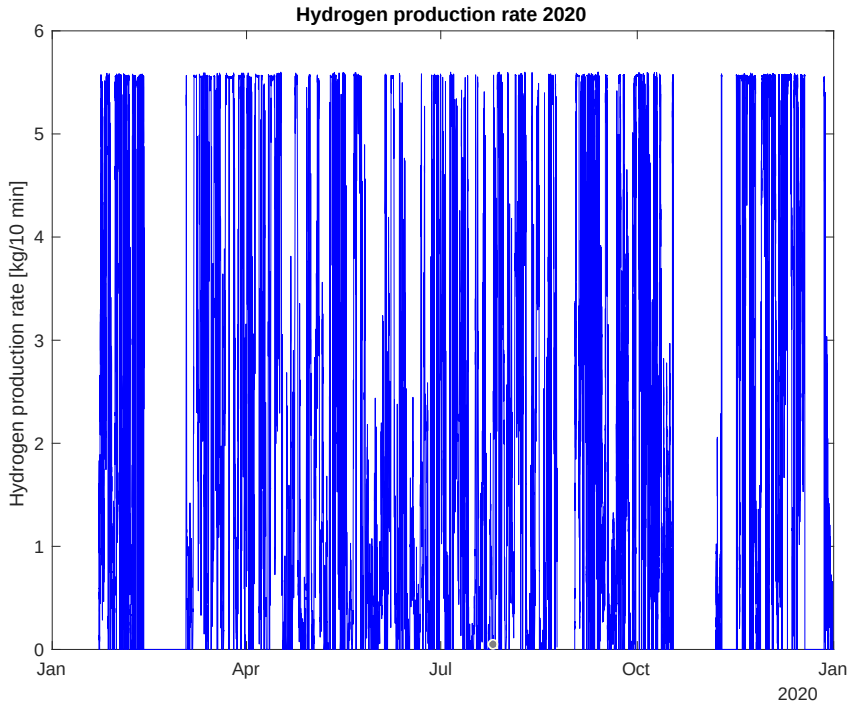

Figure 43: Hydrogen production rate 2020 [kg/10 min]

The cumulative sum of the hydrogen production rates for every 10-minute sample yields the accumulated hydrogen in 2020. This is shown in Figure 44.

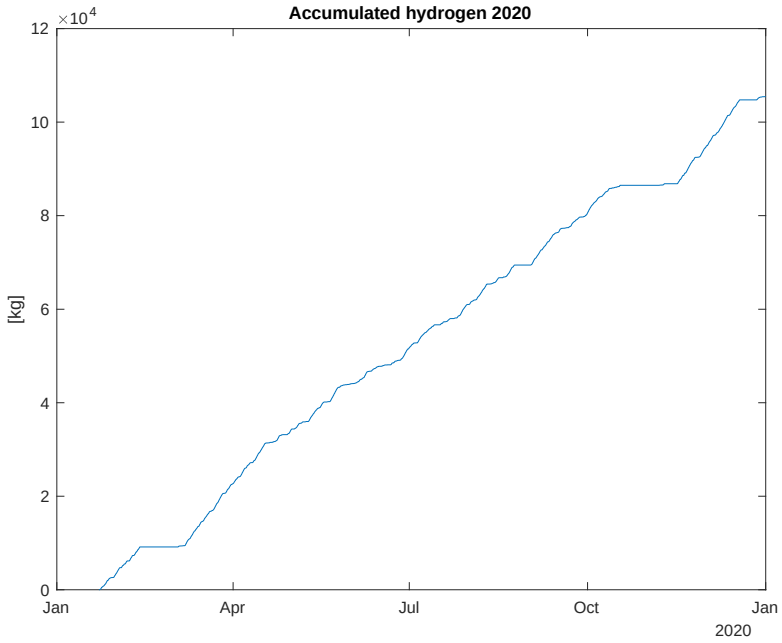

Figure 44: Accumulated hydrogen 2020 [kg]

By the end of the year 2020, the accumulated hydrogen is 110830 kg hydrogen. To compare, the hydrogen yield from the large-scale hydrogen production system powered by a constant power source at 2.3 MW, such that it would operate at its rated load throughout 2020, would be 318780 kg. The average energy efficiency of the electrolyser modelled in case 2 is 44.5 % in 2020. The maximum energy efficiency of the electrolyser, occurring at 0.15 A/cm^2, is 60.5 %.

5. Discussion

In this chapter, the methodology and results of the thesis, along with any assumptions and simplifications, are discussed. The value of the results to UNITECH is discussed, and the research questions raised in the introduction chapter are discussed.

5.1. SCADA dataset

The provided dataset [53] has a sample rate of 10 minutes or 1.67×10^{-3} Hz. The values of the measured variables in between the 10-minute samples are unknown. In the thesis, the values of the variables are treated as constant for the 10-minute duration until new measurements are available. A more representative method would be to use linear interpolation between the sampled values, thus, manipulating a higher sampling frequency of the dataset. Figure 45 is made to illustrate the different methodologies.

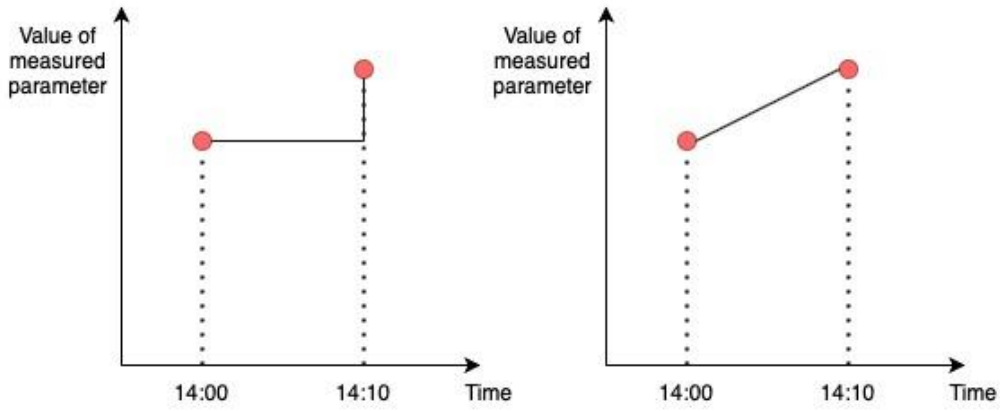

Figure 45: Methodologies of treating the provided dataset. To the left; As used in the thesis, treating a value as constant during the sampling interval. To the right; linear interpolation between the measured parameters in the dataset.

Linear interpolation would better represent the variability of the power generation from a wind turbine compared to the methodology used in this thesis; if the sampling frequency of the data was manipulated. By having a data value of the used parameters every second instead of every 10 minutes, the estimation of hydrogen yield and efficiency would better represent what could be expected in a real-life implementation. Due to the additional data that had to be included in the model, hardware limitations, and time restrictions, the sampling frequency is not manipulated. The data is then treated as shown in Figure 45 to the left; the value of a sample is treated as constant for the 10-duration. For the in-turbine electrolyser this means that for the state of the operation mode at a given time, it is assumed that it stays in the same operation mode for the 10-minute duration until a new data sample is available. By doing this, the time required to run the simulations is minimized.

For the large-scale hydrogen production system, case 2, the load of the electrolyser estimated from the dataset varies less than it would in a real-life integration due to the sampling interval of the dataset. Thus, the estimated energy efficiency of the electrolyser also varies less. For cases 1 and 2, the load response time of the electrolyser when in standby, less than 10 seconds, cannot be included in the calculation due to the sampling frequency of the dataset. With a higher sampling frequency, the loss in hydrogen production due to the load response time from standby to operating mode could be included. New SCADA systems in wind turbines typically have a sampling frequency of 1 Hz [163]. This sampling frequency would show the variability of the measurement variables, such as the power generation, more accurately, thus, better representing the real-life case of the variables. With a higher sampling frequency, the data could be used for more detailed modelling, such as for the degradation of the electrolyser.

5.2. Case 1, in-turbine hydrogen production system

In this chapter, the method of estimating the hydrogen production of the in-turbine hydrogen production system, case 1, and the hydrodynamic response of the turbine is discussed, along with the result of these analyses.

5.2.1. In-turbine hydrogen production

For the in-turbine electrolyser, the space constraints stated by UNITECH have resulted in an electrolyser with a very low hydrogen production rate. The annual yield of the in-turbine electrolyser is 581 kg. This amount of hydrogen translates to approximately 19.4 MWh, which is the same amount of energy as eight and a half hours of production from Zefyros at its rated wind speed. When UNITECH had ambitions to perform hydrogen production at Zefyros, the annual hydrogen yield and the economics of such as concept were not their focus area. The in-turbine electrolyser was suspected to be used as a testing infrastructure available for third parties and to prove that in-turbine offshore hydrogen production was feasible; that the technology required to achieve this is readily available on the market. This thesis points to components that can be used in such a system, proving the technological feasibility of in-turbine electrolysis.

The proposed in-turbine hydrogen production system consists of three main components; the electrolyser, the compressor, and the desalination unit. These components must be powered according to their specifications regarding voltage and current. The power electronics required

for such a system are not considered in the thesis. Zefyros has a 230 V DC power supply inside the turbine, and it is assumed that it can supply power to the components included in the in-turbine hydrogen production system. The energy consumption of the electrolyser, compressor, and desalination unit is assumed to be constant per mass of product. This assumption is acceptable since the in-turbine electrolyser operates at a constant load when Zefyros converts enough power to cover the energy demand for the in-turbine hydrogen production system. When the electrolyser produces hydrogen, the compressor and the desalination unit will also operate at a constant load.

Zefyros was built in 2009 and is not designed for in-turbine hydrogen production. The limited space for an electrolyser inside the turbine tower shows this. In the thesis, challenges regarding the safety of an in-turbine electrolyser have been identified. Standards and regulations for in-turbine electrolysis do not exist, so a potential pilot project would have to go through an extensive process to ensure acceptable safety measures applied for such a system. DNV will perform a safety study of the main safety implications regarding offshore hydrogen production for the Lhyfe hydrogen project [128]. This project is planning for hydrogen production at an offshore platform. The DNV study most probably will identify several safety implications for hydrogen production at an offshore platform that also applies to in-turbine hydrogen production. Extensive modifications and the addition of new components would have to be performed at Zefyros. Another potential issue is for the existing and potential future inter-connected FOWT's at the MENCENTRE. They would have to receive guarantees that no increased risk of failure of their grid connection would occur by the addition of an in-turbine electrolyser at Zefyros. Insurance of the turbine would also prove a challenge in the case of in-turbine hydrogen production. These factors are potential project-stoppers and show that in-turbine hydrogen production at UNITECH Zefyros is deemed unlikely.

Hydrogen storage for the produced hydrogen from the in-turbine electrolyser is assumed to be compressed gaseous storage at 250 bar, stored in pressure vessels onboard the turbine. This assumption is made due to the low amount of hydrogen to be stored. For large-scale production of hydrogen from offshore wind farms, this would not be feasible due to the volume of the produced hydrogen. There are several alternatives for hydrogen storage in such a case. The Deep Purple concept by Technip FMC is planning to store compressed hydrogen at the seabed, with the water pressure adding to the storage pressure [17]. The hydrogen is stored at the site to be able to convert the hydrogen back to electrical energy, using fuel cells, in periods of no

production from the wind turbines. In this way, hydrogen can be produced when the electricity prices are low. Later the electrical energy can be sold when prices are high, improving the economic feasibility of offshore hydrogen production. Another storage method receiving increased attention is the storage of compressed hydrogen in salt caverns or depleted oil fields. Here, large volumes of compressed hydrogen can be stored without requiring pressure vessels.

The hydrogen produced by the in-turbine electrolyser at Zefyros is assumed to be sold. Another possibility would be to convert the hydrogen to electricity using fuel cells. In this way, the turbine can produce and sell electrical energy even if the wind turbine is not converting any energy. This is deemed infeasible in the thesis due to the low volume of hydrogen produced by the in-turbine electrolyser and the space constraints inside the turbine tower. The Lhyfe offshore hydrogen project [42] is planning to sell the hydrogen produced offshore, where the hydrogen shall be transported by pipelines onshore. In the thesis, the hydrogen produced by the in-turbine electrolyser is assumed to be compressed from its storage at Zefyros onboard a vessel. If the hydrogen produced at Zefyros was to be transported by hydrogen pipelines, a new subsea pipeline would have to be built and installed. Due to the low amount of hydrogen produced by the in-turbine electrolyser, this is seemed as infeasible.

5.2.2. Hydrodynamic model

Regarding special considerations of the offshore location at UNITECH Zefyros, the response of the turbine is studied. This thesis identifies Zefyros' response in heave, roll, and pitch. Zefyros would experience responses in all six degrees of freedom. Environmental factors, including waves, wind, and current, would all influence this response. In the thesis, only the heave, roll, and pitch responses of the turbine caused by the incoming wavefield are considered. Wind and current would further increase these responses. The response in yaw, surge, and sway is suspected to be relatively similar to the response in heave, pitch, and roll due to the symmetry of the turbine. The response of the turbine is estimated to identify the response the in-turbine electrolyser, case 1, would experience. No studies have been found on how displacement and acceleration would affect the electrolyser. Cross-correlation of the turbine's response to waves, wind, and current with potential hydrogen leaks, gas mixing, and the decrease of electrolyser efficiency would be an important area to better understand for future commercialization of an in-turbine electrolyser solution. Since the PEM electrolyser has a solid electrolyte, compared to the liquid electrolyte of the AE, it is deemed possible that movements affect the PEM electrolyser less than for AE. This is one of the reasons why PEM electrolysis is assumed to be

used in cases 1 and 2 of the thesis. The displacement and acceleration are deemed as possible to influence an in-turbine electrolyser in terms of mixing of the product gasses; oxygen and hydrogen. This would increase the risk of gas explosion and decrease the energy efficiency of the electrolyser [66]. Other considerations identified in the thesis are the increased possibility of corrosion of the materials and the electrical equipment that could ignite accumulated hydrogen.

5.3. Case 2, large-scale hydrogen production system

This chapter will discuss the modelling approach and the model's limitations for the large-scale hydrogen production system. Simplifications and assumptions mentioned in this chapter are made to reduce the number of electrolyser-specific design choices and narrow the thesis's scope.

Important to mention is the assumption that the operating temperature of the electrolyser in case 2 is constant. This is not accurate for a real-life application. Factors such as the operating load and ambient temperature would contribute to changes in the operating temperature. The change in electrolyser efficiency due to operating temperature is illustrated in Figure 36. For the electrolyser to maintain its optimal operating temperature, a cooling system must be implemented. This is not considered in the thesis. The cooling would increase the energy demand of the hydrogen production system, decreasing the amount of hydrogen produced. The electrolyser modelled in case 2 is not considering the start-up time from a non-operational state. It is thereby assumed that when in a non-operational state, the electrolyser is in standby mode. The pressure difference across the cells is assumed to be constant. This is done to reduce the number of variables in the model and a lack of relevant literature on PEM electrolysis modelling with variable cell pressure. The assumption of pressure in the cell, 1 bar at the anode and 30 bar at the cathode, was made because this is found to be a reoccurring operating pressure found in the relevant literature [45]. The end pressure of the hydrogen would change depending on the load of the electrolyser, increasing the energy demand for further compression if lower than 30 bar.

The energy consumption of the compressor and desalination unit is assumed to be constant per mass of product. This is not accurate for a real-life application. The compressor would have to follow the electrolysers load curve, in that the amount of hydrogen to be compressed changes depending on the input of hydrogen. Compressors have their own efficiency curves [164],

where the energy efficiency changes depending on the amount of gas to compress and to what pressure. This efficiency curve would influence the hydrogen production from the large-scale hydrogen production system in case 2. Assuming a specific energy demand per mass unit is feasible for the desalination process. Seawater can be desalinated at the rate that gives the optimal energy efficiency of the desalination unit, and the freshwater product can be stored for use at a later time. In the thesis, the estimated hydrogen production from the electrolyser is used as the input for estimating the energy consumption from the compressor and desalination unit. These energy consumptions are subtracted from the energy generated from Zefyros and are used to calculate a new input for estimating the hydrogen production from the electrolyser. This will result in higher energy consumption from the compressor and desalination unit because their energy consumption is based on the hydrogen production without their energy consumption subtracted. This mismatch in energy is assumed to be negligible due to the energy consumption of the compressor and desalination unit being much lower compared to the electrolyser.

For research question two, a model has been developed to study the energy efficiency of the electrolyser when directly coupled to the variable power supply from Zefyros. The model's results show that during the year 2020, the average energy efficiency of the electrolyser is 44.5 %. The optimal efficiency is 60.5 % and occurs at a current density of 0.15 A/cm^2. What is deemed more critical is the degradation effects that the intermittency of wind could cause. Degradation will eventually decrease electrolyser efficiency and an increased risk of failure by relevant components in the electrolyser [77]. In the thesis, no degradation effects are included to narrow the scope of the thesis. The degradation of the electrolyser components is deemed a critical area to study further to prove the feasibility of offshore hydrogen production and is suggested in the future research chapter.

5.4. Value of results to UNITECH

This thesis is written in cooperation with UNITECH Energy Group. One of UNITECH's potential future directions within the company is hydrogen as energy storage. In 2021, UNITECH received funding from Innovation Norway's Green Platform funding scheme to perform a pre-study of the concept of in-turbine hydrogen production at UNITECH Zefyros [165]. The project did not receive funding for a pilot project. The results of this thesis may

shorten the process of performing a new pre-study in case of new ambitions regarding offshore hydrogen production from UNITECH.

UNITECH's expertise is in designing and assembling pressurized subsea equipment that does not leak [166]. A natural branching of their product line-up is to include hydrogen-compatible equipment. This thesis identifies the safety considerations hydrogen production introduces and reviews how to address these. Testing potential new products in an in-turbine hydrogen production system would also prove its compatibility in an offshore environment.

6. Conclusions

For an in-turbine electrolyser at UNITECH Zefyros, the available space inside the turbine tower largely constrains the rated power of the electrolyser. A Nel S-series PEM electrolyser is assumed to be used for in-turbine hydrogen production. The low rated power of the electrolyser results in that if Zefyros is generating power, the electrolyser is producing hydrogen at its rated load. Seawater is desalinated and deionized and used as a feedstock for the electrolyser. A compressor increases the pressure of the produced hydrogen from 13.8 bar to 250 bar. A 5 kWh battery was found suitable to provide the electrolyser with energy for standby mode in case of no energy generation from Zefyros. The hydrogen yield from the in-turbine hydrogen production system in 2020 would be 581 kg.

The heave and pitch response of Zefyros for short-term statistics are simulated. The most probable maximum displacement and acceleration in 1-year and 10-year return period seas have been identified. The largest response is from the 10-year response level; 1.7890 m, 0.7011 °, and 0.3684 m/s^2 and 0.2172 $°/s^2$ for displacement and acceleration in heave and pitch, respectively. Considerations regarding storage, safety, transport, and utilization of the produced hydrogen by the in-turbine electrolyser have been made. The technological feasibility of the system is proved by implementing existing market-available components, compatible with an offshore environment. UNITECH's ambition for in-turbine offshore hydrogen production is thus proved to be technically feasible.

The effect of wind power intermittency on the electrolyser is studied without considering the location of the large-scale hydrogen production system. Hence, without space restrictions it was possible to consider a larger electrolyser compared with the in-turbine case. The system is assumed to have the same rated power as Zefyros (2.3 MW) to ensure that the hydrogen production covers the whole load range of the turbine. A model to estimate the energy efficiency of the electrolyser from the cell voltage is proposed, where a difference in the electrolyser's energy efficiency of approximately 10 % throughout the load range occurs. The maximum energy efficiency (60.5 %) occurs at approximately 10 % of the rated current density, and the minimum energy efficiency occurs at the rated current density. The electrolyser's average energy efficiency in 2020 is 44.5 %. The hydrogen yield of the large-scale hydrogen production system in 2020 would be 110.8 ton hydrogen, approximately a third of the yield if operated at its rated load throughout the year.

7. Further research

In this chapter, areas not included in the thesis but are seen as important areas for further study for the concept that is offshore hydrogen production and in-turbine electrolysis are identified.

- Further study of the possibility of an in-turbine electrolyser. UNITECH Zefyros was constructed in 2009 and is now used as a test infrastructure for new technologies. This results in a lack of available space for an electrolyser with any meaningful hydrogen output. In 2023, the Flagship wind turbine, a 10 MW FOWT, will be installed at the METCENTRE next to Zefyros [160]. Using this turbine as the design basis for an in-turbine electrolyser would more accurately predict how this technology may be implemented in the future.

- To reduce the scope of this thesis and due to the lack of publicly available data, the economics of the proposed systems are not included. For an isolated turbine already grid connected, it is deemed as infeasible that on-site in-turbine hydrogen production would yield a positive economic result. In the case of an offshore wind farm connected to an onshore grid, curtailment may happen. This would make the financial case of offshore hydrogen production stronger. A suggested area for future study is a review of the economic feasibility of large-scale hydrogen production from an offshore wind farm.

- UNITECH Zefyros has a land-based grid connection, facilitating not only for the potential sale of hydrogen, but also for the sale of electrical energy. In the case of electricity generation from hydrogen by fuel cells at an offshore wind turbine, a methodology of when to produce hydrogen and when to sell and to study the financial gain this would yield is a suggested area for further study.

- The intermittency of the wind speed yields a variable power supply from the generator in the turbine. The variable load profile the electrolyser would experience may lead to accelerated degradation of the components in the electrolyser, which in turn decreases the energy efficiency of the electrolyser. Constructing a model that predicts the degradation and the consequences of degradation due to the variable load would answer an important question for the methodology directly coupling an electrolyser to wind power.

- In this thesis, the large-scale hydrogen production system is assumed to have an electrolyser with the same rated power as Zefyros. From the energy efficiency curve, the maximum energy efficiency occurs at approximately 10 % of the rated current density while the hydrogen production rate increases with the current density. Optimizing the electrolyser's rated power with respect to energy efficiency and cost would be an important field to study.

- The displacement and acceleration the electrolyser would experience in heave, roll, and pitch are identified in this thesis. By implementing the anchor system, the yaw, surge, and sway may also be identified. In the thesis, only the response of the turbine due to waves is included. No research has been found about the implications of these movements to the electrolyser. An interesting field of study is how and if the response of the turbine, in all degrees of freedom, from on-site waves, wind, and current affects the electrolyser.

8. References

[1] Miljøstatus. "Klima." https://miljostatus.miljodirektoratet.no/miljomal/klima/ (accessed 04.05, 2022).

[2] Regjeringen. "Storstilt satsing på havvind." https://www.regjeringen.no/no/aktuelt/storstilt-satsing-pa-havvind/id2900436/ (accessed 2022, 04.05).

[3] The Federation of Norwegian Industries. "Viktig dag for havvind – avklaringer om Sørlige Nordsjø II og Utsira Nord." https://www.norskindustri.no/dette-jobber-vi-med/energi-og-klima/aktuelt/viktig-dag-for-havvind--avklaringer-om-sorlige-nordsjo-og-utsira-nord/ (accessed 04.05, 2022).

[4] Regjeringen. "Kraftfull satsing på havvind." https://www.regjeringen.no/no/aktuelt/kraftfull-satsing-pa-havvind/id2912297/ (accessed 13.05, 2022).

[5] Regjeringen. "Milliardstøtte til hydrogenprosjekter." https://www.regjeringen.no/no/aktuelt/milliardstotte-til-hydrogenprosjekter/id2892615/ (accessed 04.05, 2022).

[6] European Commission. "REPowerEU: Joint European action for more affordable, secure and sustainable energy." https://ec.europa.eu/commission/presscorner/detail/en/ip_22_1511 (accessed 08.04, 2022).

[7] International Energy Forum. "Energy Storage: The Key to a Stable Energy Future." https://www.ief.org/news/energy-storage-the-key-to-a-stable-energy-future (accessed 08.04, 2022).

[8] Equinor. "Hywind Demo." https://www.equinor.com/no/what-we-do/floating-wind/hywind-demo.html (accessed 21.03, 2022).

[9] UNITECH. "Press Release January 8th 2019." https://unitechenergy.com/2019/01/08/press-release-january-8th-2019/ (accessed 21.03, 2022).

[10] Sustainable Energy Norwegian Catapult Centre. "Fasiliteter." https://sustainableenergy.no/fasiliteter/#facility_tax-laboratorier (accessed 14.03, 2022).

[11] Norwegian Offshore Wind. "Verdens første flytende vindturbin får forlenget liv." https://offshore-wind.no/news/verdens-forste-flytende-vindturbin-far-forlenget-liv/ (accessed 28.05, 2022).

[12] Offshore Engineer. "Solstad Offshore Installs Subsea Cable for TetraSpar Floater." https://www.oedigital.com/news/490673-solstad-offshore-installs-subsea-cable-for-tetraspar-floater (accessed 2022, 28.05).

[13] FLAGSHIP. "FLoAtinG offSHore wInd oPtimization for commercialization." https://www.flagshiproject.eu (accessed 29.05, 2022).

[14] FLAGSHIP. "FLAGSHIP's choice for its grid-connection architecture." https://www.flagshiproject.eu/flagships-choice-for-its-grid-connection-architecture/ (accessed 2022, 29.05).

[15] B. Skaare, F. G. Nielsen, T. D. Hanson, R. Yttervik, O. Havmøller, and A. Rekdal, "Analysis of measurements and simulations from the Hywind Demo floating wind turbine: Dynamic analysis of the Hywind Demo floating wind turbine," *Wind energy (Chichester, England)*, vol. 18, no. 6, pp. 1105-1122, 2015, doi: 10.1002/we.1750.

[16] Norwegian Technology Transfers. "Dynamic cables for offshore wind farms." https://techtransfer.no/en/renewable-energy/unitech/ (accessed 28.05, 2022).

[17] TechnipFMC. "Deep Purple™ Pilot." https://www.technipfmc.com/en/what-we-do/subsea/energy-transition-deep-purple/deep-purple-pilot/ (accessed 23.03, 2022).

[18] Lhyfe. "Offshore ecological hydrogen." https://www.lhyfe.com/hydrogen-production-facilities/offshore-ecological-hydrogen/ (accessed 23.03, 2022).

[19] NorthH2. "OFFSHORE ELECTROLYSIS." https://www.north2.eu/en/blog-en/offshore-electrolysis/ (accessed 2022, 23.03).

[20] Siemens Gamesa. "Green hydrogen Fuel for the future " https://www.siemensgamesa.com/products-and-services/hybrid-and-storage/green-hydrogen (accessed 23.03, 2022).

[21] POSHYDON. "About PosHYdon." https://poshydon.com/en/home-en/about-poshydon/ (accessed 08.02, 2022).

[22] TechnipFMC. "Energy Transition, Deep Purple™." https://www.technipfmc.com/en/what-we-do/subsea/energy-transition-deep-purple/# (accessed 09.02, 2022).

[23] J. Z. Zhang, *Hydrogen generation, storage, and utilization*, Hoboken, New Jersey: Wiley : ScienceWise Publishing, 2014.

[24] ndla. "Hydrogen som energibærer." https://ndla.no/nb/subject:1:671bd263-eee6-4c56-9e23-a6bbd3130f33/topic:3:183351/topic:2:191074/resource:1:4025 (accessed 09.09, 2021).

[25] J. F. Manwell, J. G. McGowan, and A. L. Rogers, *Wind energy explained : theory, design and application*, 2nd ed. ed. Chichester: Wiley, 2009.

[26] Rystad Energy. "Global installed offshore wind capacity to see 37% growth in 2021, fueled by China." https://www.rystadenergy.com/newsevents/news/press-releases/global-installed-offshore-wind-capacity-to-see-37pct-growth-in-2021-fueled-by-china/ (accessed 08.11, 2021).

[27] B. Lange, S. Larsen, J. Højstrup, and R. Barthelmie, "Importance of thermal effects and sea surface roughness for offshore wind resource assessment," *Journal of Wind Engineering and Industrial Aerodynamics*, vol. 92, no. 11, pp. 959-988, 2004/09/01/ 2004, doi: https://doi.org/10.1016/j.jweia.2004.05.005.

[28] G. Ren, J. Liu, J. Wan, Y. Guo, and D. Yu, "Overview of wind power intermittency: Impacts, measurements, and mitigation solutions," *Applied Energy*, vol. 204, pp. 47-65, 2017/10/15/ 2017, doi: https://doi.org/10.1016/j.apenergy.2017.06.098.

[29] Y. Qi, W. Dong, C. Dong, and C. Huang. "Fixing wind curtailment with electric power system reform in China." https://www.brookings.edu/research/fixing-wind-curtailment-with-electric-power-system-reform-in-china/ (accessed 2021, 08.11).

[30] L. Bird, J. Cochran, and X. Wang, "Wind and solar energy curtailment: Experience and practices in the United States," National Renewable Energy Lab.(NREL), Golden, CO (United States), 2014. [Online]. https://www.nrel.gov/docs/fy14osti/60983.pdf.

[31] M. Specht. "Renewable Energy Curtailment 101: The Problem That's Actually Not a Problem At All." https://blog.ucsusa.org/mark-specht/renewable-energy-curtailment-101/ (accessed 08.11, 2021).
[32] Statistisk Sentralbyrå. "Produksjon og forbruk av energi, energibalanse og energiregnskap." https://www.ssb.no/energi-og-industri/energi/statistikk/produksjon-og-forbruk-av-energi-energibalanse-og-energiregnskap (accessed 08.11, 2021).
[33] K. Meier, "Hydrogen production with sea water electrolysis using Norwegian offshore wind energy potentials," *International Journal of Energy and Environmental Engineering*, vol. 5, no. 2, p. 104, 2014/05/13 2014, doi: 10.1007/s40095-014-0104-6.
[34] G. Calado and R. Castro, "Hydrogen Production from Offshore Wind Parks: Current Situation and Future Perspectives," *Applied Sciences*, vol. 11, no. 12, p. 5561, 2021. [Online]. Available: https://www.mdpi.com/2076-3417/11/12/5561.
[35] B. Miao, L. Giordano, and S. H. Chan, "Long-distance renewable hydrogen transmission via cables and pipelines," *International Journal of Hydrogen Energy*, vol. 46, no. 36, pp. 18699-18718, 2021/05/25/ 2021, doi: https://doi.org/10.1016/j.ijhydene.2021.03.067.
[36] Air Liquide. "Applications." https://energies.airliquide.com/resources-planet-hydrogen/uses-hydrogen (accessed 08.11, 2021).
[37] O. Atlam and M. Kolhe, "Equivalent electrical model for a proton exchange membrane (PEM) electrolyser," *Energy Conversion and Management*, vol. 52, no. 8, pp. 2952-2957, 2011/08/01/ 2011, doi: https://doi.org/10.1016/j.enconman.2011.04.007.
[38] M. Rashid, M. K. Al Mesfer, H. Naseem, and M. Danish, "Hydrogen production by water electrolysis: a review of alkaline water electrolysis, PEM water electrolysis and high temperature water electrolysis," *International Journal of Engineering and Advanced Technology*, 2015.
[39] J. Adolf *et al.*, "Shell Hydrogen Study Energy of the Future? Sustainable Mobility through Fuel Cells and H2," 2017. [Online]. https://epub.wupperinst.org/frontdoor/deliver/index/docId/6786/file/6786_Hydrogen_Study.pdf.
[40] T. Taner, "Energy and exergy analyze of PEM fuel cell: A case study of modeling and simulations," *Energy*, vol. 143, pp. 284-294, 2018/01/15/ 2018, doi: https://doi.org/10.1016/j.energy.2017.10.102.
[41] T. Taner, "The novel and innovative design with using H2 fuel of PEM fuel cell: Efficiency of thermodynamic analyze," *Fuel*, vol. 302, p. 121109, 2021/10/15/ 2021, doi: https://doi.org/10.1016/j.fuel.2021.121109.
[42] Lhyfe. "Lhyfe Hydrogen." https://www.lhyfe.com/lhyfe-hydrogen/ (accessed 09.02, 2022).
[43] C. Schnuelle, T. Wassermann, D. Fuhrlaender, and E. Zondervan, "Dynamic hydrogen production from PV & wind direct electricity supply – Modeling and techno-economic assessment," *International Journal of Hydrogen Energy*, vol. 45, no. 55, pp. 29938-29952, 2020/11/06/ 2020, doi: https://doi.org/10.1016/j.ijhydene.2020.08.044.
[44] Z. Abdin, C. J. Webb, and E. M. Gray, "Modelling and simulation of a proton exchange membrane (PEM) electrolyser cell," *International Journal of Hydrogen*

Energy, vol. 40, no. 39, pp. 13243-13257, 2015/10/19/ 2015, doi: https://doi.org/10.1016/j.ijhydene.2015.07.129.

[45] J. F. Jensen, "Proton Exchange Membrane Water Electrolyzer Modeling Performance during dynamic operation," Master of Science in Renewable Energy Systems, Department of Technology Systems, University of Oslo, [Online]. https://www.duo.uio.no/handle/10852/87510, 2021.

[46] D. S. Falcão and A. M. F. R. Pinto, "A review on PEM electrolyzer modelling: Guidelines for beginners," *Journal of cleaner production*, vol. 261, p. 121184, 2020, doi: 10.1016/j.jclepro.2020.121184.

[47] V. Liso, G. Savoia, S. S. Araya, G. Cinti, and S. K. Kær, "Modelling and Experimental Analysis of a Polymer Electrolyte Membrane Water Electrolysis Cell at Different Operating Temperatures," *Energies*, vol. 11, no. 12, p. 3273, 2018. [Online]. Available: https://www.mdpi.com/1996-1073/11/12/3273.

[48] X. Wu *et al.*, "Foundations of offshore wind turbines: A review," *Renewable and Sustainable Energy Reviews*, vol. 104, pp. 379-393, 2019/04/01/ 2019, doi: https://doi.org/10.1016/j.rser.2019.01.012.

[49] Stiesdal. "The TetraSpar full-scale demonstration project." https://www.stiesdal.com/offshore-technologies/the-tetraspar-full-scale-demonstration-project/ (accessed 09.09, 2021).

[50] Dr. Techn. Olav Olsen. "Breakthrough for OO-Star Wind Floater." https://www.olavolsen.no/no/aktuelt/post-hdQPQ-breakthrough-for-oo-star-wind-floater (accessed 09.09, 2021).

[51] Office of Energy Efficiency & Renewable Energy. "How Do Wind Turbines Survive Severe Storms?" https://www.energy.gov/eere/articles/how-do-wind-turbines-survive-severe-storms (accessed 09.11, 2021).

[52] wind-turbine-models. "Siemens SWT-2.3-82." https://en.wind-turbine-models.com/turbines/204-siemens-swt-2.3-82 (accessed 21.05, 2022).

[53] G. Birkeland, "SCADA data UNITECH Zefyros " Unpublished.

[54] W. Xue, "Design, numerical modelling and analysis of a spar floater supporting the DTU 10MW wind turbine," M.Sc, Department of Marine Technology, NTNU, [Online]. https://ntnuopen.ntnu.no/ntnu-xmlui/handle/11250/2402261, 2016.

[55] J. Journée and W. Massie, "Offshore hydromechanics," 2001. [Online]. https://ocw.tudelft.nl/wp-content/uploads/OffshoreHydromechanics_Journee_Massie.pdf.

[56] K. Tangen, "Dynamisk respons av vindturbiner plassert offshore," M.Sc, Det matematisk-naturvitenskapelige fakultet University of Oslo, [Online]. https://www.duo.uio.no/handle/10852/10878, 2012.

[57] T. C. Thuestad. "Irregulær sjø & havmiljøstatistikk." https://home.hvl.no/ansatte/tct/FTP/V2022%20Hydrodynamikk/Forelesninger/14_1_Irregulær_sjø_korttidsstatistikk.pdf (accessed 23.05, 2022).

[58] J. Aarnes, G. P. Haugom, and B. Norheim, "PRODUKSJON OG BRUK AV HYDROGEN I NORGE," 2019. [Online]. https://www.regjeringen.no/contentassets/0762c0682ad04e6abd66a9555e7468df/hydrogen-i-norge---synteserapport.pdf.

[59] V. Rievaj, J. Gaňa, and F. Synák, "Is hydrogen the fuel of the future?," *Transportation Research Procedia*, vol. 40, pp. 469-474, 2019/01/01/ 2019, doi: https://doi.org/10.1016/j.trpro.2019.07.068.

[60] R. Soltani, M. A. Rosen, and I. Dincer, "Assessment of CO2 capture options from various points in steam methane reforming for hydrogen production," *International Journal of Hydrogen Energy*, vol. 39, no. 35, pp. 20266-20275, 2014/12/03/ 2014, doi: https://doi.org/10.1016/j.ijhydene.2014.09.161.

[61] A. Godula-Jopek, D. Stolten, and C. Bourasseau, *Hydrogen production : by electrolysis*, Weinheim, Germany: WILEY-VCH Verlag GmbH & Co. KGaA, 2015.

[62] M. Carmo, D. L. Fritz, J. Mergel, and D. Stolten, "A comprehensive review on PEM water electrolysis," *International Journal of Hydrogen Energy*, vol. 38, no. 12, pp. 4901-4934, 2013/04/22/ 2013, doi: https://doi.org/10.1016/j.ijhydene.2013.01.151.

[63] K. Hofstad. "strømtetthet." Store Norske Leksikon. https://snl.no/strømtetthet (accessed 27.09, 2021).

[64] Y. Guo, G. Li, J. Zhou, and Y. Liu, "Comparison between hydrogen production by alkaline water electrolysis and hydrogen production by PEM electrolysis," in *IOP Conference Series: Earth and Environmental Science*, 2019, vol. 371, no. 4: IOP Publishing, p. 042022.

[65] Nel. "M SERIES - PEM Electrolyser." https://nelhydrogen.com/product/m-series-3/ (accessed 27.09, 2021).

[66] H. Ito, N. Miyazaki, M. Ishida, and A. Nakano, "Cross-permeation and consumption of hydrogen during proton exchange membrane electrolysis," *International Journal of Hydrogen Energy*, vol. 41, no. 45, pp. 20439-20446, 2016/12/07/ 2016, doi: https://doi.org/10.1016/j.ijhydene.2016.08.119.

[67] I. Vincent and D. Bessarabov, "Low cost hydrogen production by anion exchange membrane electrolysis: A review," *Renewable and Sustainable Energy Reviews*, vol. 81, pp. 1690-1704, 2018/01/01/ 2018, doi: https://doi.org/10.1016/j.rser.2017.05.258.

[68] A. Nechache and S. Hody, "Alternative and innovative solid oxide electrolysis cell materials: A short review," *Renewable and Sustainable Energy Reviews*, vol. 149, p. 111322, 2021/10/01/ 2021, doi: https://doi.org/10.1016/j.rser.2021.111322.

[69] A. Brisse, J. Schefold, and M. Zahid, "High temperature water electrolysis in solid oxide cells," *International Journal of Hydrogen Energy*, vol. 33, no. 20, pp. 5375-5382, 2008/10/01/ 2008, doi: https://doi.org/10.1016/j.ijhydene.2008.07.120.

[70] L. Bi, S. Boulfrad, and E. Traversa, "Steam electrolysis by solid oxide electrolysis cells (SOECs) with proton-conducting oxides," *Chemical Society Reviews*, vol. 43, no. 24, pp. 8255-8270, 2014.

[71] Bosch. "How stationary fuel cells are revolutionizing the power supply." https://www.bosch.com/stories/sofc-system/ (accessed 16.03, 2022).

[72] E. Taibi, R. Miranda, W. Vanhoudt, T. Winkel, J.-C. Lanoix, and F. Barth, "Hydrogen from renewable power: Technology outlook for the energy transition," 2018. [Online]. https://www.irena.org/publications/2018/sep/hydrogen-from-renewable-power.

[73] A. O. Sæbø *et al.*, "Optimal utnyttelse av energi fra havvind i Sørlige Nordsjø II ", 2021. [Online]. https://greenstat.no/downloads/optimal-utnyttelse-av-energi-fra-havvind-i-sorlige-nordsjo-ii_hr-tn.pdf.

[74] S. Shiva Kumar and V. Himabindu, "Hydrogen production by PEM water electrolysis – A review," *Materials Science for Energy Technologies*, vol. 2, no. 3, pp. 442-454, 2019/12/01/ 2019, doi: https://doi.org/10.1016/j.mset.2019.03.002.
[75] A. A. Rahim, A. S. Tijani, and F. H. Shukri, "Simulation analysis of the effect of temperature on overpotentials in PEM electrolyzer system," *Journal of Mechanical Engineering*, vol. 12, no. 1, pp. 47-65, 2015.
[76] S. Sood *et al.*, "Generic dynamical model of PEM electrolyser under intermittent sources," *Energies*, vol. 13, no. 24, p. 6556, 2020.
[77] E. Taibi, H. Blanco, R. Miranda, and M. Carmo, "Green Hydrogen Cost Reduction, Scaling up electrolysers to meet the 1.5 °C climate goal," 2020. [Online]. https://www.irena.org/publications/2020/Dec/Green-hydrogen-cost-reduction.
[78] F. Scheepers *et al.*, "Improving the Efficiency of PEM Electrolyzers through Membrane-Specific Pressure Optimization," *Energies*, vol. 13, no. 3, p. 612, 2020. [Online]. Available: https://www.mdpi.com/1996-1073/13/3/612.
[79] M. Schalenbach, M. Carmo, D. L. Fritz, J. Mergel, and D. Stolten, "Pressurized PEM water electrolysis: Efficiency and gas crossover," *International journal of hydrogen energy*, vol. 38, no. 35, pp. 14921-14933, 2013, doi: 10.1016/j.ijhydene.2013.09.013.
[80] H. Görgün, "Dynamic modelling of a proton exchange membrane (PEM) electrolyzer," *International Journal of Hydrogen Energy*, vol. 31, no. 1, pp. 29-38, 2006/01/01/ 2006, doi: https://doi.org/10.1016/j.ijhydene.2005.04.001.
[81] J. J. Hwang, L. K. Lai, W. Wu, and W. R. Chang, "Dynamic modeling of a photovoltaic hydrogen fuel cell hybrid system," *International Journal of Hydrogen Energy*, vol. 34, no. 23, pp. 9531-9542, 2009/12/01/ 2009, doi: https://doi.org/10.1016/j.ijhydene.2009.09.100.
[82] M. Ni, M. K. H. Leung, and D. Y. C. Leung, "Energy and exergy analysis of hydrogen production by a proton exchange membrane (PEM) electrolyzer plant," *Energy Conversion and Management*, vol. 49, no. 10, pp. 2748-2756, 2008/10/01/ 2008, doi: https://doi.org/10.1016/j.enconman.2008.03.018.
[83] P. Choi, D. G. Bessarabov, and R. Datta, "A simple model for solid polymer electrolyte (SPE) water electrolysis," *Solid State Ionics*, vol. 175, no. 1, pp. 535-539, 2004/11/30/ 2004, doi: https://doi.org/10.1016/j.ssi.2004.01.076.
[84] T. Yigit and O. F. Selamet, "Mathematical modeling and dynamic Simulink simulation of high-pressure PEM electrolyzer system," *International Journal of Hydrogen Energy*, vol. 41, no. 32, pp. 13901-13914, 2016/08/24/ 2016, doi: https://doi.org/10.1016/j.ijhydene.2016.06.022.
[85] K. Hofstad. "hydrogendrivstoff." https://snl.no/hydrogendrivstoff (accessed 09.11, 2021).
[86] K. Hofstad. "energivare." https://snl.no/energivare (accessed 23.03, 2022).
[87] Office of Energy Efficiency & Renewable Energy. "Hydrogen Storage." https://www.energy.gov/eere/fuelcells/hydrogen-storage (accessed 09.11, 2021).
[88] B. Pedersen. "hydrogen." Store Norske Leksikon https://snl.no/hydrogen (accessed 09.11, 2021).

[89] K. Mazloomi and C. Gomes, "Hydrogen as an energy carrier: Prospects and challenges," *Renewable and Sustainable Energy Reviews,* vol. 16, pp. 3024-3033, 06/01 2012, doi: 10.1016/j.rser.2012.02.028.

[90] M. Aziz, "Liquid Hydrogen: A Review on Liquefaction, Storage, Transportation, and Safety," *Energies (Basel),* vol. 14, no. 18, p. 5917, 2021, doi: 10.3390/en14185917.

[91] A. Godula-Jopek, W. Jehle, and J. Wellnitz, *Hydrogen storage technologies : new materials, transport, and infrastructure*, 2nd ed. ed. Weinheim: Wiley-VCH Verlag GmbH & Co. KGaA, 2012.

[92] D. Grouset and C. Ridart, "Chapter 6 - Lowering Energy Spending Together With Compression, Storage, and Transportation Costs for Hydrogen Distribution in the Early Market," in *Hydrogen Supply Chains*, C. Azzaro-Pantel Ed.: Academic Press, 2018, pp. 207-270.

[93] Department of Energy Hydrogen and Fuel Cells Program Record, "Energy requirements for hydrogen gas compression and liquefaction as related to vehicle storage needs," 2009. [Online]. https://www.hydrogen.energy.gov/pdfs/9013_energy_requirements_for_hydrogen_gas_compression.pdf.

[94] L. Van Hoecke, L. Laffineur, R. Campe, P. Perreault, S. Verbruggen, and S. Lenaerts, "Challenges in the use of hydrogen as a maritime fuel," *Energy & Environmental Science,* vol. 14, 01/01 2020, doi: 10.1039/D0EE01545H.

[95] E. Rivard, M. Trudeau, and K. Zaghib, "Hydrogen Storage for Mobility: A Review," *Materials,* vol. 12, no. 12, p. 1973, 2019. [Online]. Available: https://www.mdpi.com/1996-1944/12/12/1973.

[96] M. Aziz, A. T. Wijayanta, A. B. D. Nandiyanto, M. Aziz, A. T. Wijayanta, and A. B. D. Nandiyanto, "Ammonia as Effective Hydrogen Storage: A Review on Production, Storage and Utilization," *Energies (Basel),* vol. 13, no. 12, p. 3062, 2020, doi: 10.3390/en13123062.

[97] W. S. Chai, Y. Bao, P. Jin, G. Tang, and L. Zhou, "A review on ammonia, ammonia-hydrogen and ammonia-methane fuels," *Renewable and Sustainable Energy Reviews,* vol. 147, p. 111254, 2021/09/01/ 2021, doi: https://doi.org/10.1016/j.rser.2021.111254.

[98] N. A. A. Rusman and M. Dahari, "A review on the current progress of metal hydrides material for solid-state hydrogen storage applications," *International Journal of Hydrogen Energy,* vol. 41, no. 28, pp. 12108-12126, 2016/07/27/ 2016, doi: https://doi.org/10.1016/j.ijhydene.2016.05.244.

[99] K. Turani-I-Belloto, C. A. Castilla-Martinez, D. Cot, E. Petit, S. Benarib, and U. B. Demirci, "Nanosized ammonia borane for solid-state hydrogen storage: Outcomes, limitations, challenges and opportunities," *International Journal of Hydrogen Energy,* vol. 46, no. 10, pp. 7351-7370, 2021/02/08/ 2021, doi: https://doi.org/10.1016/j.ijhydene.2020.11.224.

[100] J. O. Abe, A. P. I. Popoola, E. Ajenifuja, and O. M. Popoola, "Hydrogen energy, economy and storage: Review and recommendation," *International Journal of Hydrogen Energy,* vol. 44, no. 29, pp. 15072-15086, 2019/06/07/ 2019, doi: https://doi.org/10.1016/j.ijhydene.2019.04.068.

[101] Hexagon. "Hydrogen Type 4 cylinders." https://s3.eu-central-1.amazonaws.com/hexagonpurus-website/HexagonPurus_HydrogenType4_DataSheet.pdf (accessed 10.03, 2022).
[102] SINTEF. "HyLINE - Safe Pipelines for Hydrogen Transport." https://www.sintef.no/en/projects/2019/hyline-safe-pipelines-for-hydrogen-transport/ (accessed 15.11, 2021).
[103] DNV. "Transportation of hydrogen gas in offshore pipelines - H2Pipe." https://www.dnv.com/oilgas/joint-industry-projects/gas-value-chain/transportation-of-hydrogen-gas-in-offshore-pipelines-jip.html (accessed 2021, 15.11).
[104] ARENA. "Hydrogen to be trialled in NSW gas networks." https://arena.gov.au/news/hydrogen-to-be-trialled-in-nsw-gas-networks/ (accessed 15.11, 2021).
[105] H21. "Pioneering a UK hydrogen network…Led by Northern Gas Networks." https://h21.green (accessed 15.11, 2021).
[106] CRISTIN. "Safe Pipelines for Hydrogen Transport." https://app.cristin.no/projects/show.jsf?id=2062917 (accessed 15.11, 2021).
[107] Lloyd's Register. "World first for liquid hydrogen transportation." https://www.lr.org/en/insights/articles/world-first-for-liquid-hydrogen-transportation/ (accessed 10.11, 2021).
[108] K. Hyde and A. Ellis, "Feasibility of Hydrogen Bunkering," 2019. [Online]. https://northsearegion.eu/media/9385/feasibility-of-hydrogen-bunkering-final-080419.pdf.
[109] Dennis van der Meulen and J. Douma, "SuAc 1.1b Hydrogen Bunkering Scenarios," 2021. [Online]. https://www.rh2ine.eu/wp-content/uploads/2021/10/RH2INE-Kickstart-Study-Scenario-building-Hydrogen-Bunkering-Scenarios.pdf.
[110] D. N. Qin, D. A. Raissi, and D. P. Brooker, "Analysis of Fuel Cell Vehicle Developments ", 2014. [Online]. http://fsec.ucf.edu/en/publications/pdf/fsec-cr-1987-14.pdf.
[111] Statistisk Sentralbyrå. "Bilparken." https://www.ssb.no/transport-og-reiseliv/landtransport/statistikk/bilparken (accessed 11.11, 2021).
[112] Hynion. "Om oss." http://www.hynion.com/no/om-oss (accessed 11.11, 2021).
[113] Greenstat. "Everfuel og Greenstat inngår samarbeid om kostnadseffektiv verdkjede for hydrogen i Norge." https://greenstat.no/hvaskjer/everfuel-og-greenstat-inngar-samarbeid-om-kostnadseffektiv-verdkjede-for-hydrogen-i-norge (accessed 11.11, 2021).
[114] Toyota. "HYDROGEN FOR ALLE." https://www.toyota.no/world-of-toyota/articles-news-events/2021/hydrogen-fyllestasjoner.json (accessed 11.11, 2021).
[115] Skipsrevyen. "Ukens Skipsbesøk: MF "Hydra"." https://www.skipsrevyen.no/article/ukens-skisbesoek-mf-hydra/ (accessed 12.11, 2021).
[116] T. I. Jøssang. "Nok en forsin-kelse for verdens-nyheten." https://www.aftenbladet.no/lokalt/i/z7PBL5/ny-forsinkelse-for-verdens-foerste-hydrogenferje (accessed 29.04, 2022).

[117] Eidesvik. "Viking Energy with ammonia-driven fuel cell." https://eidesvik.no/viking-energy-with-ammonia-driven-fuel-cell/ (accessed 12.11, 2021).
[118] Airbus. "ZEROe." https://www.airbus.com/en/innovation/zero-emission/hydrogen/zeroe (accessed 15.11, 2021).
[119] Bloomberg Green. "This Village in England Is Already Using Hydrogen to Heat Homes." https://www.bloomberg.com/news/articles/2021-09-08/this-village-in-england-is-already-using-hydrogen-to-heat-homes (accessed 15.11, 2021).
[120] EnergiRike. "Enova investerer 122 millioner i Tizir, Tyssedal." https://www.energirike.no/sider/hjem/nyheter/enova-investerer-122-millioner-i-tizir-tyssedal/480/ (accessed 15.11, 2021).
[121] *Forskrift om håndtering av brannfarlig, reaksjonsfarlig og trykksatt stoff samt utstyr og anlegg som benyttes ved håndteringen,* Justis- og beredskapsdepartementet, 2009.
[122] *Forskrift om trykkpåkjent utstyr,* Arbeids- og sosialdepartementet and Justis- og beredskapsdepartementet, 2017.
[123] *Forskrift om tiltak for å forebygge og begrense konsekvensene av storulykker i virksomheter der farlige kjemikalier forekommer (storulykkeforskriften),* Justis- og beredskapsdepartementet, 2016.
[124] *Forskrift om landtransport av farlig gods,* Justis- og beredskapsdepartementet, 2009.
[125] *Forskrift om utstyr og sikkerhetssystem til bruk i eksplosjonsfarlig område,* Arbeids- og inkluderingsdepartementet and Justis- og beredskapsdepartementet, 2017.
[126] R. Koelewijn, M. v. Dam, and C. Hulsbosch-Dam, "Report on offshore structural integrity and safety performance of H2 production, processing, storage and transport," 2020. [Online]. https://north-sea-energy.eu/static/0803c088fdf41a7050eb91051dba1218/FINAL-NSE3_D4.2-Report-on-offshore-structural-integrity-and-safety-performance-of-H2-production-processing-storage-and-transport.pdf.
[127] Direktoratet for samfunnssikkerhet og beredskap. "Krav til merking av utstyr til bruk i eksplosjonsfarlige områder." https://www.dsb.no/nyhetsarkiv/2021/krav-til-merking-av-utstyr-til-bruk-i-eksplosjonsfarlige-omrader/ (accessed 27.05, 2022).
[128] DNV. "DNV to study safety implications of world-first offshore green hydrogen production facility." https://www.dnv.com/news/dnv-to-study-safety-implications-of-world-first-offshore-green-hydrogen-production-facility-204179 (accessed 09.02, 2022).
[129] G. Birkeland, "UNITECH Zefyros space restrictions," Unpublished.
[130] Nel. "S SERIES PEM Electrolyser." https://nelhydrogen.com/product/s-series/ (accessed 03.11, 2021).
[131] G. Matute, J. M. Yusta, and L. C. Correas, "Techno-economic modelling of water electrolysers in the range of several MW to provide grid services while generating hydrogen for different applications: A case study in Spain applied to mobility with FCEVs," *International Journal of Hydrogen Energy,* vol. 44, no. 33, pp. 17431-17442, 2019/07/05/ 2019, doi: https://doi.org/10.1016/j.ijhydene.2019.05.092.
[132] Siemens Energy. "Overview of the PEM Silyzer Family." https://4echile-datastore.s3.eu-central-1.amazonaws.com/wp-

content/uploads/2020/10/10132733/20200930-SE-NEB-PEM-Electrolyzer-and-Applications_EW.pdf (accessed 23.03, 2022).
[133] DNV. "DNV Sesam software." https://rapid-models.dnvgl.com/about/use-cases/sesam.html#background (accessed 12.04, 2022).
[134] DNV. "SeSam Genie." https://www.dnv.com/Images/Sesam-Genie-brochure-spread_tcm8-58836.pdf (accessed 12.04, 2022).
[135] DNV. "Hydrodynamic analysis and stability analysis software - HydroD." https://www.dnv.com/services/hydrodynamic-analysis-and-stability-analysis-software-hydrod-14492 (accessed 12.04, 2022).
[136] DNV. "Graphical post-processor software - Postresp." https://www.dnv.com/services/graphical-post-processor-software-postresp-2415 (accessed 24.03, 2022).
[137] G. Birkeland, "Zefyros As Built," Unpublished.
[138] *Structural design of offshore ship-shaped units*, DNV, https://rules.dnv.com/docs/pdf/DNV/OS/2020-07/DNVGL-OS-C102.pdf, 2020. [Online]. Available: https://rules.dnv.com/docs/pdf/DNV/OS/2020-07/DNVGL-OS-C102.pdf
[139] K. Ayers, "High efficiency PEM water electrolysis: Enabled by advanced catalysts, membranes, and processes," *Current Opinion in Chemical Engineering*, vol. 33, p. 100719, 2021.
[140] G. Birkeland, "Hywind Metocean Design Basis," UNITECH, 13.03, Unpublished.
[141] MathWorks. "MathWorks." https://www.mathworks.com/?s_tid=gn_logo (accessed 08.04, 2022).
[142] J. Tiktak, "Heat Management of PEM Electrolysis," M.Sc, Maritime and Materials Engineering, TU Delft Mechanical, [Online]. https://repository.tudelft.nl/islandora/object/uuid:c046820a-72bc-4f05-b72d-e60a3ecb8c89?collection=education, 2019.
[143] F. Barbir, "PEM electrolysis for production of hydrogen from renewable energy sources," *Solar Energy*, vol. 78, no. 5, pp. 661-669, 2005/05/01/ 2005, doi: https://doi.org/10.1016/j.solener.2004.09.003.
[144] M. Kopp, D. Coleman, C. Stiller, K. Scheffer, J. Aichinger, and B. Scheppat, "Energiepark Mainz: Technical and economic analysis of the worldwide largest Power-to-Gas plant with PEM electrolysis," *International Journal of Hydrogen Energy*, vol. 42, no. 19, pp. 13311-13320, 2017/05/11/ 2017, doi: https://doi.org/10.1016/j.ijhydene.2016.12.145.
[145] Nel. "Alkaline and Proton PEM Electrolysers." https://nelhydrogen.com/resources/electrolysers-brochure/ (accessed 2022, 14.02).
[146] L&W Compressors. "EX-PROOF PLANTS." https://www.lw-compressors.com/sites/default/files/product-files/Ex_proof_plants_en.pdf (accessed 28.04, 2022).
[147] L&W Compressors. "Product Range." https://www.lw-compressors.com/sites/default/files/product-files/ProductRange.pdf (accessed 2022, 28.04).

[148] A. H. Zimmerman, "Self-discharge losses in lithium-ion cells," *IEEE aerospace and electronic systems magazine*, vol. 19, no. 2, pp. 19-24, 2004, doi: 10.1109/MAES.2004.1269687.
[149] Hydrogen Tools. "Hydrogen Density at different temperatures and pressures." https://h2tools.org/hyarc/hydrogen-data/hydrogen-density-different-temperatures-and-pressures (accessed 03.10, 2021).
[150] A. Di Blasi *et al.*, "Evaluation of materials and components degradation of a PEM electrolyzer for marine applications," *International Journal of Hydrogen Energy*, vol. 38, no. 18, pp. 7612-7615, 2013/06/18/ 2013, doi: https://doi.org/10.1016/j.ijhydene.2012.10.062.
[151] Mehrer. "RECIPROCATING COMPRESSORS." https://www.mehrer.de/en/products/reciprocating-compressors/112-trx200 (accessed 24.03, 2022).
[152] C. San March, "Technical Reference on Hydrogen Compatibility of Materials," 2006. [Online]. https://www.sandia.gov/app/uploads/sites/158/2021/12/4001TechRef_Cu.pdf.
[153] J. Shi *et al.*, "Corrosion behaviors of pure copper and Cu-Ni-Zn alloy in NaCl solution and artificial salt water," in *IOP Conference Series: Materials Science and Engineering*, 2018, vol. 292, no. 1: IOP Publishing, p. 012004.
[154] Hexagon. "Hydrogen high-pressure Type 4 cylinders." https://s3.eu-central-1.amazonaws.com/hexagonpurus-website/HexagonPurus_Broschüre_HighPressureType4.pdf (accessed 01.04, 2022).
[155] D. K. Jesthi and R. K. Nayak, "Evaluation of mechanical properties and morphology of seawater aged carbon and glass fiber reinforced polymer hybrid composites," *Composites Part B: Engineering*, vol. 174, p. 106980, 2019/10/01/ 2019, doi: https://doi.org/10.1016/j.compositesb.2019.106980.
[156] Offshore magazine. "DORIS, Lhyfe pursuing floating wind turbine/green hydrogen development." https://www.offshore-mag.com/renewable-energy/article/14214796/doris-lhyfe-pursuing-floating-wind-turbinegreen-hydrogen-development (accessed 30.03, 2022).
[157] Exponential Power. "Hydrogen Gas Ventilation for Battery Rooms." https://www.exponentialpower.com/sbs-exhaust-ventilation-fan.html (accessed 30.03, 2022).
[158] Shell. "Shell Marine Gasoil (0,05%)." https://prodepc.blob.core.windows.net/epcblobstorage/GPCDOC_X_cbe_26724_key_140007515295_201302281447.pdf (accessed 14.03, 2022).
[159] U.S Energy Information Administration. "Oil tanker sizes range from general purpose to ultra-large crude carriers on AFRA scale." https://www.eia.gov/todayinenergy/detail.php?id=17991 (accessed 14.03, 2022).
[160] Siva. "Unitech Teknologisenter." https://siva.no/virkemidler/byggeprosjekter/unitech-teknologisenter/ (accessed 14.03, 2022).
[161] SICGILSOL. "OXYGEN." https://www.sicgilsol.com/oxygen/# (accessed 13.05, 2022).

[162] A. Buttler and H. Spliethoff, "Current status of water electrolysis for energy storage, grid balancing and sector coupling via power-to-gas and power-to-liquids: A review," *Renewable and Sustainable Energy Reviews*, vol. 82, pp. 2440-2454, 2018/02/01/ 2018, doi: https://doi.org/10.1016/j.rser.2017.09.003.

[163] E. Gonzalez, B. Stephen, D. Infield, and J. J. Melero, "Using high-frequency SCADA data for wind turbine performance monitoring: A sensitivity study," *Renewable Energy*, vol. 131, pp. 841-853, 2019/02/01/ 2019, doi: https://doi.org/10.1016/j.renene.2018.07.068.

[164] F. Fagotti, M. Todescat, R. Ferreira, and A. Prata, "Heat transfer modeling in a reciprocating compressor," 1994. [Online]. http://citeseerx.ist.psu.edu/viewdoc/download?doi=10.1.1.898.4226&rep=rep1&type=pdf.

[165] T. G. Tollaksen. "Han vil bygge verdens første drivstoffstasjon ute i havet." https://e24.no/det-groenne-skiftet/i/QmjLK4/han-vil-bygge-verdens-foerste-drivstoffstasjon-ute-i-havet (accessed 27.05, 2022).

[166] UNITECH Energy. "Making a Difference." https://unitechenergy.com/making-a-difference/ (accessed 2022, 27.05).